



US Army Corps
of Engineers

AD-A231 703



DTIC FILE COPY

TECHNICAL REPORT SL-91-2

2

EVALUATION OF PARAMETERS AFFECTING THERMAL STRESSES IN MASS CONCRETE

by

Anthony A. Bombich, Sharon Garner, C. Dean Norman

Structures Laboratory

DEPARTMENT OF THE ARMY

Waterways Experiment Station, Corps of Engineers
3909 Halls Ferry Road, Vicksburg, Mississippi 39180-6199



January 1991

Final Report

Approved for Public Release; Distribution Unlimited

DTIC
ELECTE
FEB 13 1991
S B D

Prepared for US Army Engineer District, St. Louis
St. Louis, Missouri 63101-1986



91 2 12 095

**Destroy this report when no longer needed. Do not return
it to the originator.**

**The findings in this report are not to be construed as an official
Department of the Army position unless so designated
by other authorized documents.**

**The contents of this report are not to be used for
advertising, publication, or promotional purposes.
Citation of trade names does not constitute an
official endorsement or approval of the use of
such commercial products.**

REPORT DOCUMENTATION PAGE

Form Approved
OMB No. 0704-0188

Public reporting burden for this collection of information is estimated to average 1 hour per response, including the time for reviewing instructions, searching existing data sources, gathering and maintaining the data needed, and completing and reviewing the collection of information. Send comments regarding this burden estimate or any other aspect of this collection of information, including suggestions for reducing this burden, to Washington Headquarters Services, Directorate for Information Operations and Reports, 1215 Jefferson Davis Highway, Suite 1204, Arlington, VA 22202-4302, and to the Office of Management and Budget, Paperwork Reduction Project (0704-0188), Washington, DC 20503.

| | | | |
|---|---|--|-----------------------------------|
| 1. AGENCY USE ONLY (Leave blank) | 2. REPORT DATE January 1991 | 3. REPORT TYPE AND DATES COVERED Final | |
| 4. TITLE AND SUBTITLE Evaluation of Parameters Affecting Thermal Stresses in Mass Concrete | | 5. FUNDING NUMBERS | |
| 6. AUTHOR(S) Anthony A. Bombich Sharon Garner C. Dean Norman | | 8. PERFORMING ORGANIZATION REPORT NUMBER Technical Report SL-91-2 (CTIAC Report 88) | |
| 7. PERFORMING ORGANIZATION NAME(S) AND ADDRESS(ES) USAE Waterways Experiment Station Structures Laboratory 3909 Halls Ferry Road Vicksburg, MS 39180-6199 | | 10. SPONSORING / MONITORING AGENCY REPORT NUMBER | |
| 9. SPONSORING / MONITORING AGENCY NAME(S) AND ADDRESS(ES) US Army Engineer District, St. Louis St. Louis, MO 63101-1986 | | 11. SUPPLEMENTARY NOTES Available from National Technical Information Service, 5285 Port Royal Road, Springfield, VA 22161 | |
| 12a. DISTRIBUTION / AVAILABILITY STATEMENT Approved for public release; distribution unlimited | | 12b. DISTRIBUTION CODE | |
| 13. ABSTRACT (Maximum 200 words) This report describes an investigation to evaluate parameters that affect thermal stresses in mass concrete. This investigation, conducted at the US Army Engineer Waterways Experiment Station (WES) was part of a cooperative effort conducted at Corps District Offices, Corps research laboratories, and several universities to support construction of the second lock in Melvin Price Locks and Dam (MPL&D). The investigation was based upon implementation of ABAQUS, a finite-element program capable of performing complete incremental construction analyses of complex mass concrete structures during and following construction. The report describes a user-defined aging creep material model, UMAT, used with ABAQUS to account for the changes in concrete material strength, modulus of elasticity, creep, shrinkage, etc. following placement in a mass concrete structure. UMAT also contains a smeared cracking model to evolve the onset and effects of cracking. In addition to material aging, ABAQUS includes the | | | |
| | | | (Continued) |
| 14. SUBJECT TERMS Aging-creep model Incremental construction Thermal stress Concrete properties Mass concrete Finite-element analysis Temperature | | 15. NUMBER OF PAGES 104 | |
| | | 16. PRICE CODE | |
| 17. SECURITY CLASSIFICATION OF REPORT UNCLASSIFIED | 18. SECURITY CLASSIFICATION OF THIS PAGE UNCLASSIFIED | 19. SECURITY CLASSIFICATION OF ABSTRACT | 20. LIMITATION OF ABSTRACT |

Unclassified

13. (Concluded).

capability to simulate placement of incremental stages (lifts) of concrete in a structure, time-stepping, modeling of thermal and mechanical boundaries, model environmental conditions, and provides other user-defined subroutines to model parameters such as heat evolution of cement in the concrete mixtures.

The report describes calibration of the UMAT aging creep material model for use in the overall research project. Initially, test data for MPL&D were not available; therefore, the initial UMAT calibration was based on properties of "similar" mixtures. Modulus and creep were predicted using two different equations, and the results compared with the test data for three mass concrete mixtures. Due to limited data available for shrinkage, a curve was assumed based on previous test results at WES. Upon completion of testing MPL&D concrete mixture C2-2 for modulus of elastic modulus, creep, and shrinkage, actual test data were compared with the predicted curves used in the model. The UMAT curve was in fairly good agreement with elastic modulus for the mixture. However, test creep strains were less than half of the UMAT creep equation. The UMAT shrinkage curve approximated the total test strains, but not the shape of the test shrinkage curves. Both shrinkage and creep depend on variables whose contributions to the final properties are not easily determined, such as volumes and properties of the aggregates and chemical composition of the cement paste. It is recommended that properties of mass concretes used in UMAT, especially those at early ages, should be based on test results rather than assumed properties.

The report also describes the development of an incremental construction formulation to address aspects of nonlinear finite-element analysis of mass concrete structures that are not common in conventional structural analysis. Accurate computation of thermal stresses during incremental construction finite-element analysis is dependent upon accurate computation of thermal loads produced by variation in concrete temperatures during simulations of construction. The final section addresses requirements and methodologies needed for computation of thermal loads. Through a series of finite-element thermal analyses, grid size and time-step length sensitivity are examined. These analyses were performed using constant and varying ambient temperature boundary conditions. Evaluation of material, placement, and construction parameters were included. Multiple heat generation input curves were implemented, and boundary conditions were varied to simulate curing conditions, ambient conditions, surface insulation, and lift interface equilibration. The thermal analyses were conducted in a sequence of simple-to-more-complex conditions which finally simulated actual conditions.

The analyses were based upon finite-element models of an instrumented, incrementally constructed model lock wall, the WES Test Wall, constructed for a related research program. In order to evaluate critical parameters for incremental analyses, computed results from thermal simulations with ABAQUS were compared with measurements made during construction of the WES Test Wall.

The report discusses the sequence of analyses including problems and solutions relating to incremental construction methodology in computation of thermal loads. Based upon the results of the investigation, criteria are presented to be applied in the selection of certain parameters used in incremental construction analyses and to identify the state of the art.

Unclassified

PREFACE

The investigation described in this report was conducted for the US Army Engineer District, St. Louis. Authorization was given by DA Form 2544, No. ED87-30, dated 10 April 1987. Funds for publication of the report were provided from those made available for operation of the Concrete Technology Information Analysis Center at the US Army Engineer Waterways Experiment Station (WES). This is CTIAC Report No. 88.

The investigation was performed at WES by members of the staff of the Structures Laboratory, under the general supervision of Messers. Bryant Mather, Chief, and J. T. Ballard, Assistant Chief. Direct supervision was provided by K. L. Saucier, Chief, Concrete Technology Division (CTD). Project management was provided by Dr. C. Dean Norman, Structural Mechanics Division, formerly Chief, Evaluation and Monitoring Unit, Concrete and Grout Group, CTD. This report was prepared by Mr. Anthony A. Bombich, Ms. Sharon Garner, Applied Mechanics Group, Engineering Mechanics Branch, CTD, and Dr. Norman. The authors acknowledge Messrs. Donald Smith, Michael Hammons, Dan Wilson, and Brent Lamb, and Ms. Linda Mayfield, CTD, for their help during this investigation.

Commander and Director of WES during preparation of this report was COL Larry B. Fulton, EN. Technical Director was Dr. Robert W. Whalin.



| | |
|---------------------------|-------------------------------------|
| Accession For | |
| NTIS GRA&I | <input checked="" type="checkbox"/> |
| DTIC TAB | <input type="checkbox"/> |
| Unannounced | <input type="checkbox"/> |
| Justification | |
| By _____ | |
| Distribution/ | |
| Availability Codes | |
| Dist | Avail and/or Special |
| A-1 | |

CONTENTS

| | <u>Page</u> |
|--|-------------|
| PREFACE | i |
| LIST OF TABLES | iv |
| LIST OF FIGURES | v |
| CONVERSION FACTORS, NON-SI TO METRIC (SI) UNITS OF MEASUREMENT . . . | vii |
| PART I: INTRODUCTION | 1 |
| Background | 1 |
| Objectives | 3 |
| Scope | 7 |
| PART II: ANALYSIS PROCEDURE | 10 |
| Heat Transfer and Structural Analysis | 10 |
| Aging Creep Model with Cracking | 10 |
| PART III: MATERIAL MODEL CALIBRATION | 13 |
| Details of Model Calibration | 13 |
| Initial Model Calibration | 17 |
| Testing | 22 |
| Final Model Calibration | 26 |
| PART IV: INCREMENTAL CONSTRUCTION FORMULATION | 35 |
| Background | 35 |
| The WES Test Wall | 37 |
| Construction and surface preparation | 37 |
| Instrumentation of WES Test Wall | 39 |
| Incremental Formulation | 39 |
| Lift heights | 48 |
| Finite element models | 48 |
| Concrete placement schemes | 53 |
| Weather conditions | 53 |
| Concrete placement times | 55 |
| Placement temperatures | 57 |
| Normal curing conditions | 57 |
| Curing convection film coefficient | 57 |
| Insulation curing condition | 59 |
| Insulation curing film coefficients | 59 |
| Concrete Mixture and Properties | 60 |
| DFLUX subroutine and the adiabatic temperature rise of concrete | 61 |
| Summary of Thermal Analyses | 62 |
| Discussion of Results | 66 |
| Element size and time step sensitivity analyses with constant air temperature | 67 |
| Element size and time step sensitivity with variable ambient air temperatures | 75 |
| Comparison of measured and predicted results | 80 |

| | |
|---|----|
| Lift interface equilibrium | 85 |
| Conclusions | 87 |
| Element size and time step sensitivity with constant air temperatures | 87 |
| Element size and time step sensitivity with variable ambient air temperature | 90 |
| Concrete properties | 90 |
| Curing, boundary conditions, and modeling of surface heat transfer film coefficients | 91 |
| Recommended future efforts | 92 |
| REFERENCES | 93 |

LIST OF TABLES

| <u>No.</u> | | <u>Page</u> |
|------------|--|-------------|
| 1 | Concrete Mixture Proportions for Melvin Price Lock and Dam Mixtures | 17 |
| 2 | Compressive Strength Test Results for Melvin Price Lock and Dam Mixture C2-2 | 18 |
| 3 | Comparison of Mixtures used in Calibrating the UMAT Model | 19 |
| 4 | Creep and Elastic Modulus Test Specimens | 25 |
| 5 | Average Modulus Results from Uniaxial Compression and Creep Tests | 26 |
| 6 | Finite Element Investigation - Grid Size Variation | 53 |
| 7 | WES Test Wall Concrete Mixture Proportions | 61 |
| 8 | Thermal Properties of Concrete used in Finite Element Investigation | 62 |
| 9 | Thermal Analysis Run Summary Showing Grid Size/Time Step/ Ambient and Adiabatic Temperature Relationship | 64 |
| 10 | Incremental Construction Formulation Thermal Analyses Computer Runs | 65 |
| 11 | Minimum Time Step Lengths, t (days) Required by ABAQUS from Equation 13 for Incremental Construction Thermal Analyses of WES Test Wall | 71 |
| 12 | Final Sequence of Heat Transfer Film Coefficients used for Lift 6 | 83 |

LIST OF FIGURES

| <u>No.</u> | | <u>Page</u> |
|------------|---|-------------|
| 1 | Three-dimensional finite element grid for monolith L13 | 2 |
| 2 | Two-dimensional finite element grid for monolith L17 | 2 |
| 3 | Specific creep predictions for early time loading of a silica fume concrete for ABAQUS with an aging, creep model | 4 |
| 4 | Shrinkage measurements showing significant increase at early ages, $f'c = 3000$ psi. | 5 |
| 5 | Elastic modulus showing significant increase at early ages, $f'c = 3000$ psi. | 5 |
| 6 | Effects of including aging, creep, and shrinkage in the finite element analysis of a generic mass concrete placement problem (ABAQUS) | 6 |
| 7 | Incrementally constructed mass concrete model of lock wall with observed crack patterns | 8 |
| 8 | Verification of creep prediction from ABAQUS for a 3-day age at loading test | 9 |
| 9 | Bounding adiabatic temperature rise curves | 14 |
| 10 | UMAT specific strains vs time | 16 |
| 11 | Test modulus curves for the Dworshak Dam, Portuguese Dam and Tenn-Tom mixtures | 20 |
| 12 | Predicted and test moduli | 20 |
| 13 | Initial UMAT modulus vs time curve | 21 |
| 14 | Predicted and tested 3-day specific creep curves | 23 |
| 15 | Comparison of UMAT 3-day specific creep curve and Dworshak specific creep | 23 |
| 16 | UMAT shrinkage curve | 24 |
| 17 | Series 2: 1/2-day creep test strains | 27 |
| 18 | Series 2: 3/4-day creep test strains | 27 |
| 19 | Series 1: 3-day and 7-day creep test strains | 28 |
| 20 | Series 2: 1-day and 3-day creep test strains | 28 |
| 21 | Three-day specific creep curves calculated from Series 1 and Series 2 test data | 29 |
| 22 | Typical autogenous shrinkage test specimen | 30 |
| 23 | Average shrinkage strain results, mixture C2-2 | 31 |
| 24 | Average shrinkage strain results, mixture C3-3 | 31 |
| 25 | UMAT and tested elastic modulus vs time curves | 33 |
| 26 | Upper bound, lower bound and tested specific creep curves | 33 |
| 27 | Upper bound, lower bound and tested shrinkage strain curves | 34 |
| 28 | WES Test Wall | 38 |
| 29 | Instrumentation measurement planes in WES Test Wall | 40 |
| 30 | Locations of Carlson strain gages in longitudinal plane in Test Wall | 41 |
| 31 | Locations of in-plane Carlson strain gages in transverse plane in Test Wall | 42 |
| 32 | Locations of longitudinal Carlson strain gages in transverse plane in Test Wall | 43 |
| 33a | Measured temperatures along vertical centerline of lift 5 in Test Wall | 44 |

| | | |
|-----|--|----|
| 33b | Measured temperatures across width of lift 5 in Test Wall | 44 |
| 33c | Measured temperatures along vertical centerline of lift 6 in Test Wall | 45 |
| 34a | Measured strains along vertical centerline of lift 5 in Test Wall due to thermal gradient in Figure 33a | 46 |
| 34b | Measured strains across width of lift 5 in Test Wall due to thermal gradient in Figure 33b | 46 |
| 34c | Measured strains along vertical centerline of lift 6 in Test Wall due to thermal gradient in Figure 33c | 47 |
| 35 | Finite element model for the very coarse grid "W-model" | 49 |
| 36 | Finite element model for the coarse grid "C-model" | 50 |
| 37 | Finite element model for the medium grid "M-model" | 51 |
| 38 | Finite element model for the fine grid "F-model" | 52 |
| 39 | Ambient air temperature curves used in Test Wall analyses | 54 |
| 40 | Actual resultant daily wind velocities during construction of Test Wall lifts 4-6 | 56 |
| 41 | Adiabatic temperature rise curves of concrete for Test Wall | 63 |
| 42 | Predicted temperatures versus element size for time step of 0.125 days | 68 |
| 43 | Predicted temperatures versus element size for time step of 0.25 days | 69 |
| 44 | Predicted temperatures versus element size for time step of 0.50 days | 70 |
| 45 | Horizontal temperature gradients versus element size at 0.25 days after placement of lift 5 | 72 |
| 46 | Horizontal temperature gradients versus element size at 0.50 days after placement of lift 5 | 73 |
| 47 | Horizontal temperature gradients versus element size at 1.0 days after placement of lift 5 | 74 |
| 48 | Predicted temperatures versus time step length in W-model | 76 |
| 49 | Predicted temperatures versus time step length in C-model | 77 |
| 50 | Predicted temperatures versus time step length in M- and F-models | 78 |
| 51 | Predicted temperatures versus element size with actual daily air temperatures | 79 |
| 52 | Predicted temperatures versus time step length in F-Model with actual daily air temperatures | 81 |
| 53 | Measured and predicted temperatures at the center and vertical surface of lift 5 with mean daily and actual daily air temperatures | 82 |
| 54 | Measured and predicted temperatures in insulated lift 6 with actual daily air temperatures | 84 |
| 55 | Comparison of predicted surface temperatures with variation in measured surface temperatures in insulated lift 6 | 86 |
| 56 | Measured temperatures at lift 5/lift 6 interface before and after placing lift 6 | 88 |

CONVERSION FACTORS, NON-SI TO SI (METRIC)
UNITS OF MEASUREMENT

Non-SI units of measurement used in this report can be converted to SI (metric) units as follows:

| <u>Multiply</u> | <u>By</u> | <u>To Obtain</u> |
|---|-------------|-------------------------------|
| Btu (International Table) per pound (mass) × degree Fahrenheit | 4,186.8 | joules per kilogram kelvin |
| Btu (International Table) × feet per hour × square foot × degree Fahrenheit | 1.73073 | watts per metre kelvin |
| Btu (International Table) × inch per day × square inch × degree Fahrenheit | 3.46146 | watts per metre kelvin |
| Btu (International Table) per hour × square foot × degree Fahrenheit | 5.67826 | watts per square metre kelvin |
| Btu (International Table) per day × square foot × degree Fahrenheit | 0.946377 | watts per square metre kelvin |
| Calories per gram | 4.184 | Kilojoules per kilogram |
| Fahrenheit degrees | 5/9 | Celsius degrees or kelvins* |
| feet | 0.3048 | metres |
| inches | 25.4 | millimetres |
| miles per hour (US Statute) | 1.609347 | kilometres per hour |
| pounds (force) per square inch | 0.006894757 | megapascals |
| pounds (mass) per cubic inch | 27,679.899 | kilograms per cubic metre |
| pounds (mass) per cubic foot | 16.01846 | kilograms per cubic metre |

* To obtain Celsius (C) temperature readings from Fahrenheit (F) readings, use the following formula: $C = (5/9)(F - 32)$. To obtain kelvin (K) readings, use $K = (5/9)(F - 32) + 273.15$.

Evaluation of Parameters Affecting Thermal Stresses
In Mass Concrete

PART I: INTRODUCTION

Background

1. In support of the St. Louis District, U.S. Army Corps of Engineers, personnel of the Waterways Experiment Station (WES) conducted a series of nonlinear finite-element thermal stress analyses for selected monoliths of Melvin Price Locks and Dam (MPL&D)(1)*. Several two-and three-dimensional grids were developed and verified for monoliths L13 (Figure 1) and L17 (Figure 2). Two-dimensional thermal stress analyses were performed for monoliths L13 and L17. A modern general purpose heat transfer and structural analysis code (ABAQUS) and a 2D code (WES2D), used in many previous thermal studies at WES, were used to perform these analyses.

2. A very important feature of this work was that for the first time a deliberate effort was made to perform complete incremental construction analyses of a complex mass concrete structure with a modern state-of-the-art analysis procedure. The basic approach taken in the study was to use verified material formulations and analysis procedures, assess predicted results, and define areas for refinement in the analysis. After reviewing the literature and assessing the state of current practice in the analysis of mass concrete construction, a number of parameters were identified as critical in terms of having potentially significant effects on final stresses, structural displacements, and distributions of loads. These parameters include:

- a. The incremental construction formulation.
- b. Concrete aging (i.e. compressive strength, tensile strength, elastic modulus, etc.)
- c. Creep/stress relaxation.
- d. Shrinkage.
- e. Cracking.

* Numbers in parenthesis refer to references at the end of this report.

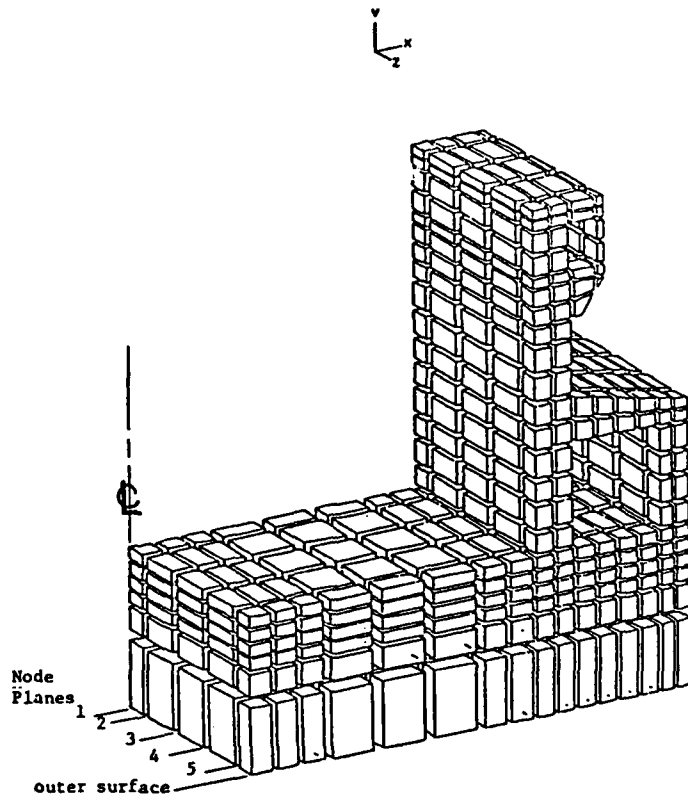


Figure 1. Three-dimensional finite element grid for monolith L13.

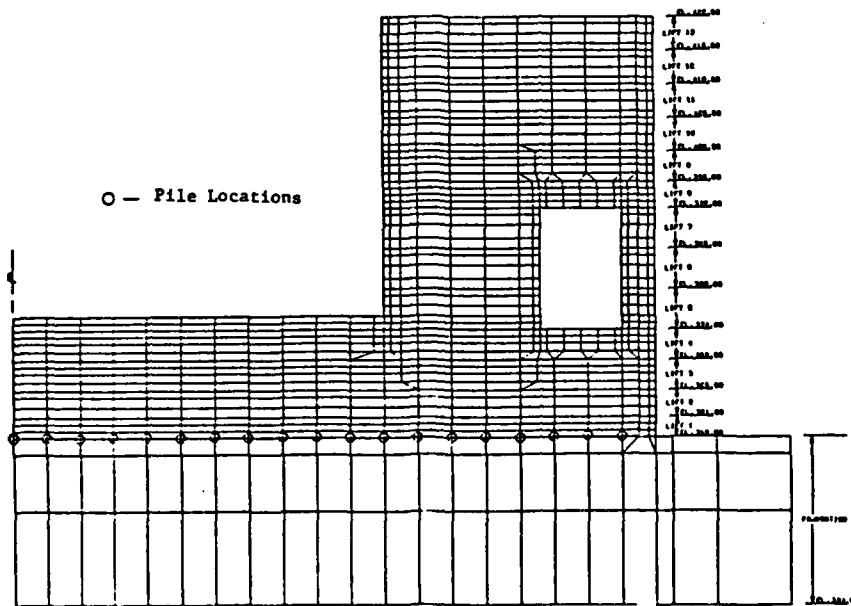


Figure 2. Two-dimensional finite element grid for monolith L17.

- f. Mesh size.
- g. Boundary conditions.

3. In preliminary assessments of the above parameters, an important observation was made which is relevant to essentially the entire list. Test results defining time variations of creep functions, shrinkage, modulus, etc., for early time (i.e. 1 to 7 days) were seen to have a significant effect on predicted stresses and displacements for early and later times. This observation can be justified by comparing specific strains for age at loading of one day versus age at loading of seven days (Figure 3). It can be seen in Figure 3 that creep strains are much greater at one-day loading versus seven-day loading. Early age shrinkage (Figure 4)* and change in modulus (Figure 5) are also seen to be quite significant. When various combinations of these parameters are included in a finite element analysis of a generic two-dimensional concrete placement problem, as shown in Figure 6, the relative effects of different parameters can be evaluated. For this particular problem, when all effects (i.e. aging, creep, and shrinkage) were included in the analysis, the concrete cracked at about 2.5 days, which is what was observed in the actual structure. From the observations made in this section, it is obvious that many parameters significantly affect stresses developed in mass concrete structures.

Objectives

4. The objectives of this research program were to:
- a. Define parameters which have a significant effect on stresses developed in mass concrete structures.
 - b. Evaluate the effects of variations in these parameters based on analysis of mass concrete structures and structural components.
 - c. Define and conduct critical material properties tests to calibrate, refine and verify the analysis procedure.
 - d. Develop design aids which can be used by analysts and designers of mass concrete structures to better define appropriate analysis parameters, material properties and boundary conditions.

* A table of factors for converting non-SI units of measurement to SI (metric) is presented on page vii.

TOTAL UNIAXIAL SPECIFIC STRAIN

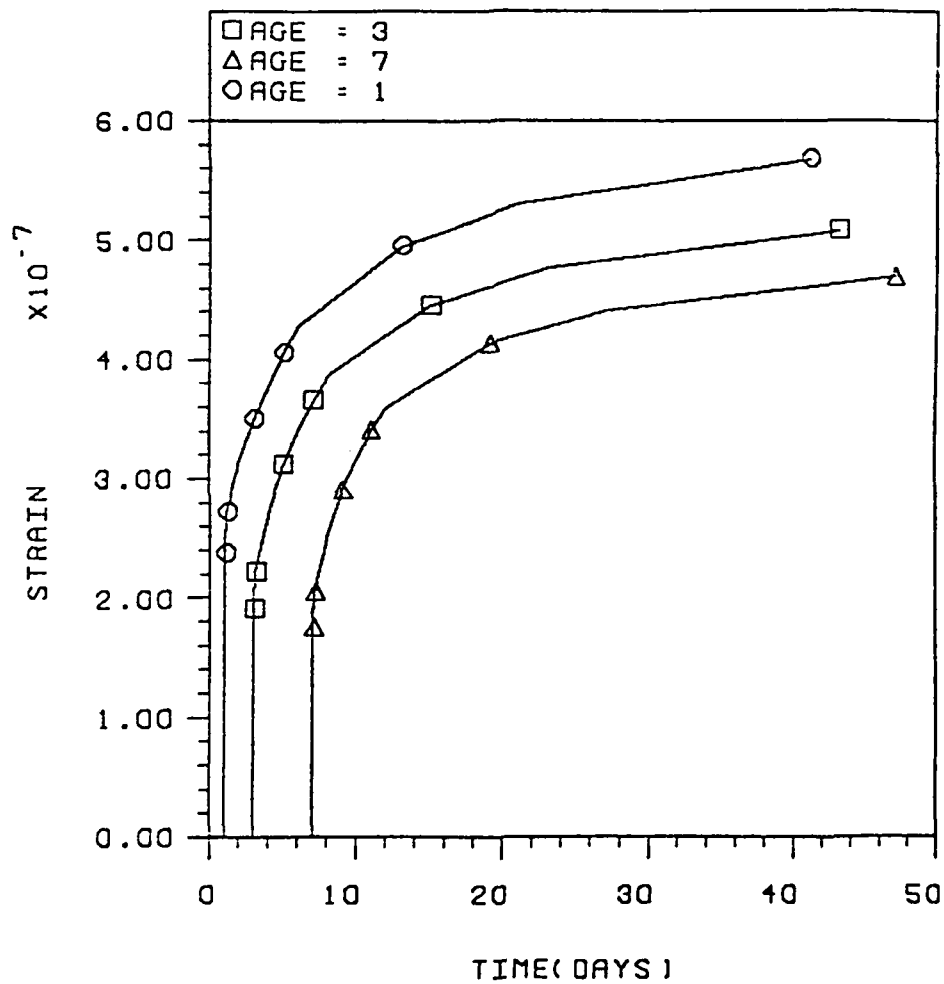


Figure 3. Specific creep predictions for early time loading of a silica-fume concrete, ABAQUS with aging, creep model.

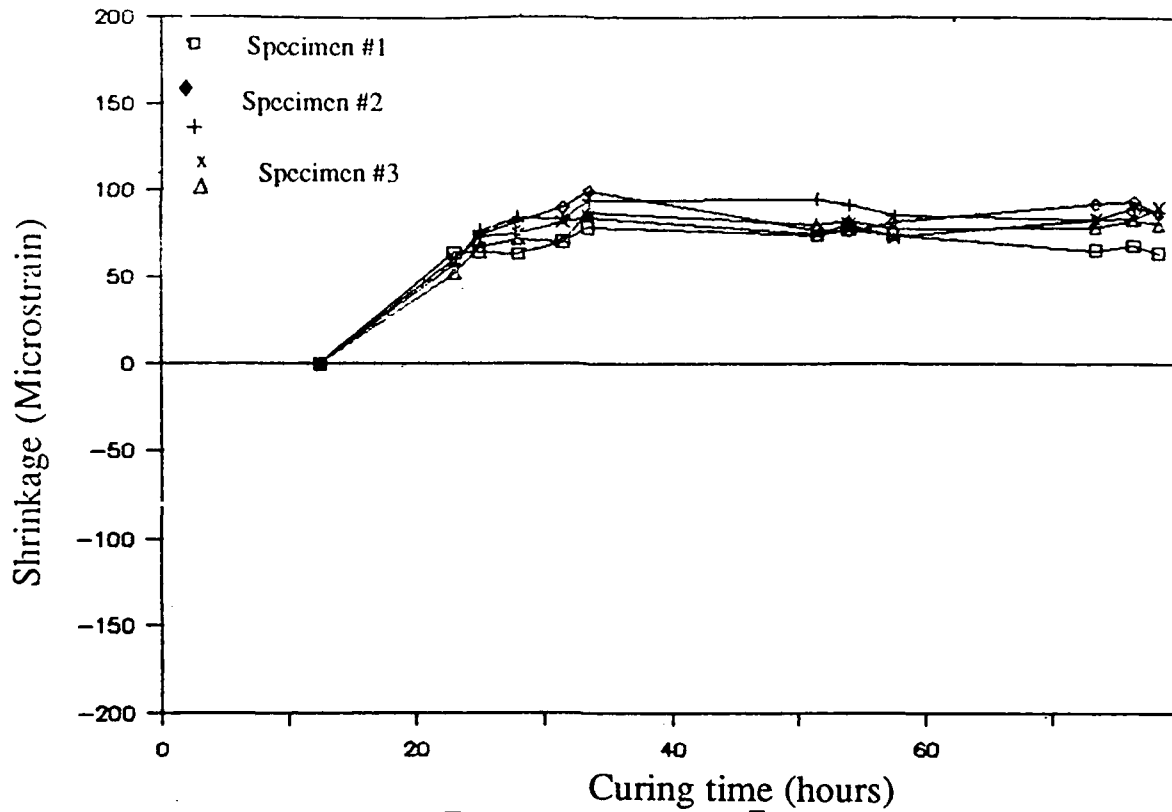


Figure 4. Shrinkage measurements showing significant increase at early ages, $f'c = 3000$ psi.

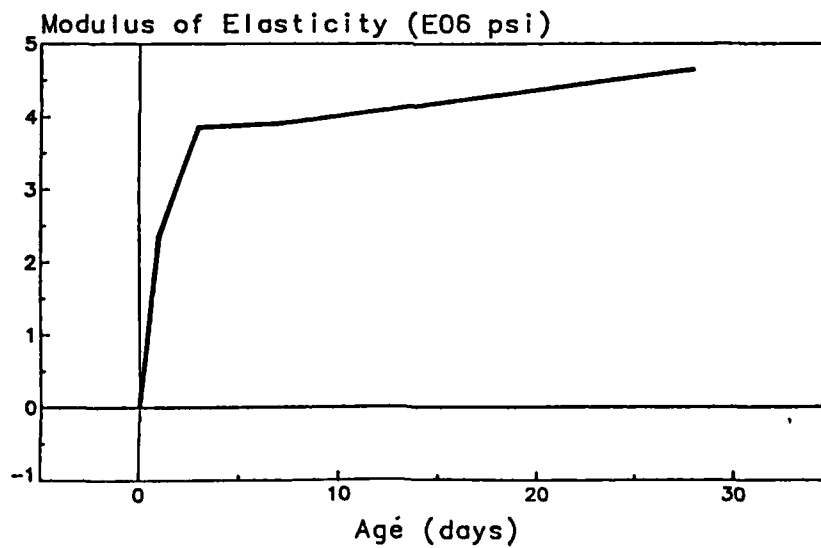


Figure 5. Elastic modulus showing significant increase at early ages, $f'c = 3000$ psi.

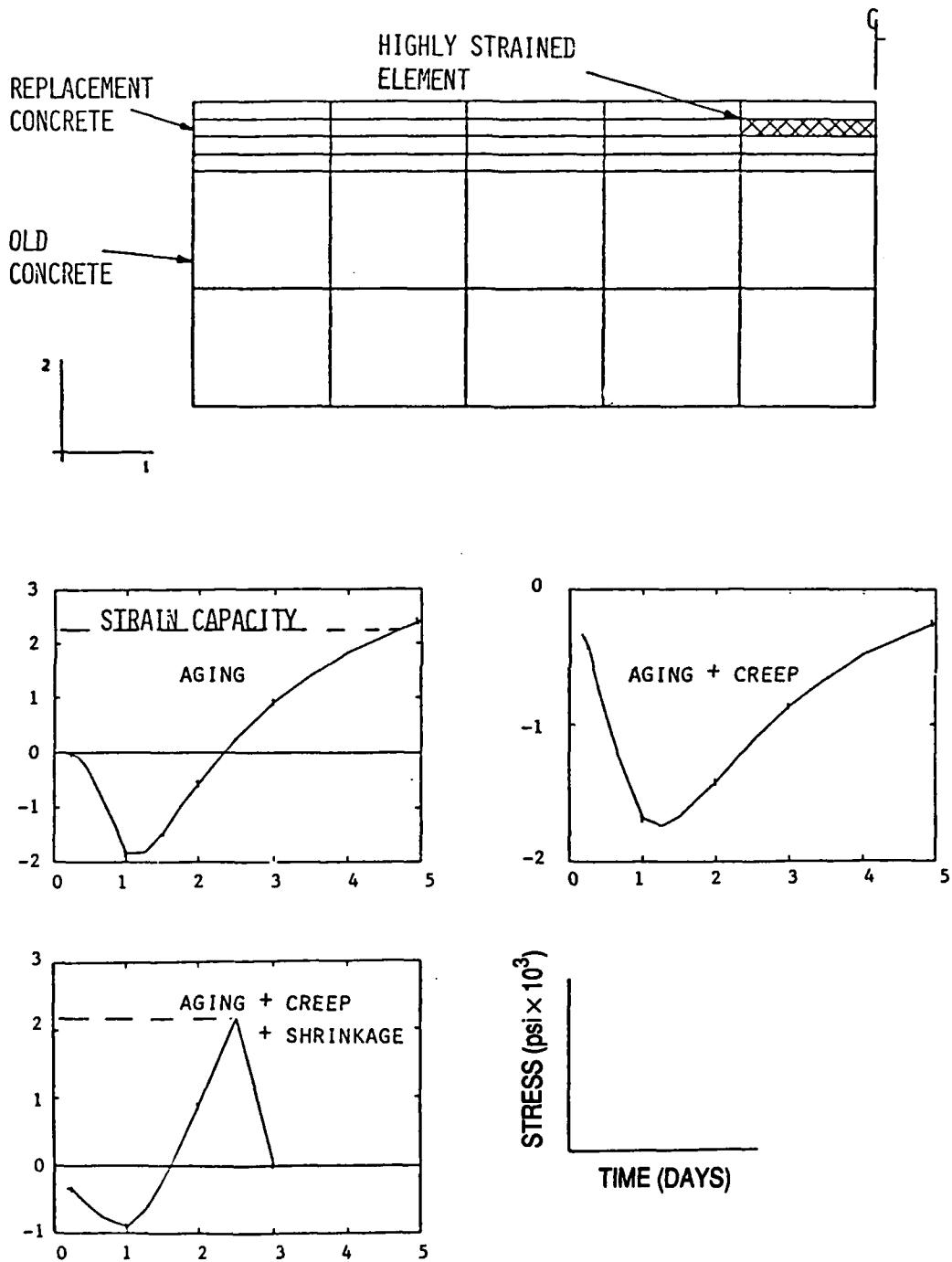


Figure 6. Effects of including aging, creep, and shrinkage effects in the finite-element analysis of a generic mass concrete placement problem (ABAQUS).

Scope

5. In order to accomplish the objectives of this research program, a cooperative effort among Corps District Offices, Government research laboratories, and universities was conducted. Analysis work supporting this program was performed at different agencies but all used the most current version of CTD's 2D aging, creep model with cracking capabilities in the ABAQUS finite-element code.

6. Critical parameters are determined based on the results of tests and finite-element analysis of typical mass concrete structures and structural components such as the model lock-wall monolith shown in Figure 7. This rather large model structure was incrementally constructed at CTD in a related research program and contains over 100 channels of instrumentation, including temperature and thermal strain measurements. Results from other smaller structural component tests at CTD, as well as pertinent tests at other laboratories, universities and field experiences, will be used to carefully define critical parameters, calibrate and verify the analysis procedure.

7. After defining the critical parameters, required material properties tests were designed and carefully conducted to refine the constitutive model in ABAQUS. Material properties (e.g. creep, shrinkage, and modulus of elasticity as functions of age) will be calibrated, refined, and verified within the code by actually conducting analysis of specific tests such as the early time creep test shown in Figure 8.

8. After the material model was refined and verified, a detailed evaluation of critical parameters was conducted by carefully analyzing typical structures as previously discussed. Also the effects of parameter variation on distribution of pile forces was studied by analyzing mass concrete structures with slab and wall components of various flexibilities.

9. Efficient mesh characteristics for the analysis of typical structures and components was determined. Effects of various boundary conditions (both thermal and force-displacement) was evaluated.

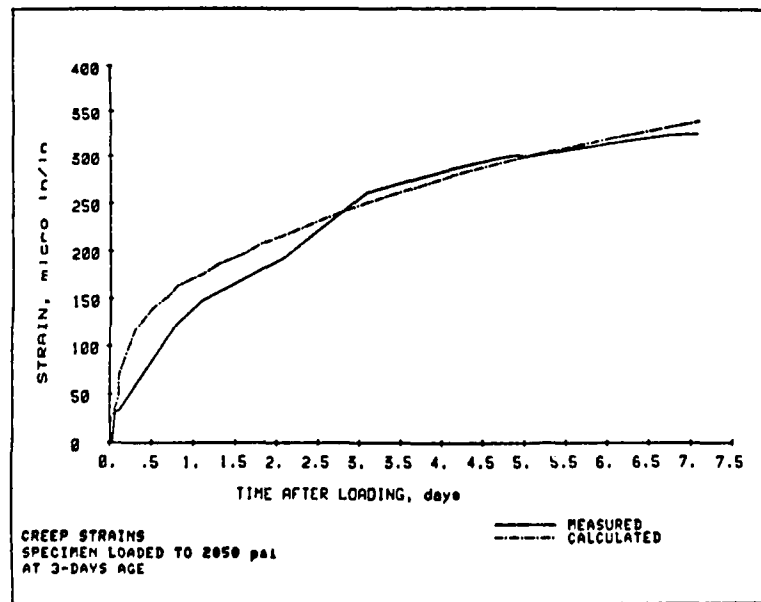
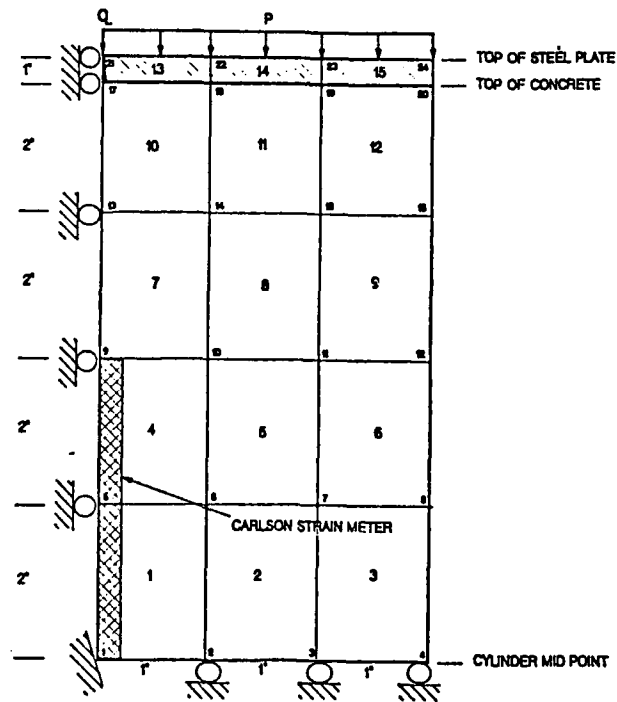


Figure 8. Verification of creep prediction from ABAQUS for a 3-day age at loading test

PART II: ANALYSIS PROCEDURE

Heat Transfer and Structural Analysis

10. As mentioned previously, a well established general-purpose finite-element code was selected for use in analyzing and evaluating the monoliths of MPL&D. ABAQUS, developed by Hibbitt, Karlsson, and Sorensen(2) was the finite-element code selected for this problem based on its flexibility, and demonstrated effectiveness which are discussed in detail in Reference 1. A wide variety of constitutive models is provided in ABAQUS, and these models can be used essentially with any element type. User-defined material models are incorporated with relative ease through the UMAT subroutine. Also, reinforcement can be added to any element. Static and dynamic response in stress analysis can be conducted as well as steady-state and transient heat transfer problems. Incremental construction problems can be simulated effectively through the "model change" option where previously defined elements can be included or removed from the analysis in a specified solution step.

Aging Creep Model with Cracking

11. The fact that the material properties of concrete change with time (aging) presents special computational problems for the thermal stress analysis of mass concrete structures. Significant changes in material strength, modulus, creep, shrinkage, etc. must be accounted for in a consistent and numerically efficient manner in the finite-element solution procedure. This is accomplished through the two-dimensional (2-D) aging creep model with cracking capabilities in the ABAQUS-UMAT subroutine format. In this model, cracking in the xy (or rz) plane and normal to the θ direction for axisymmetric problems is included. The model also includes the effects of time-dependent change in properties on the elastic modulus and cracking strength and the effects of changing temperatures on the creep compliance, the elastic modulus, and the ultimate/cracking strength. The elastic modulus and ultimate strength can be expressed as functions of age (t) and temperature (T) as $E(t,T)$ and $\sigma_u(t,T)$, respectively. The cracking strain (ϵ_f), if not user defined, is assumed to be 10 percent of the absolute value of the compressive

strain at ultimate strength. Poisson's ratio (ν) is assumed to be constant. The creep properties, Equation 1 and the properties $E(t,T)$, $\sigma_u(t,T)$, ϵ_f , and ν are included in a separate subroutine in a form which can be easily modified by the user. The numerical values of the model parameters, namely those describing Equation 1, and the other mechanical properties are supplied by the user. Further details of the mathematical description of the model are presented by Rashid and Dunham⁽³⁾. Creep properties are given in the form

$$J(t, \tau, T) = \sum_{i=1}^2 A_i(\tau, T) \left[1 - e^{-r_i(t-\tau)} \right] + D(\tau, T)(t - \tau) \quad (1)$$

$$A_i(\tau, T) = A_{oi} e^{-Q/RT} \left[\frac{E(3)}{E(\tau)} \right]^2$$

$$D(\tau, T) = D_o e^{-Q/RT} \left[\frac{E(3)}{E(\tau)} \right]^2$$

where

J = creep strain per unit stress

t = time

τ = age at loading

T = temperature

R = gas constant

$E(\tau)$ = modulus of elasticity at time τ

r_i, A_i, D, Q = material constants

The material constants are calibrated so that J best represents the specific creep of a particular concrete during a specified time frame of interest. The effect of aging is accounted for in the term $E(3)/E(\tau)$ and will be discussed later. Temperature effects are simulated through the activation energy term $e^{-Q/RT}$, where Q is best evaluated through creep tests at different temperatures, in which $J(t, \tau, \text{ and } T_i)$ can be measured and set equal to e^{-Q/RT_i} for the two values of T_i at fixed t and τ .

12. Similar approaches are used to determine the elastic modulus as a function of time and shrinkage as a function of time. The functional form for

$E(\tau)$, where τ is concrete age in days, is

$$E(\tau) = E_0 + B_1 \left[1 - e^{-m_1(\tau-1)} \right] + B_2 \left[1 - e^{-m_2(\tau-1)} \right] + B_3 (\tau-1)$$

where E_0 is one-day modulus and constants B_1 , B_2 , and B_3 are determined based on tests at 3 days of interest. Shrinkage is determined from

$$\epsilon^s = C_1(1 - e^{-s_1 t}) + C_2(1 - e^{-s_2 t})$$

where S_1 and S_2 are selected as in the previous forms so that shrinkage becomes negligible after some time. Then C_1 and C_2 are determined from early-time and late-time sealed shrinkage tests. These tests primarily measure autogenous shrinkage (shrinkage that occurs without a loss of moisture). Most shrinkage that occurs in mass concrete structures is of this type, since only the exterior faces are subject to drying.

13. A smeared crack model is used in conjunction with a cracking criterion. This criterion consist of the following elements: (a) it is strain driven but is modified by the stress; (b) the crack surface normal is in the direction of the principal strain; and (c) the cracking criterion is interactive. Details of the smeared crack model and its implementation in the code are presented in (3).

PART III. MATERIAL MODEL CALIBRATION

Details of Model Calibration

14. The concrete heat generation and material models used in the MPL&D analyses were implemented in ABAQUS through user subroutines. These are user-supplied models, usually in the form of Fortran subroutines, which can be linked to the ABAQUS main library. Two user subroutines must be implemented in order to model the behavior of mass concrete: DFLUX and UMAT. Subroutine DFLUX is used to supply the adiabatic temperature rise curve for the concrete mixture. This is the increase in temperature due to hydration when no heat loss occurs (i.e., all boundaries are adiabatic). This subroutine converts adiabatic temperature rise to heat generation rates for use in finite-element heat transfer analyses in which general radiation and convection boundary conditions are incorporated. The UMAT subroutine contains the material model, a visco-plastic formulation which accounts for the effects of aging, creep, shrinkage, and cracking.

15. The adiabatic temperature rise curve used for the analyses reported herein was the original curve used for the MPL&D study done previously by WES (1). This curve was for a Type II cement with 7-day heat of hydration of 70 calories/gram. However, more recent heat of hydration tests on cement for MPL&D yielded 7-day heats of hydration varying from 55 calories/gram to 70 calories/gram. To provide for this range of values, the curve was factored for the lower heat of hydration and both curves were included in the DFLUX subroutine as bounding conditions. The adiabatic temperature rise curves are shown in Figure 9.

16. The material model was calibrated by fitting three internal curves to test data:

- a. Elastic modulus versus time
- b. Specific creep versus time for concrete loaded at 3 days of age
- c. Autogenous shrinkage versus time.

All curves are based on a temperature of 70 degrees Fahrenheit.

17. Three terms that may require clarification are creep, specific creep (or creep compliance) and autogenous shrinkage. Creep is defined by the American Concrete Institute (ACI) Committee 209(4) as "The time-dependent

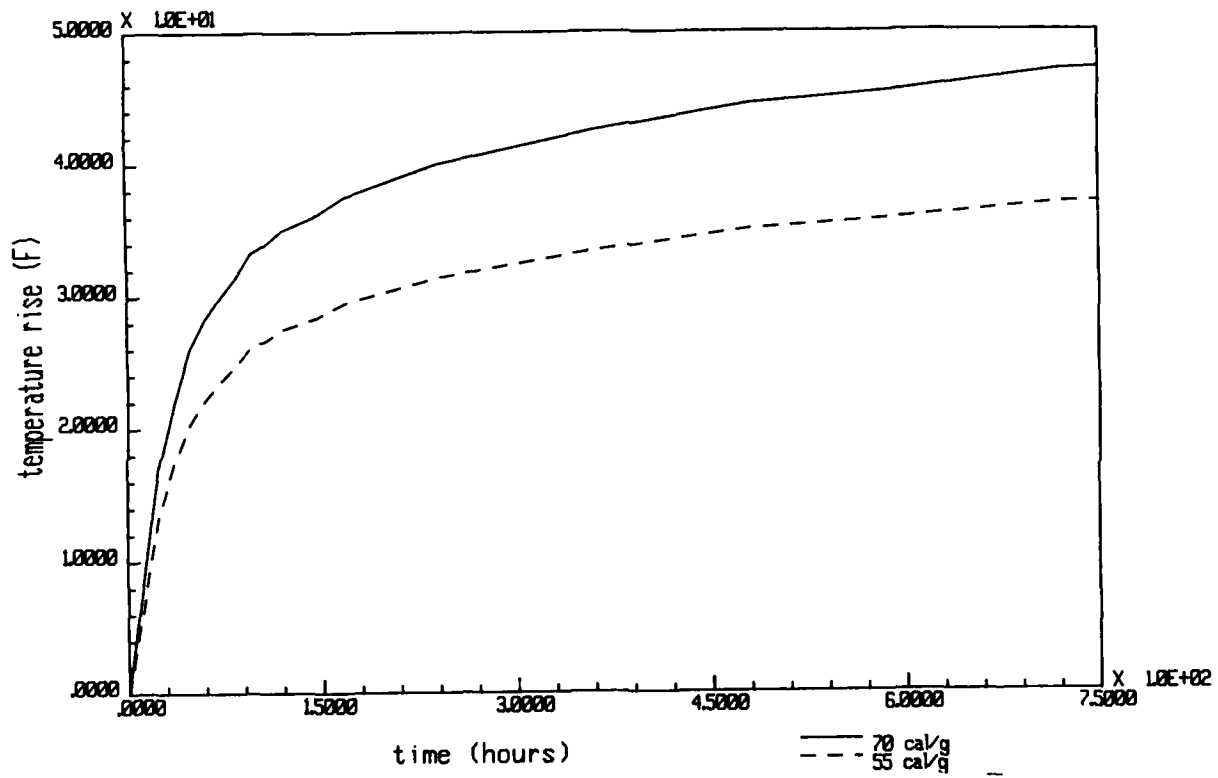


Figure 9. Bounding adiabatic temperature rise curves

increase of strain in hardened concrete subjected to sustained stress. It is obtained by subtracting from the total measured strain in a loaded specimen, the sum of the initial instantaneous (usually considered elastic) strain due to the sustained stress, the shrinkage, and the eventual thermal strain in an identical load-free specimen which is subjected to the same history of relative humidity and temperature conditions." This definition assumes that strain in a loaded specimen consists of an initial elastic strain, creep strain, shrinkage and thermal expansion or contraction. In a mass concrete structure, however, stresses and moduli are constantly changing throughout the structure and construction period, and initial elastic strain has little meaning. Calibration of the material model must be based on time-dependent modulus and creep. Creep compliance is determined from a plot of specific strain (strain per unit stress) versus time from a three-day creep test and is the difference between the total specific strain and the elastic specific strain. The relationship between total specific strain $J(t)$, creep compliance $(C(t))$ and elastic specific strain $(1/E(t))$ is shown in Figure 10.

18. The ACI (4) also defines shrinkage as "the decrease with time of concrete volume. The decrease is due to changes in the moisture content of the concrete and physico-chemical changes, which occur without stress attributable to actions external to the concrete." Shrinkage due to moisture loss, or drying shrinkage, only occurs at the surface of mass concrete structures and is not simulated in the material model. However, additional volumetric changes occur during hydration of the cement that are not directly attributable to changes in temperature. In this report, the term autogenous shrinkage refers to these volumetric changes.

19. An exponential equation with two or more terms fit to selected test data points has been found to provide an adequate fit to test data for various concrete mixtures (5), and this form was implemented in the material model for all three curves.

20. From time of setting to 1 day, the elastic modulus is assumed to be linear. For times later than 1 day, the elastic modulus is determined by the following equation:

$$E(t) = A(1 - e^{(r_1 t)}) + B(1 - e^{(r_2 t)}) + C(t - 1) + E(1) \quad (2)$$

where t is concrete age in days and $E(t)$ is modulus at age t and r_1 , r_2 , A , B and C are constants.

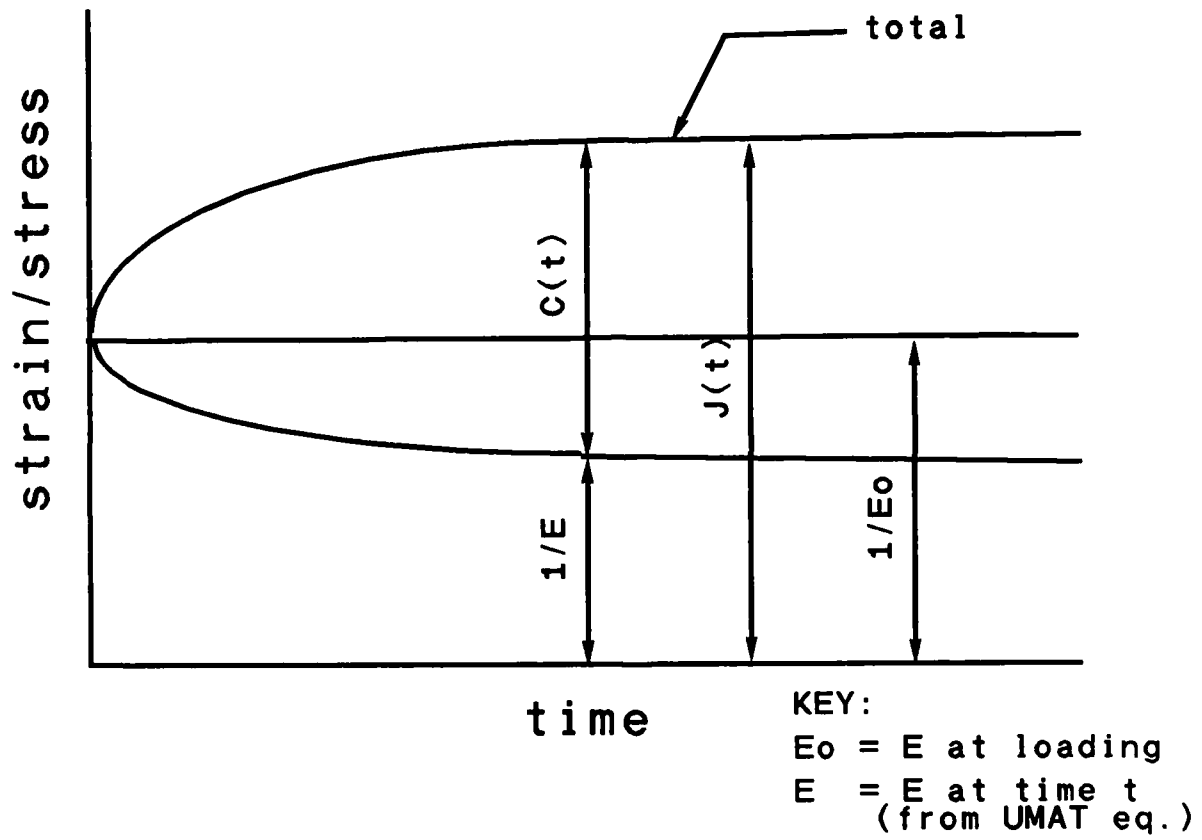


Figure 10. UMAT specific strains vs time

21. The formula for specific creep is defined by a similar equation.

$$C(t) = D(1 - e^{-x_1 t}) + F(1 - e^{-x_2 t}) + G(t) \quad (3)$$

where $C(t)$ is the creep strain per unit stress, t is time after loading, and x_1 , x_2 , D , F and G are constants.

22. The formula for autogenous shrinkage is similarly defined by

$$S(t) = H(1 - e^{-u_1 t}) + K(1 - e^{-u_2 t}) \quad (4)$$

where $S(t)$ is the shrinkage strain at age t and u_1 , u_2 , H and K are constants.

23. In order to determine the parameters required for calibration of the model, an extensive test program was undertaken. Modulus and creep tests for MPL&D mixture C2-2 (with 1-1/2-in. nominal maximum aggregate) were performed at WES, and autogenous shrinkage tests for MPL&D mixtures C2-2 and C3-3 (with 3-in. nominal maximum aggregate) were performed at the University of Michigan under contract to WES. Proportions for mixtures C2-2 and C3-3 are given in Table 1.

Table 1

Concrete Mixture Proportions for Melvin Price Lock and Dam Mixtures

| <u>Material</u> | <u>Batch Weight, lb / cu yd</u> | |
|--------------------|---------------------------------|---------------------|
| | <u>Mixture C2-2</u> | <u>Mixture C3-3</u> |
| Cement | 245 | 231 |
| Type "F" flyash | 82 | 77 |
| Sand | 1298 | 1196 |
| 3/4-in aggregate | 1182 | 825 |
| 1-1/2-in aggregate | 971 | 615 |
| Water | 186 | 175 |

Initial Model Calibration

24. To allow preliminary calculations prior to the completion of the testing, an initial calibration was performed based on existing test data for similar concrete mixtures and on predictions from the following models:

- a. The model of ACI Committee 209 (4) and
- b. Bazant and Wittmann's (6) simplified model for creep and shrinkage.

25. The ACI equation for modulus of elasticity is

$$E_c = 33 w^{1.5} \sqrt{f'_c} \quad (5)$$

where E is modulus of elasticity in psi, w is specific weight in pcf and f'_c is compressive strength in psi.

26. Compressive strength at any age can be predicted using the following equation (4):

$$f'_c(t) = \frac{t}{a + bt} (f'_{c,28}) \quad (6)$$

where t is time in days, $f'_{c,28}$ is at 28 days, and a and b are 4.0 and 0.85 respectively for Type I cement. These constants were not available for Type II cement.

27. However, compressive strength test data for mixture C2-2 at 1, 7, 28, and 90 days was available and is given in Table 2. Compressive strength calculated according to equation 6 is also given for comparison. The data show that coefficients in equation 6 need to be fitted for Type II cements.

Table 2
Compressive Strength Test Results for Melvin Price Lock and Dam Mixture C2-2

| <u>Concrete Age (days)</u> | <u>Compressive Strength (psi)</u> | <u>Eq. 6 Results (psi)</u> |
|--------------------------------|---------------------------------------|--------------------------------|
| 1 | 690 | 485 |
| 7 | 1,380 | 1,653 |
| 28 | 2,350 | |
| 90 | 3,450 | 2,627 |

28. According to Bazant, the conventional elastic modulus may be calculated as

$$E(t') = \frac{E_0}{1 + \phi'_1(t'^{-m} + \alpha)} \quad (7)$$

where

$$\phi'_1 = 10^{-3n} \phi_1$$

$$n = 1/8$$

$$m = 1/3$$

$$\alpha = 0.05$$

$$\phi_1 = 3 \text{ to } 6 \text{ and}$$

$$E_0 = 1.5(E_{28})$$

29. In addition, moduli from three similar mixtures were compared with predicted results from the ACI and Bazant equations. The three mixtures were

Dworshak Dam mixture II (7), Portuguese Dam mixture 3, and Tennessee-Tombigbee (Tenn-Tom) Waterway mixture D (8). Proportions for these mixtures are given in Table 3 with proportions for Lock and Dam 26 mixture C2-2 for comparison.

Table 3
Comparison of Mixtures used in Calibrating the UMAT Model

| <u>Material</u> | <u>Batch weight, lb / cu yd</u> | | | |
|--------------------|---------------------------------|-----------------|-------------------|-----------------|
| | <u>MPL&D, C2-2</u> | <u>Dworshak</u> | <u>Portuguese</u> | <u>Tenn-Tom</u> |
| Cement (Type II) | 245.0 | 331.7 | 219.0 | 282.0 |
| Fly ash | 82.0 | 115.2 | 92.0 | |
| Fine aggregate | 1,298.0 | 1,245.0 | 1,097.0 | 848.5 |
| Coarse aggregate | 2,153.0 | 1,972.0 | 2,557.0 | 2,704.2 |
| Water | <u>186.0</u> | <u>265.3</u> | <u>202.0</u> | <u>157.4</u> |
| Total | 3,964.0 | 3,929.2 | 4,169.0 | 3,992.1 |
| Air | 5% | 6% | 4.5% | 3.7% |
| Water-cement ratio | 0.57 | 0.59 | 0.60 | 0.56 |

30. Test moduli for the three mixtures are plotted in Figure 11. Curves for modulus of elasticity as predicted by the ACI and Bazant formulas are compared with Dworshak mixture II test data in Figure 12. The curve labeled Bazant 1 is for $\phi_1=3$, while Bazant 2 is calculated using $\phi_1=6$. As can be seen, the Dworshak data agree fairly well with the ACI formula results and with the Bazant 1 curve.

31. The initial modulus of elasticity curve was based on values predicted using the ACI modulus equation and test f'_c values and is given by Equation 8. A plot of this equation is presented in Figure 13.

$$E(t) = [1.76(1 - e^{-0.06(t-1)}) + 0.0878(1 - e^{-0.8831(t-1)}) + 1.448]10^6 \quad (8)$$

32. The linear term was omitted since no test values for E were obtained for the mixture at times beyond 90 days and a fit to existing data including a linear term gave excessively large modulus values at late times.

33. The ACI formula for creep coefficient at any age (t) is

$$\nu_t = \frac{t^c}{d + t^c} \nu_u \quad (9)$$

where c and d are constants and ν_u is the ultimate ratio of creep to initial strain.

34. ν_u is calculated by multiplying 2.35 by various creep correction factors based on curing method, relative humidity, age at loading and specimen

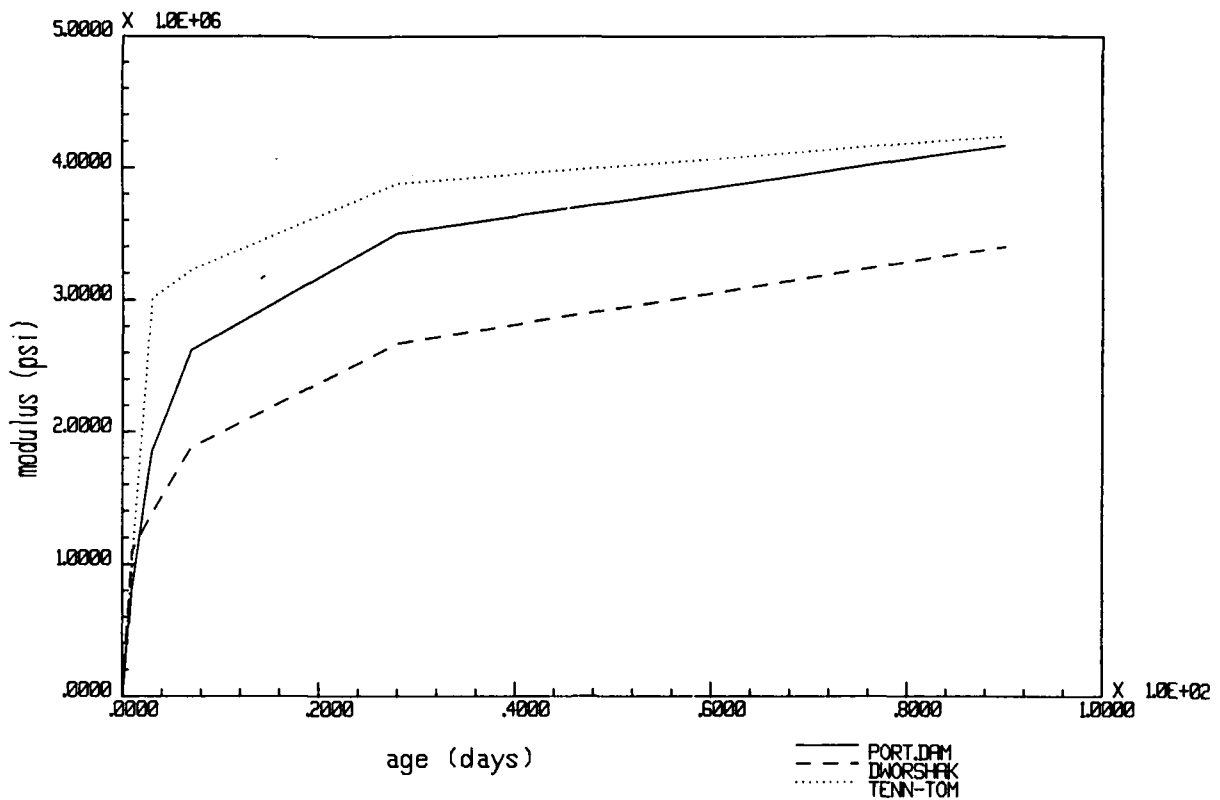


Figure 11. Test modulus curves for the Dworshak Dam, Portuguese Dam and Tenn-Tom mixtures

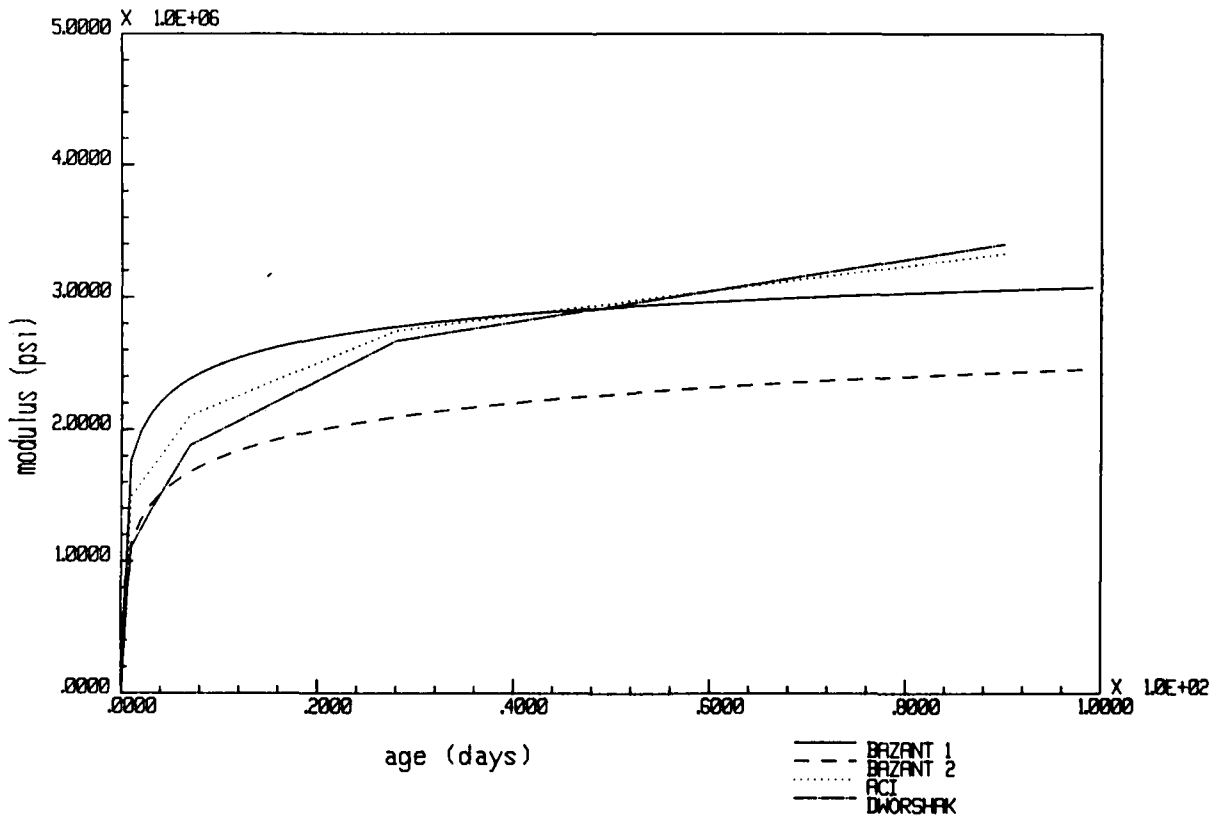


Figure 12. Predicted and test moduli

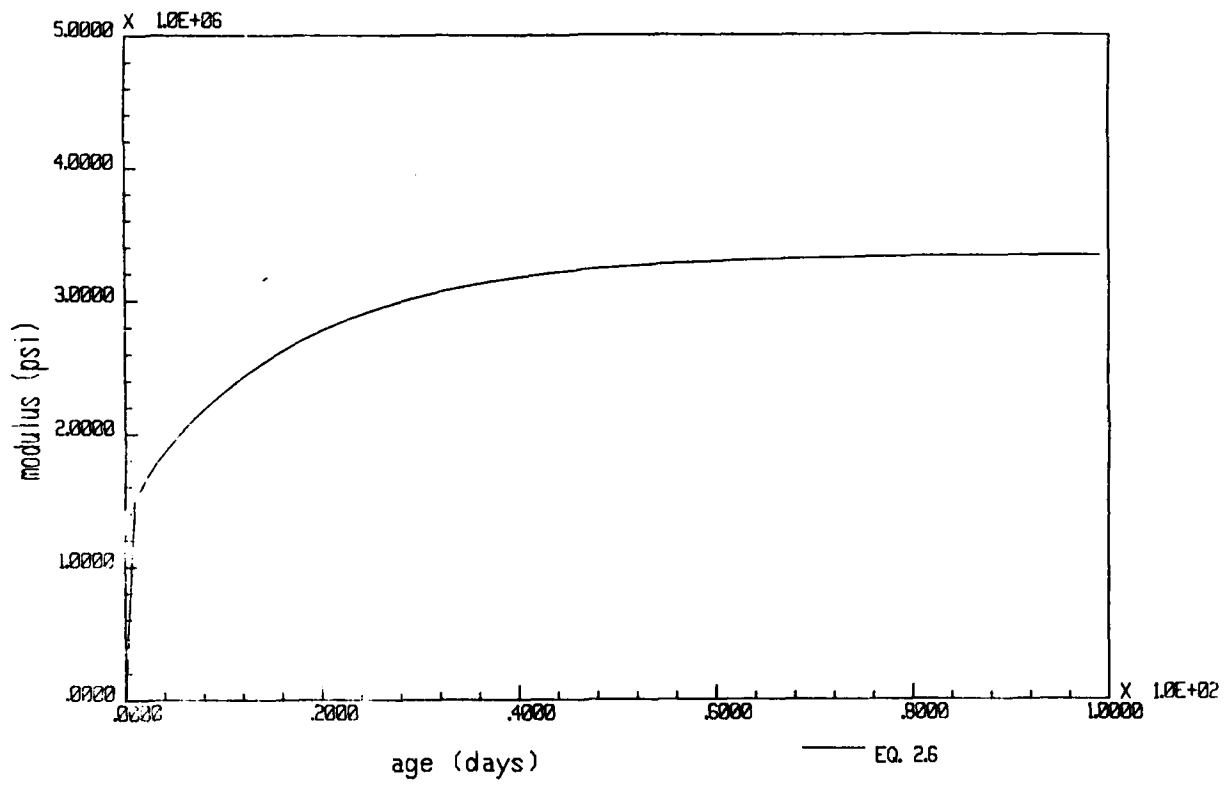


Figure 13. Initial UMAT modulus vs time curve

thickness. For a relative humidity of 50 percent and moist curing, with an age at loading of 3 days (duplicating the creep cylinder tests performed at WES) ν_u equals $2.35 \times 0.935 \times 1.098$ or 2.41. Average suggested values for c and d are 0.60 and 10.0, respectively.

35. To determine specific creep, C_t must then be multiplied by the elastic specific strain at 3 days, $1/E_3$. The modulus at 3 days, E_3 , as calculated from equation 8 is 1.76×10^6 psi.

36. Bazant's creep formula is given by the following equation:

$$J(t, t') = \frac{1}{E_0} + \frac{\phi_1}{E_0} (t'^m + \alpha)(t - t')^n \quad (10)$$

where t' is age at loading in days, t is age in days, and E_0 , m and n are as given previously.

37. Plots of predicted creep strains based on the Bazant and ACI equations are compared with 3-day creep curves for two similar concretes in Figure 14. Twenty-eight day modulus in the Bazant equation was calculated using equation 8.

38. As can be seen in Figure 14, the lower curve calculated using the Bazant equation, the ACI predictions and the Dworshak test results agree fairly well. Therefore, the Dworshak Dam 3-day creep test was selected as an initial approximation for creep strains. The resulting specific creep curve is given by the equation below.

$$C(t) = [0.333(1 - e^{-0.18(t-3)}) + 0.316(1 - e^{-5.3(t-3)}) + 1.76 \times 10^{-3}(t - 3)]10^{-6} \quad (11)$$

This equation is plotted against the Dworshak data in Figure 15.

39. An initial approximation for shrinkage strains was obtained from existing data for sealed creep test control specimens from the WES test lock wall. The resulting equation is given below. A plot of the equation is shown in Figure 16.

$$S(t) = [102.5(1 - e^{-0.15t}) + 72.5(1 - e^{-0.02263t})]10^{-6} \quad (12)$$

Testing

40. All concrete specimens tested at WES were proportioned according to design mixture C2-2, with materials furnished by the St. Louis District. Actual mixture proportions were varied in the field.

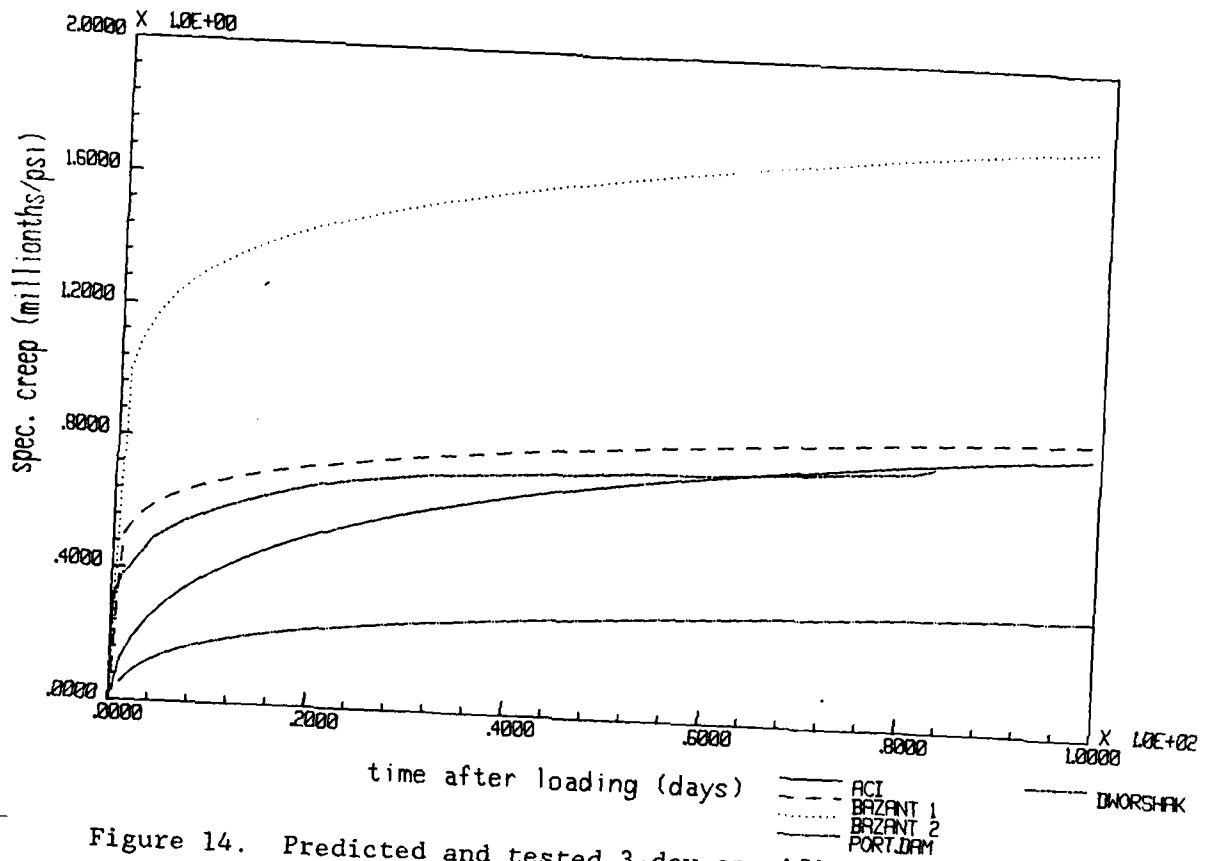


Figure 14. Predicted and tested 3-day specific creep curves

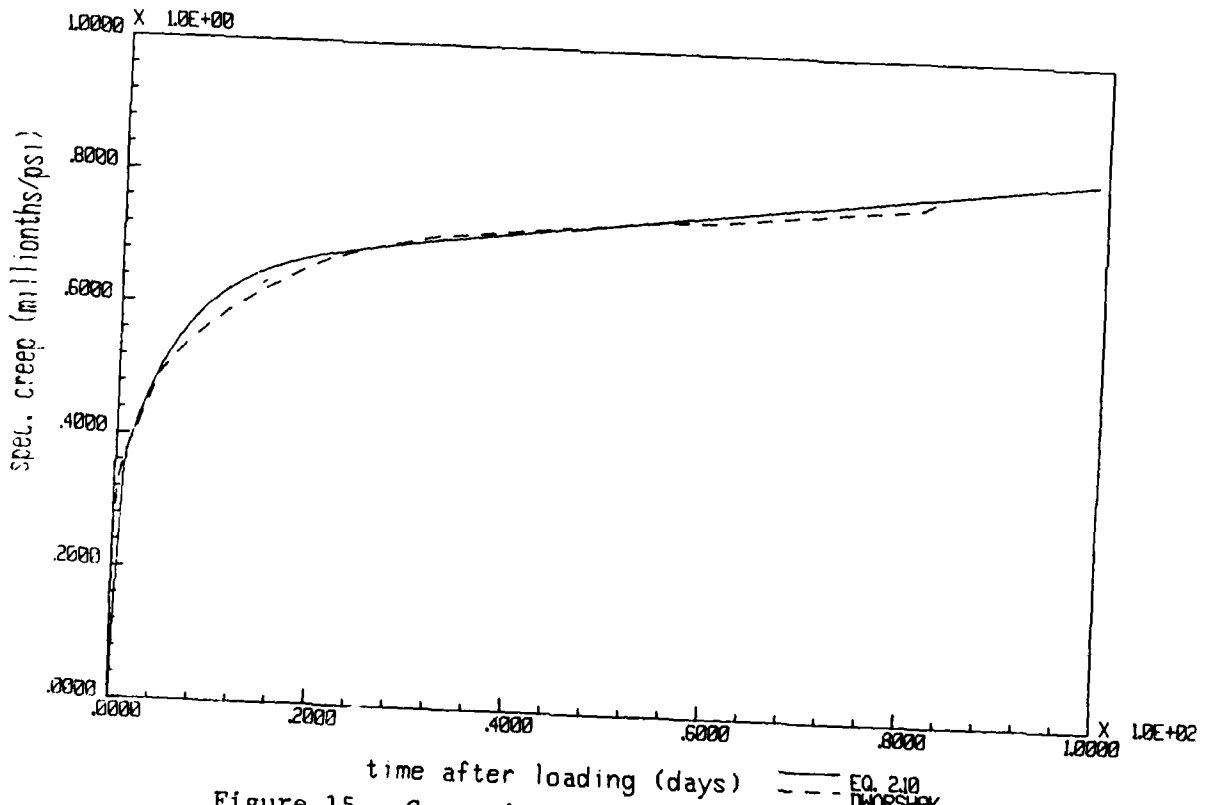


Figure 15. Comparison of UMAT 3-day specific creep curve and Dworshak specific creep

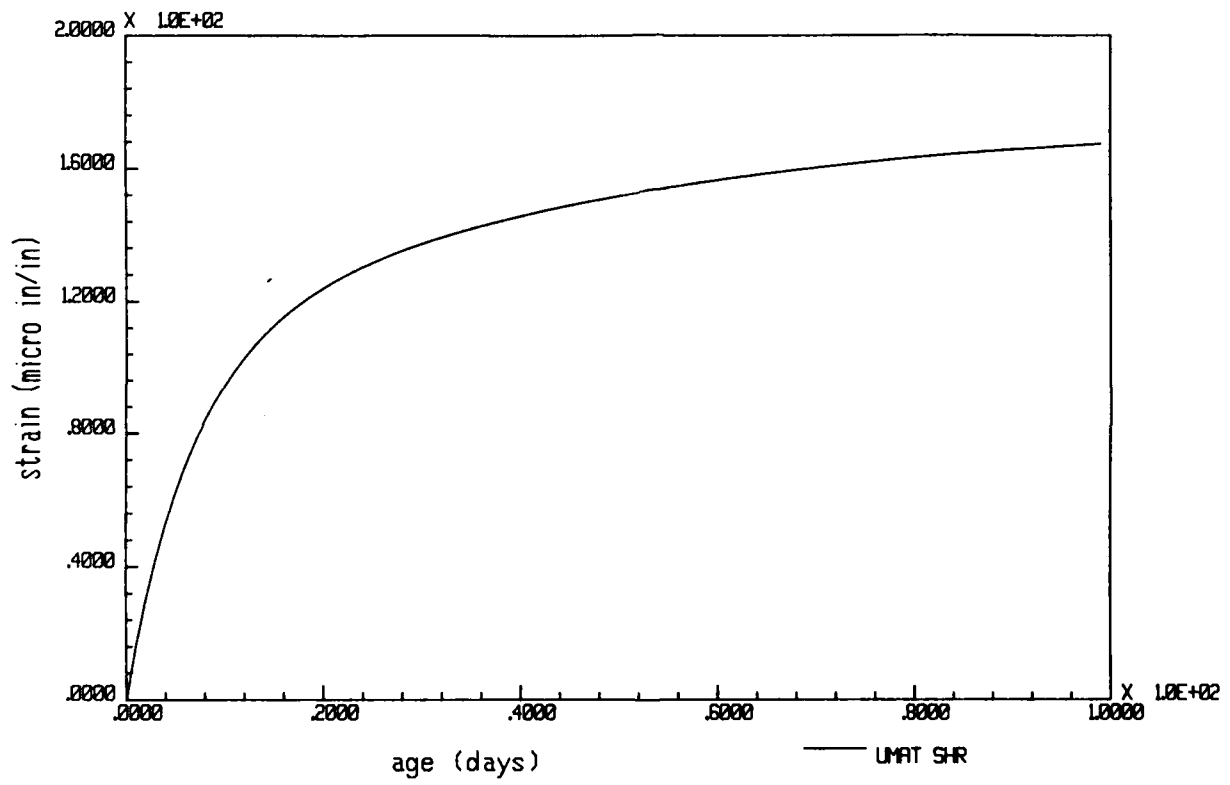


Figure 16. UMAT shrinkage curve

41. Test specimens for determination of creep, compressive strength, and modulus of elasticity were cast as indicated in Table 4. Two series of creep tests were conducted. Series 1 tests consisted of one specimen each loaded at 1, 3 and 7 days and two control specimens. These tests were continued for approximately 6 weeks. Loading was accomplished by means of a hydraulic ram system, and loads were monitored by manually reading Bourdon pressure gages. Series 2 tests were initiated to obtain early-time creep and modulus characteristics for refining the model at a later date. This series of tests consisted of two specimens each loaded at 11.75 hours and 16.75 hours after casting (1.5 and 6.5 hours after time of setting), single specimens loaded at 24 hours and 72 hours and two control specimens. Loading was continued for approximately three weeks. Loads in this series were continuously monitored by in-line pressure transducers in conjunction with a Hewlett-Packard data acquisition system. Since exact stresses were always known, specific creep could be more accurately determined in the second series.

Table 4
Creep and Elastic Modulus Test Specimens

| <u>Specimen Size (in x in)</u> | <u>Number of Specimens</u> | <u>Type of Test</u> | <u>Age at Loading (days)</u> | <u>Creep Test Load (psi)</u> |
|--------------------------------|----------------------------|---------------------|------------------------------|------------------------------|
| 6 x 12 | 2 | Elastic modulus | 1 | - |
| 6 x 12 | 2 | Elastic modulus | 3 | - |
| 6 x 12 | 2 | Elastic modulus | 28 | - |
| 6 x 16 | 1 | Creep - Series 1 | 1 | 135 |
| 6 x 16 | 1 | Creep - Series 1 | 3 | 244 |
| 6 X 16 | 1 | Creep - Series 1 | 7 | 345 |
| 6 x 16 | 2 | Control | - | - |
| 6 x 16 | 2 | Creep - Series 2 | 0.5 | 47 |
| 6 x 16 | 2 | Creep - Series 2 | 0.75 | 103 |
| 6 x 16 | 1 | Creep - Series 2 | 1 | 173 |
| 6 x 16 | 1 | Creep - Series 2 | 3 | 335 |
| 6 x 16 | 2 | Control | - | - |

42. Creep and control specimens were 6-in.-diameter by 16-in.-high cylinders each containing a single Carlson strain meter oriented axially. All creep tests were conducted in a temperature and moisture-controlled room at 70 degrees Fahrenheit and 50 percent relative humidity. Specimens were loaded as

shown in Table 4. Results of 0.5, 0.75, 1 and 3-day creep tests are shown in Figures 17 through 20. Three-day specific creep curves are shown in Figure 21. Note the sudden change in strain in the Series 1: 3-day test (Figure 19). This resulted when the stress was allowed to drop over time and then adjusted to the correct value.

43. Specimens to be tested for modulus of elasticity were 6-in.-diameter by 12-in.-high cylinders. Strains were monitored using external strain gages. Modulus values for concrete at 1, 3, and 7 days of age were calculated from the loading phase of the creep tests. Test results and moduli calculated from creep tests are shown in Table 5.

Table 5

Average Modulus Results from Uniaxial Compressive and Creep Tests

| <u>Age at Loading</u> <u>(days)</u> | <u>Uniax. Comp.</u> <u>Modulus</u> <u>(10⁶ psi)</u> | <u>Series 1</u> <u>Modulus</u> <u>(10⁶ psi)</u> | <u>Series 2</u> <u>Modulus</u> <u>(10⁶ psi)</u> |
|--|--|--|--|
| 0.50 | | | 0.70 |
| 0.75 | | | 1.20 |
| 1.00 | | 2.23 | 1.93 |
| 3.00 | | 2.80 | 3.00 |
| 7.00 | | 3.19 | |
| 28.00 | 2.95 | | |

44. Autogenous shrinkage specimens were prepared at the University of Michigan under the direction of Dr. Will Hansen. Three specimens were prepared for mixture C2-2 and two for mixture C3-3 from materials provided by the St. Louis District. Specimens were 6-in. by 6-in. by 12-in. prisms with steel inserts embedded for attaching dial gages at the center and edge of each specimen. A typical specimen is shown in Figure 22. At approximately 10 to 12 hours forms were removed and specimens were sealed in polyurethane and placed on a 2-in. strip of teflon. Strains were then monitored periodically. Average strains for the two mixtures are shown in Figures 23 and 24.

Final Material Model Calibration

45. The modulus of elasticity curve in the model is used to calculate the aging factor. The aging factor is simply the modulus at time t (from

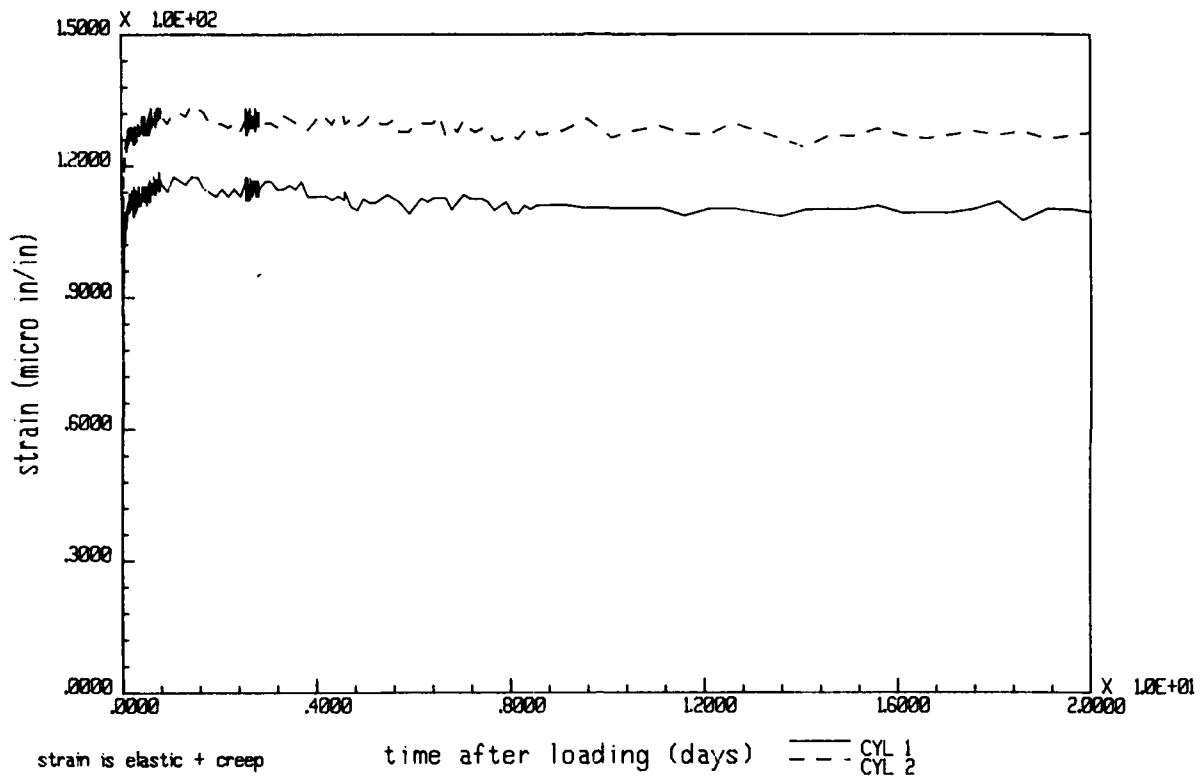


Figure 17. Series 2: 1/2-day creep test strains

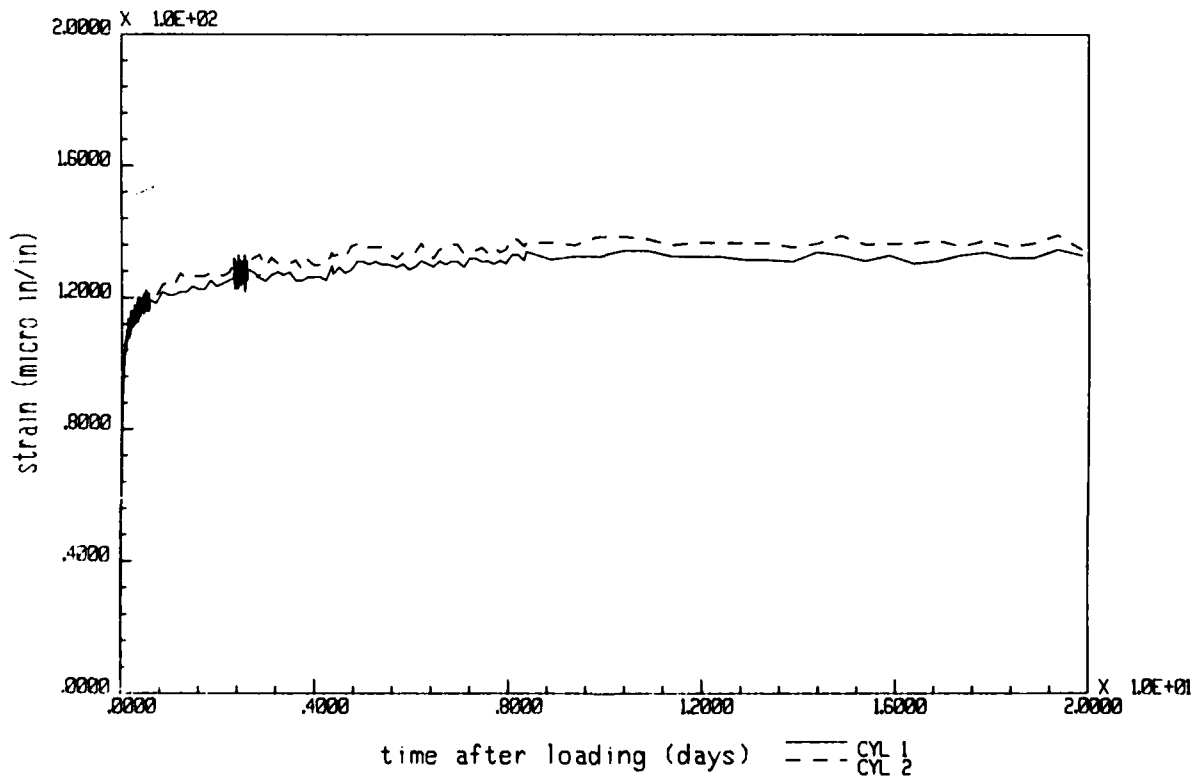


Figure 18. Series 2: 3/4-day creep test strains

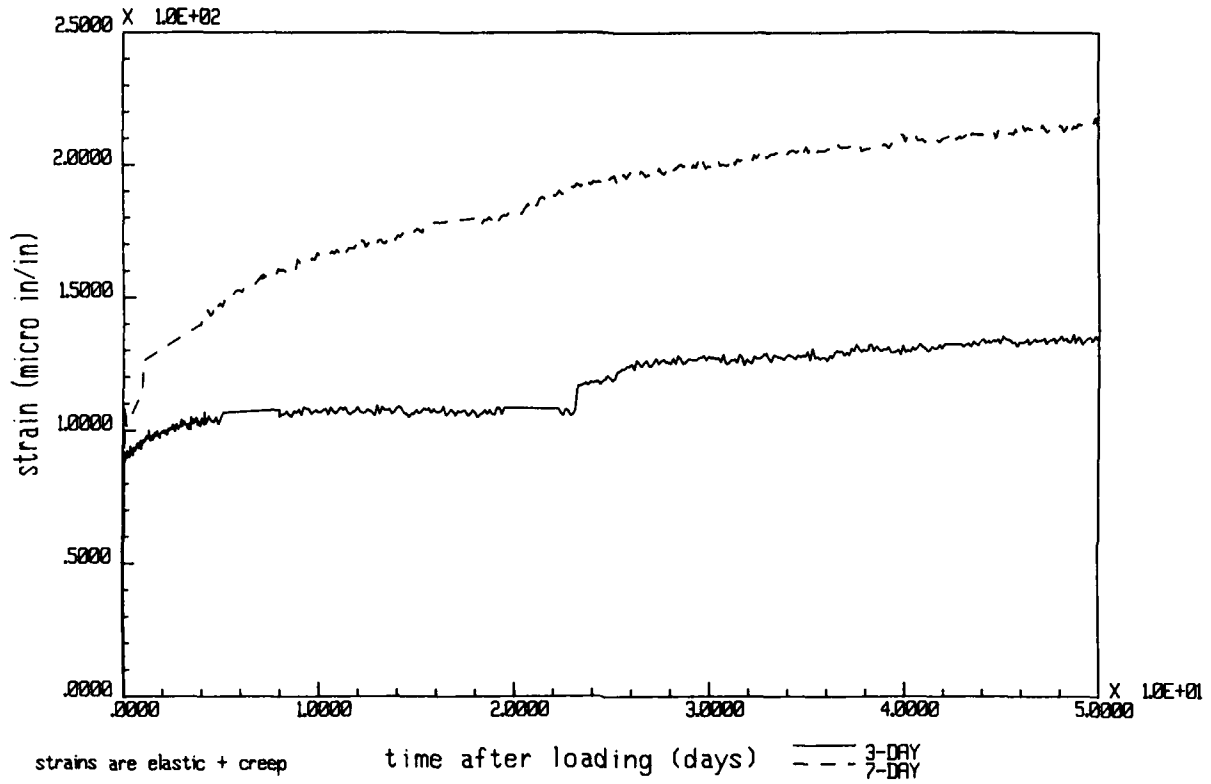


Figure 19. Series 1: 3-day and 7-day creep test strains

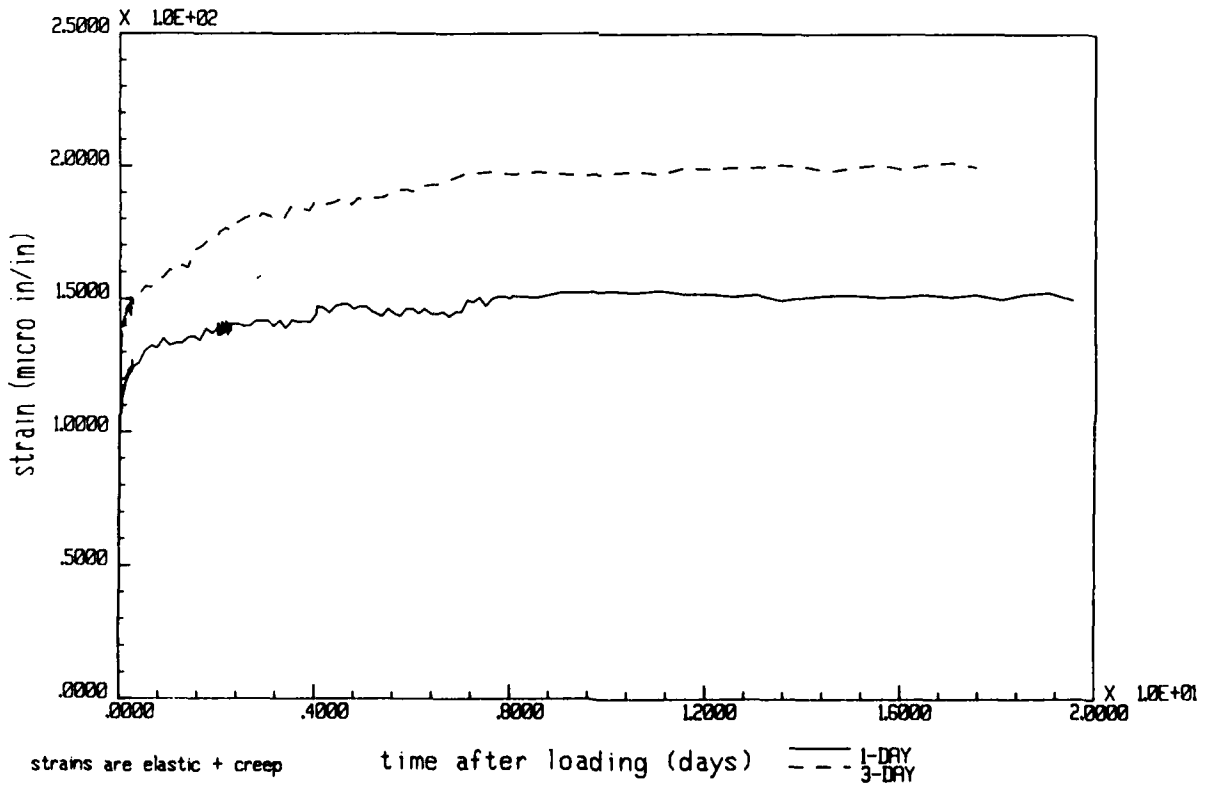


Figure 20. Series 2: 1-day and 3-day creep test strains

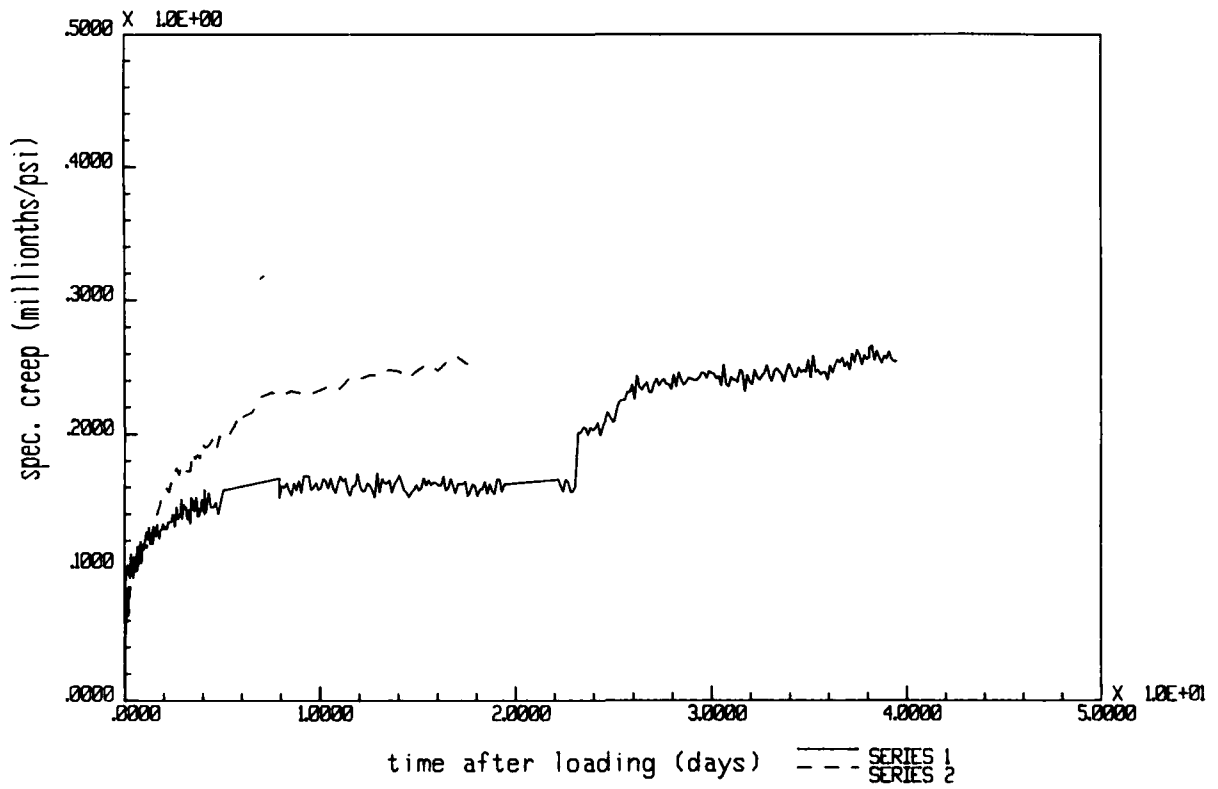


Figure 21. Three-day specific creep curves calculated from Series 1 and Series 2 test data

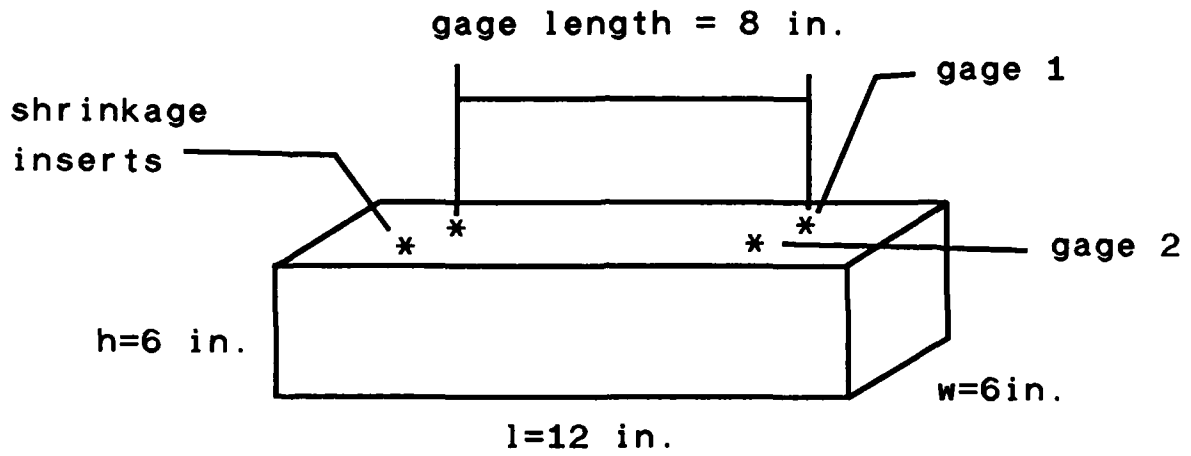


Figure 22. Typical autogenous shrinkage test specimen

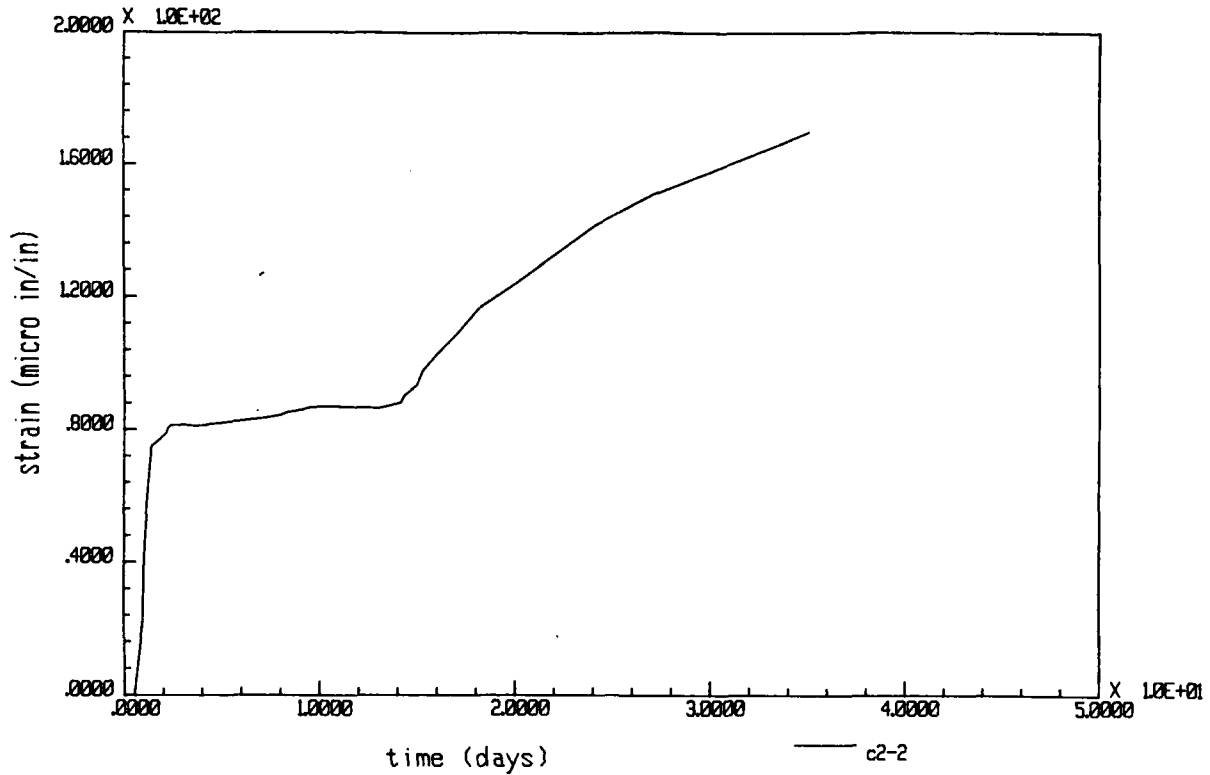


Figure 23. Average shrinkage strain results, mixture C2-2

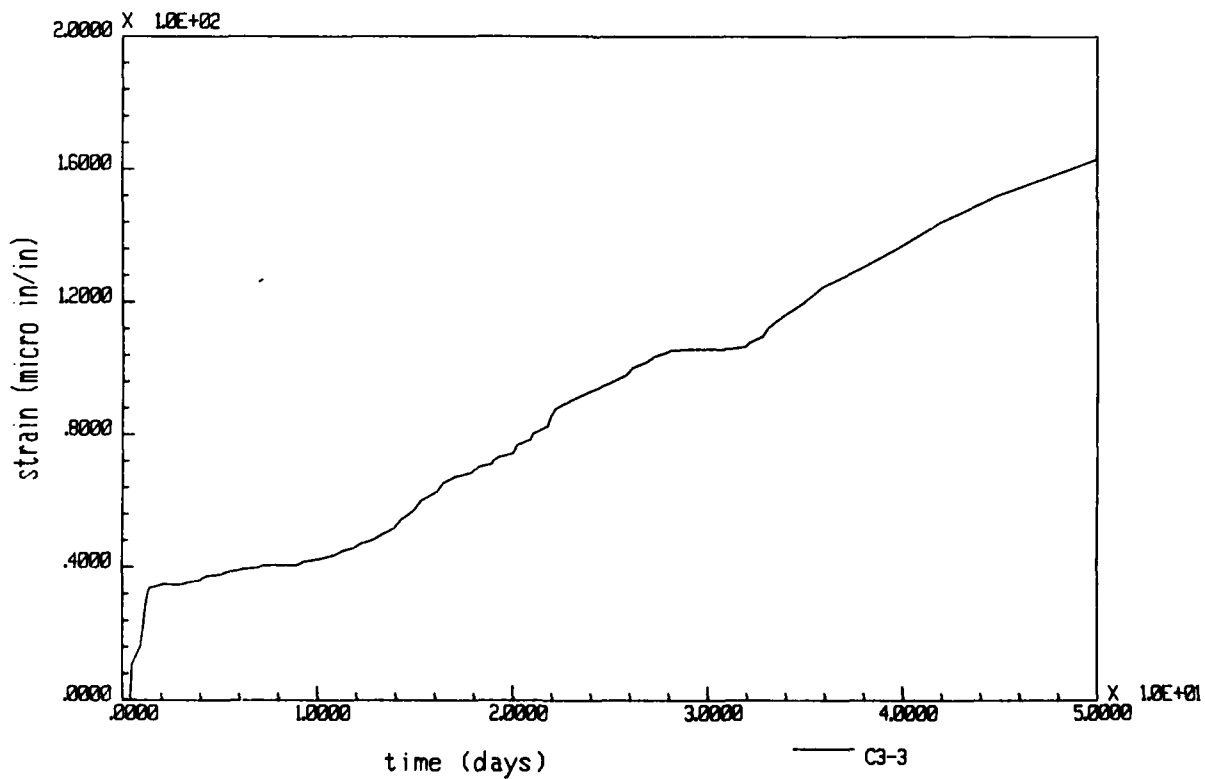


Figure 24. Average shrinkage strain results, mixture C3-3

Equation 8) divided by the 3-day modulus calculated using equation 8. This factor is then multiplied by the 3-day modulus input for a particular concrete. This means that the same curve may be used for different concretes as long as the shape of the curve is adequate to describe the change in modulus. The modulus-time curve calculated using aging factors based on equation 8 and a 3-day modulus of 2.8×10^6 psi (the approximate 3-day modulus for mixture C2-2) is plotted against test modulus values in Figure 25.

46. Test specimens exhibited much less creep than expected. In an attempt to determine the reason for this, an unconfined compression test was conducted on a specimen of the limestone aggregate used in the mixture. The modulus of elasticity of the aggregate specimen was approximately 14×10^6 psi, a relatively high value for limestone. Stiffness of the aggregate is an influential factor in creep, since the aggregate offers restraint to contractions due to creep in the "softer" cement paste (9).

47. However, the shape of the 3-day creep curve was similar to that of the curve defined by equation 11. Since the UMAT subroutine provides a convenient external method of factoring the creep and shrinkage curves using parameters input in the data statements, factored upper and lower bounding curves were used in the finite-element calculations. Factored curves representing 25 percent and 45 percent of the equation 11 curve are plotted against test data in Figure 26.

48. Shrinkage data did not fit the exponential form as readily as other parameters. Two problems were encountered in determining the optimal shrinkage curve for inclusion in the UMAT subroutine:

- a. very few data were available on autogenous shrinkage and
- b. the shapes of the average shrinkage curves for mixtures C2-2 and C3-3 were very different.

Due to these difficulties, the original curve was retained and modified externally in the same manner as the creep curve. The original curve and upper and lower bounding curves are plotted against Hansen's average shrinkage data for mixtures C2-2 and C3-3 in Figure 27. Predicted shrinkage is also plotted against Hansen's average shrinkage data for mixtures C2-2 and C3-3 in Figure 27.

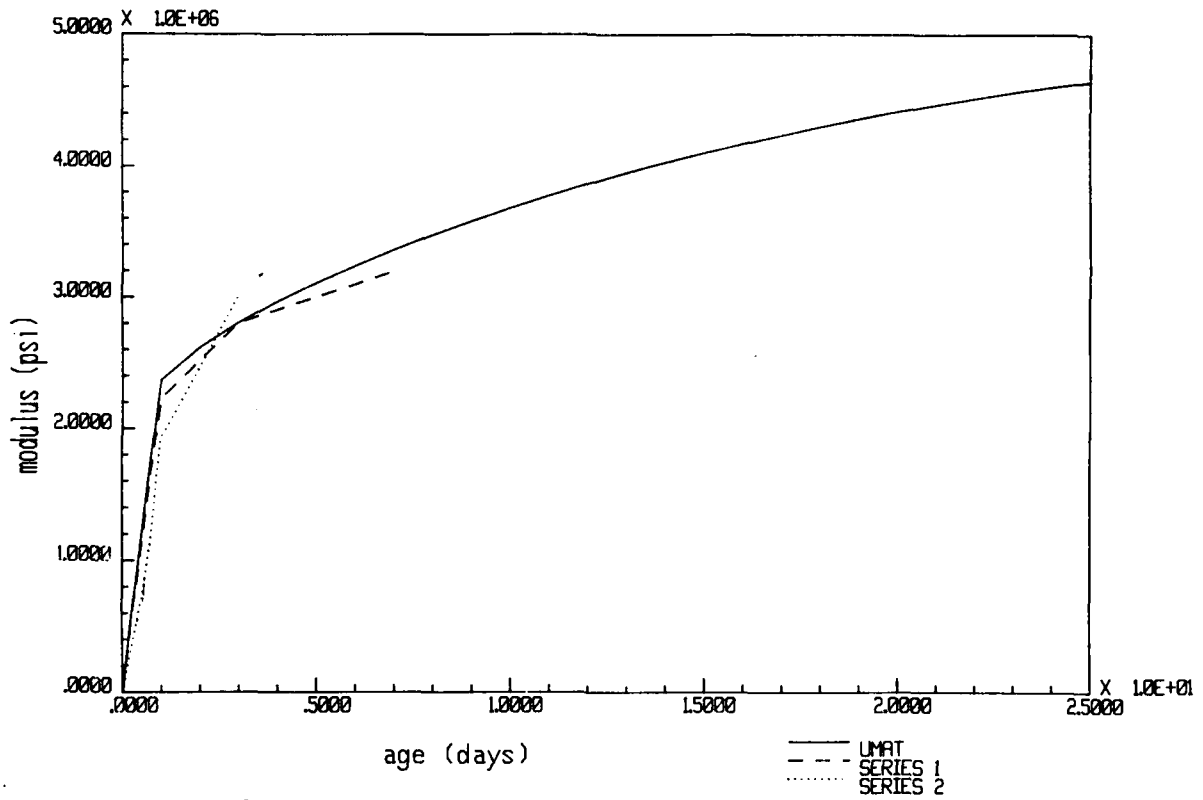


Figure 25. UMAT and tested elastic modulus vs time curves

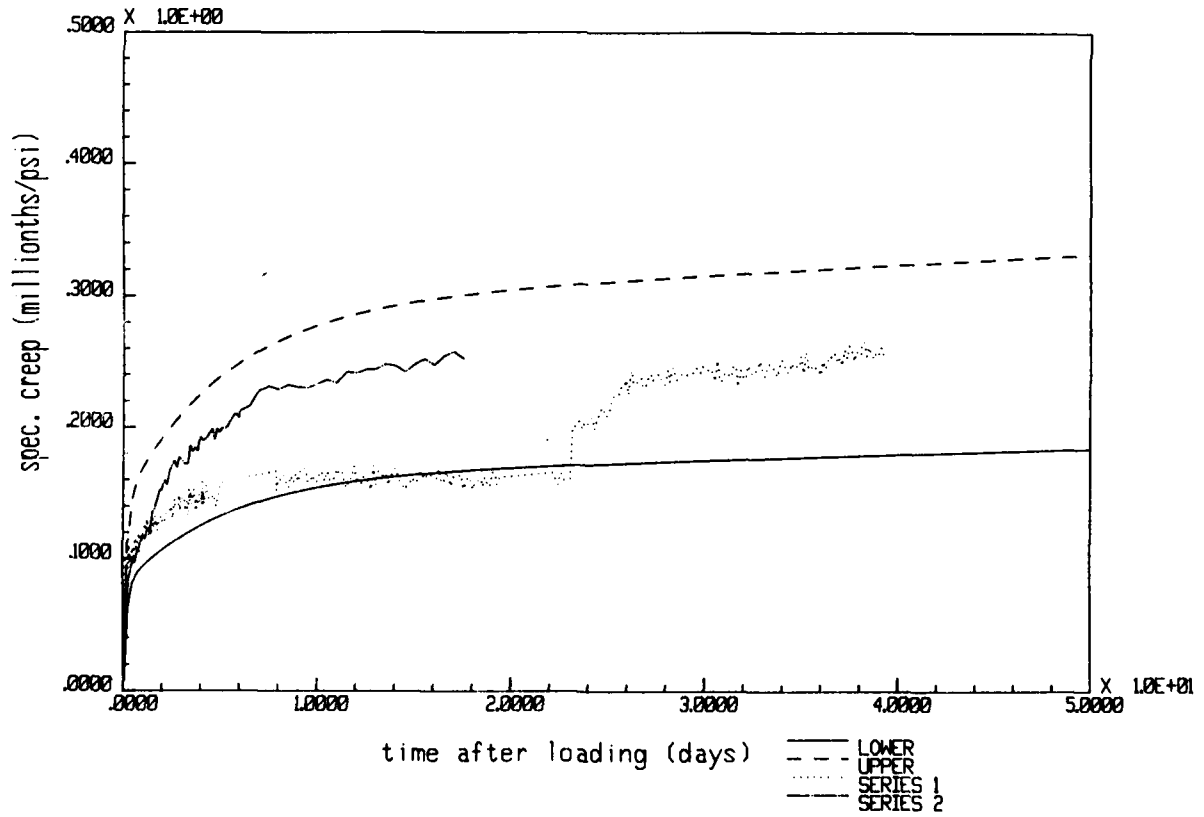


Figure 26. Upper bound, lower bound and tested specific creep curves

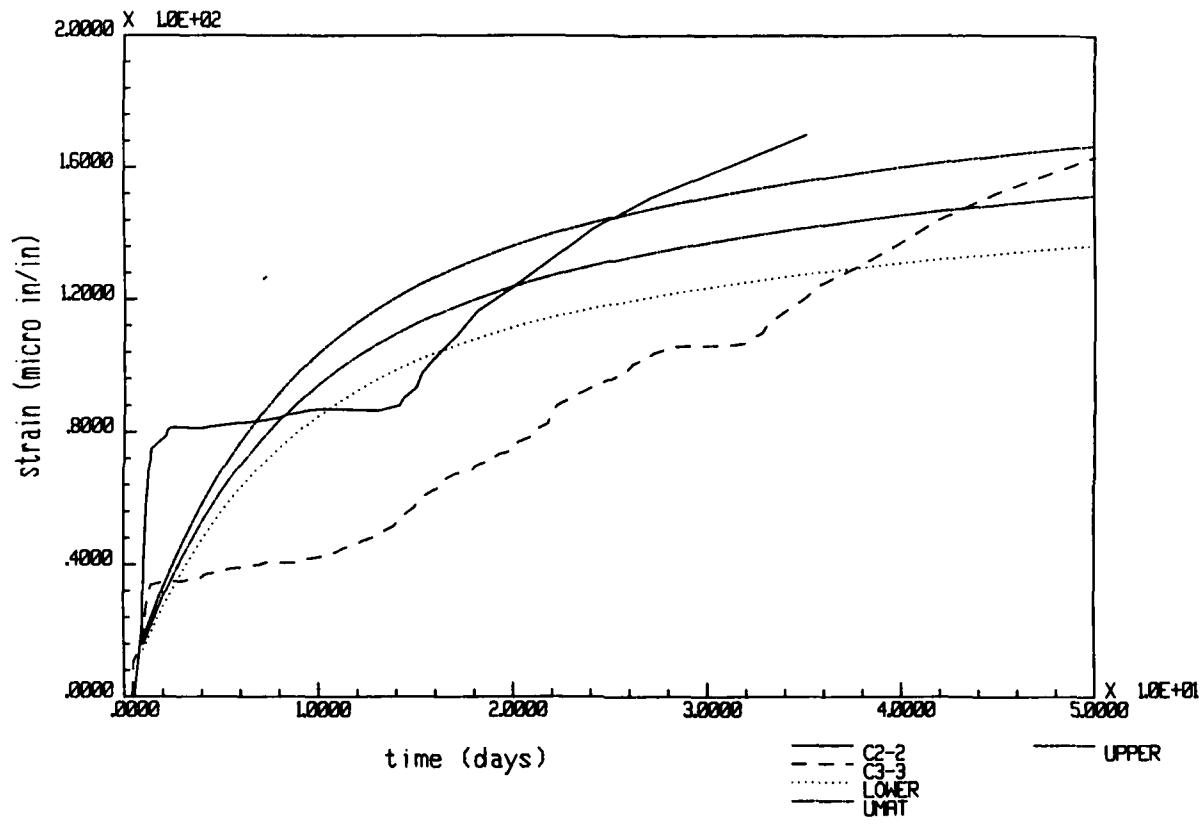


Figure 27. Upper bound, lower bound and tested shrinkage strain curves

PART IV. INCREMENTAL CONSTRUCTION FORMULATION

Background

49. The effective application of non-linear finite element analysis in the problem of incremental construction of mass concrete structures requires the development of material properties and analysis procedures which are not common in conventional structural analysis. Since incremental thermal stress analyses continue from beginning of construction through completion, it is important to minimize the number of elements in the total grid and maximize the solution time step size. However, accuracy of predicted results will be dependent on the number of elements used within a lift, type of element, and solution time step. Therefore, the criteria that guides the selection of optimum values of these parameters should be known. Time-step sensitivity is dependent upon the rate of change of the internal and external thermal environments plus the rate of change of material properties due to aging. In certain problems, daily temperature variation must be taken into consideration. In other cases only the yearly variation of expected mean daily temperatures is necessary. There are appropriate maximum time steps that will provide accurate results for each case, but what criteria should be used for their determination?

50. During transient thermal analyses the solution procedure used in ABAQUS introduces a requirement between element size and minimum time step. The requirement is

$$t > (pc/6k)l^2 \quad (13)$$

where

t = the time step

p = density

c = specific heat

k = thermal conductivity

l = a typical element dimension (such as the length of a side of an element).

This relationship specifies the minimum time step for the effects of a thermal input to span an element. ABAQUS warns that time steps smaller than defined above can introduce sporadic oscillations into the results. This requirement can change the grid density/time step length relationship that may have

otherwise been adequate for a given internal or external temperature environment. The result can be a dramatic increase in computer time required for the analysis because more, smaller elements may be needed to capture temperature changes that occur over very short time spans. Can the ABAQUS time step/element size requirement be exceeded and yield acceptable oscillation error or must the requirement be assessed by the analyst on a case by case basis?

51. An incremental construction formulation must address methodology for modeling boundary conditions, body fluxes such as concrete heat generation, surface fluxes such as solar radiation absorption or radiation heat loss, and other placement or construction parameters procedures. Complex curing conditions and application of insulation are normal practices. Use of several concrete mixtures or placement of concrete at different temperatures may require multiple heat generation capability. Lift interface equilibration effects must be examined when placement temperatures are substantially different than the temperature of the surface upon which placement occurs. Evaluation of many of these parameters requires validation of computed results against measured values.

52. In this section the questions and problems raised above pertaining to the incremental construction analysis formulation will be addressed. Through a series of finite-element thermal analyses, grid size and time step length sensitivity are examined. Several grid densities and time step lengths are used some of which intentionally violate the relationship in equation 13, to provide guidelines in this area. Analyses were performed using the following ambient temperature boundary conditions:

- a. constant temperature,
- b. mean daily temperature variation,
- c. daily temperature variation.

53. In addition, evaluation of material parameters and placement or other construction parameters were performed. These included:

- a. boundary condition testing to simulate curing conditions,
- b. surface insulation,
- c. implementing multiple heat generation input,
- d. examining lift interface equilibration.

The WES Test Wall

54. In order to evaluate critical parameters for incremental construction analyses, computed results from thermal simulations using ABAQUS were compared with data collected from an instrumented, incrementally constructed model lock wall (WES Test Wall) built for a related research program. The WES Test Wall shown in Figure 28 was constructed for the primary purpose of testing lock wall resurfacing techniques. It consists of two adjacent (east and west) fifteen-foot-wide monoliths with north- and south-facing surfaces for resurfacing demonstration tests. Each monolith was constructed in six lifts consisting of a base slab, a two-foot high by eight-foot thick second lift followed by four lifts nominally five-feet high by six-feet thick. This configuration provided a one-foot-thick resurfacing recess on each face of the east and west monoliths.

Construction and surface preparation

55. Concrete for the entire base slab (lift 1) and all of lift 2 was placed in two separate placements. Subsequent lifts were placed in two placements, the west monolith first followed by the east monolith. Nominal time between each placement was four days or about eight days between lifts in the same monolith.

56. Formwork consisted of commercially manufactured panels with angle-bar steel backing and 3/4-inch plywood faces. Typical sizes were 1 ft wide by 2.5 ft high and 2 ft wide by 2.5 ft high. Flat, steel form ties traversed the width of the monoliths at seven horizontal locations and three or four vertical locations that corresponded to the corners of the form panels. Formwork overlapped the previous lift by about 4 in. to anchor the bottom of the forms to the form ties in the existing concrete. The formwork overlap occurred in all lifts except number 3 which was formed directly upon the 1-ft resurfacing ledge of lift 2. The result was that lifts 4 and 5 were actually only 4 ft 8 in. high. An extra 1-ft row of form panels were added to lift 6 which made it 5 ft 8 in. high to complete the 20-ft structure.

57. The exposed north and south faces of lifts 3 - 6 received an exposed aggregate surface to simulate a concrete lock face with its surface concrete removed for resurfacing. The exposed aggregate surface was prepared in the following manner. Formwork was removed as soon as possible after placement of concrete. The smooth, formed surface was then removed with a

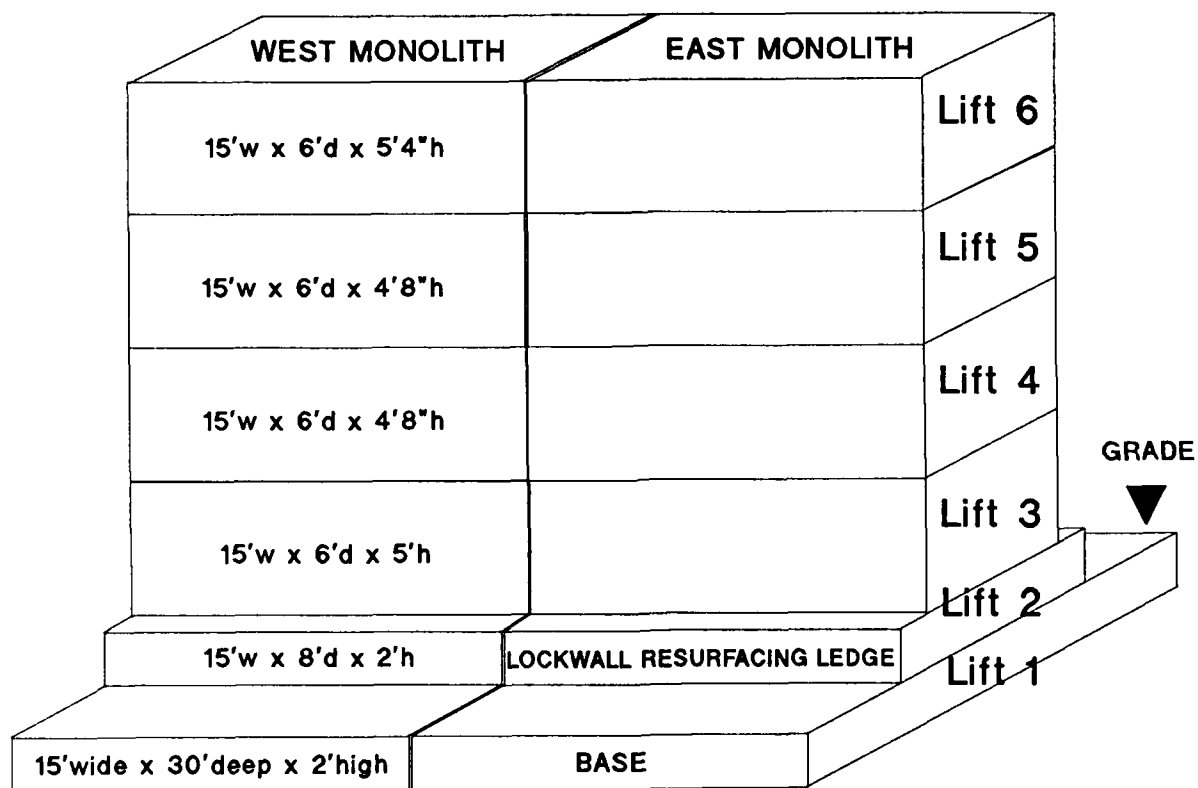


Figure 28. WES Test Wall

high pressure water spray to the desired exposed aggregate finish. The time required for form removal ranged from 2 - 3 hours after placement on mild days to 5 - 6 hours after placement on cold days. Preparing the exposed aggregate finish for one lift typically took one hour to complete.

Instrumentation of the WES Test Wall

58. Construction of the WES Test Wall offered an excellent opportunity to develop a database of temperatures and strains measured during incremental construction of a mass concrete structure. These measurements were intended for study in future analytical research efforts for comparison with and validation of computed results.

59. Instrumentation of the WES Test Wall consisted of 50 Carlson strain gages, each capable of measuring strain and temperature, supplemented by an additional 50 thermocouples to measure temperature. The Carlson gages were placed in lifts 5 and 6 of the west monolith. Primary strain and temperature measurement points were located in the longitudinal and transverse planes bisecting lifts 5 and 6. These planes are shown in Figure 29. Within these planes the Carlson gages were oriented in the vertical, transverse, or longitudinal directions depending upon location. Some of the thermocouples were placed in key locations in lifts 5 and 6 of the east monolith for comparison with data from the west monolith. Several thermocouples and two additional Carlson gages had been earlier installed in lifts 3 and 4 of the east monolith primarily to test instrumentation and data acquisition techniques and to prepare the construction crew for working carefully around the installed instrumentation. As a result, no measurements were lost.

60. Figures 30 - 32 show the locations and orientation of Carlson gages in lifts 5 and lift 6. Figures 33a - 33c are examples of typical temperature measurements from Carlson gages in the Test Wall. Figures 34a - 34c are examples of typical strain measurements from the same Carlson gages. Strains are normalized at placement time. The early strains at times up to about four to six hours may not represent actual strain behavior because the concrete is not in a fully hardened state for the Carlson gages to respond reliably.

Incremental Formulation

61. A series of two-dimensional (2-D) finite-element analyses were conducted to address the incremental construction parameter questions

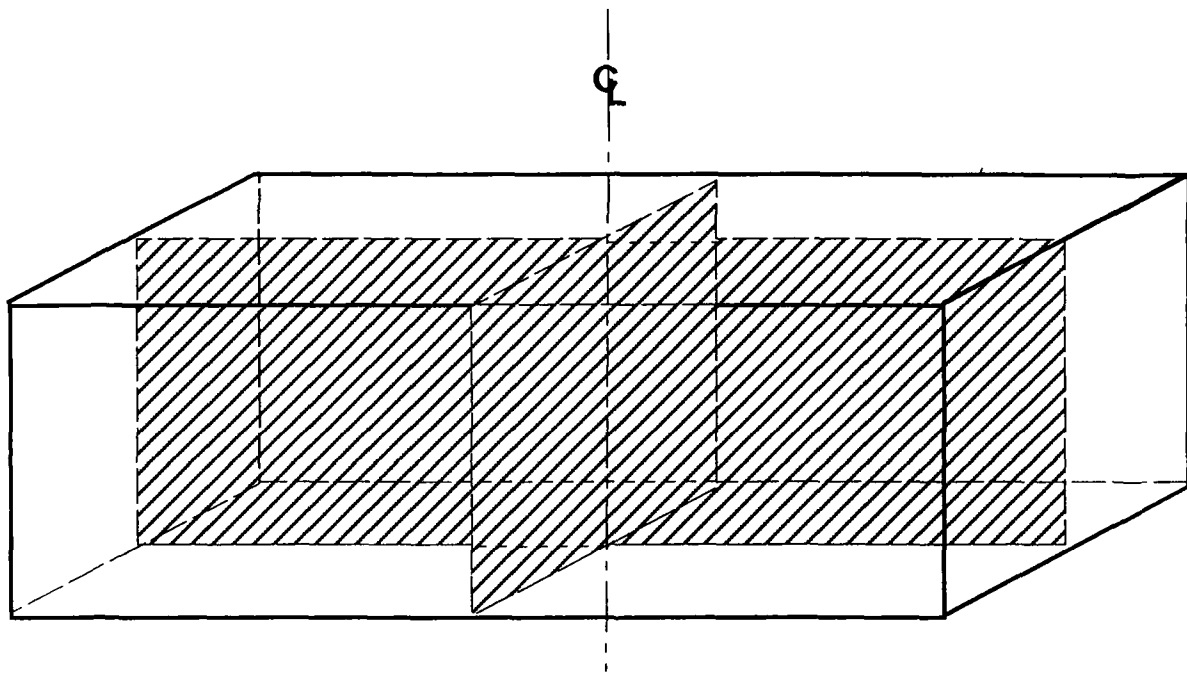


Figure 29. Instrumentation measurement planes in WES Test Wall

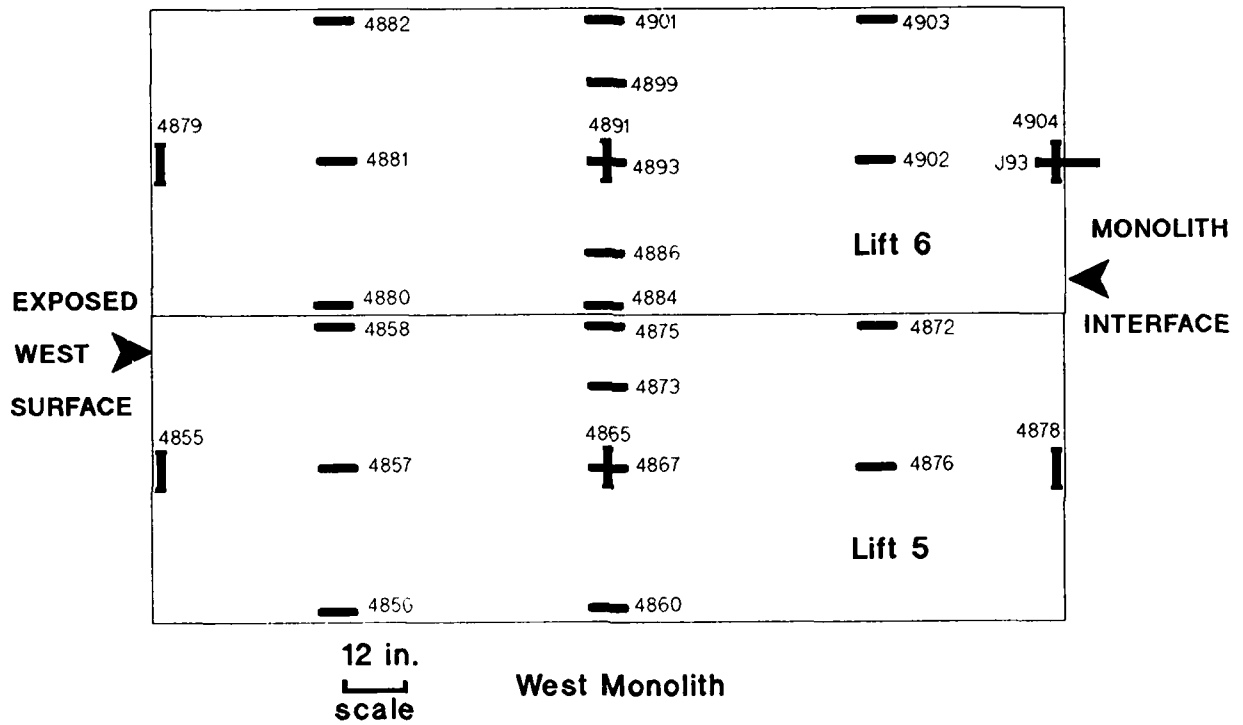


Figure 30. Locations of Carlson strain gages in longitudinal plane in WES Test Wall

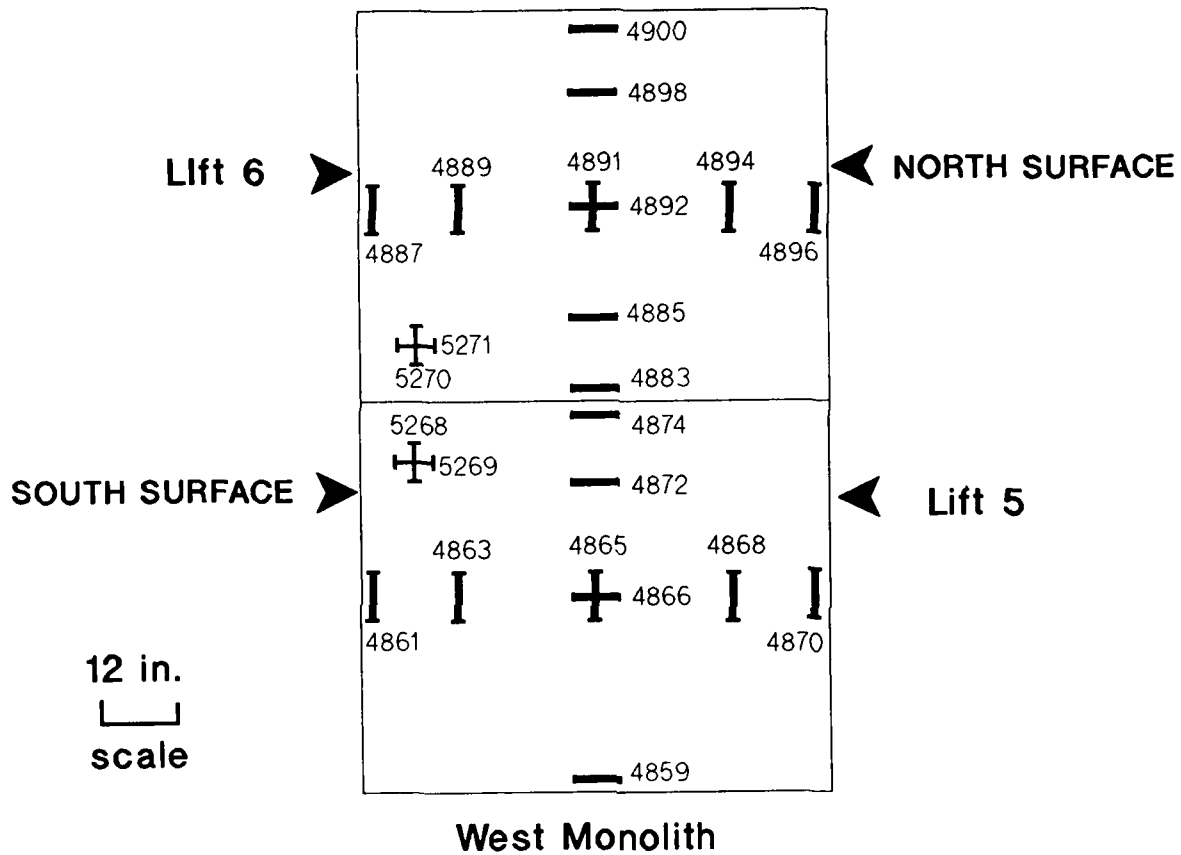


Figure 31. Locations of in-plane Carlson strain gages in transverse plane in WES Test Wall

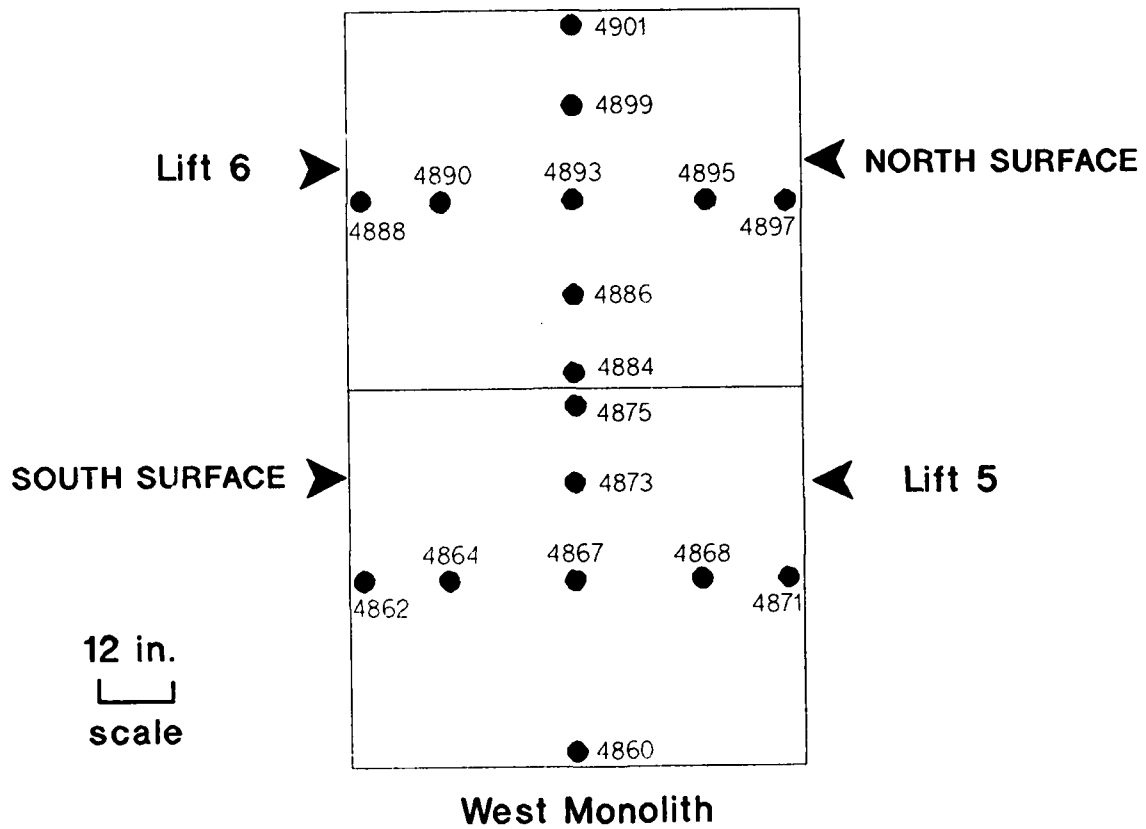


Figure 32. Locations of longitudinal Carlson strain gages in transverse plane in WES Test Wall

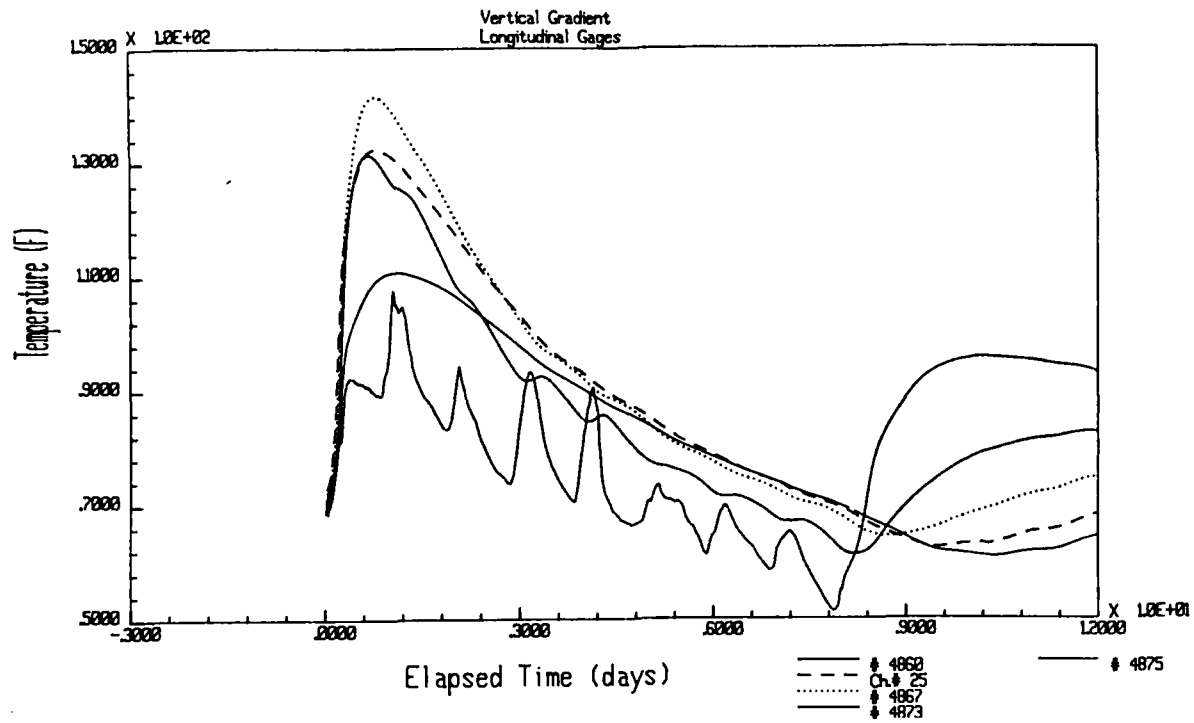


Figure 33a. Measured temperatures along vertical centerline of lift 5 in Test Wall

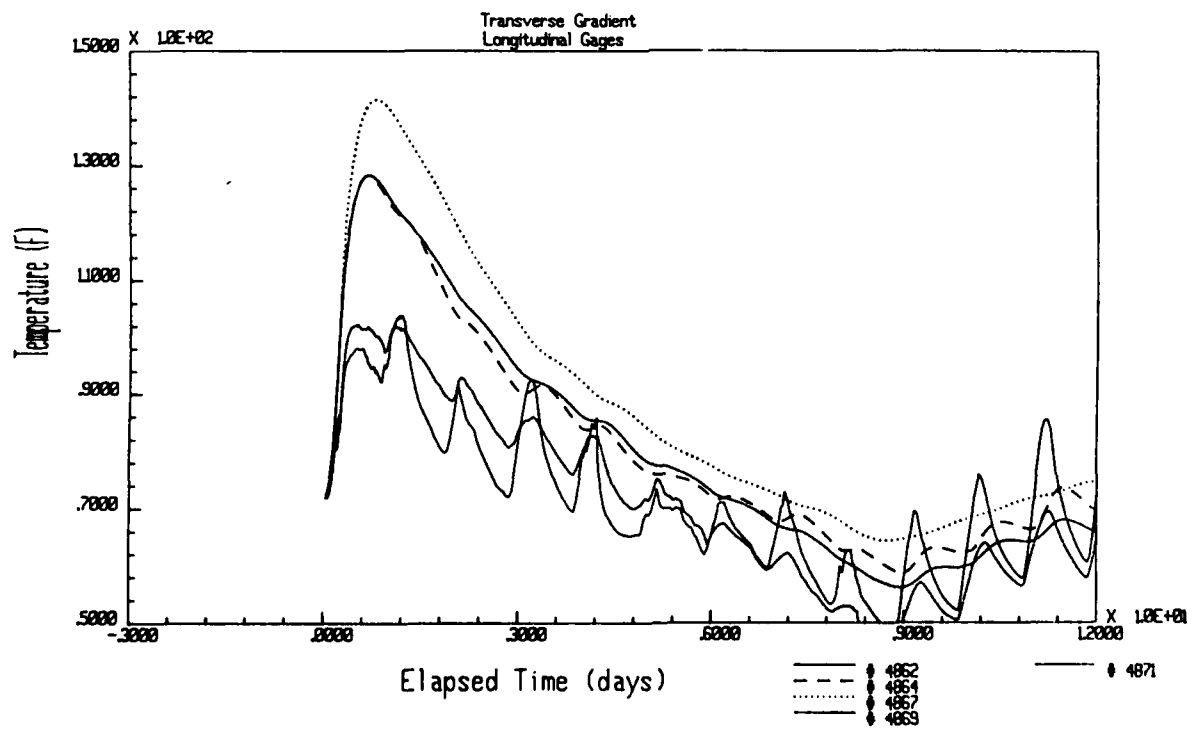


Figure 33b. Measured temperatures across width of lift 5 in Test Wall

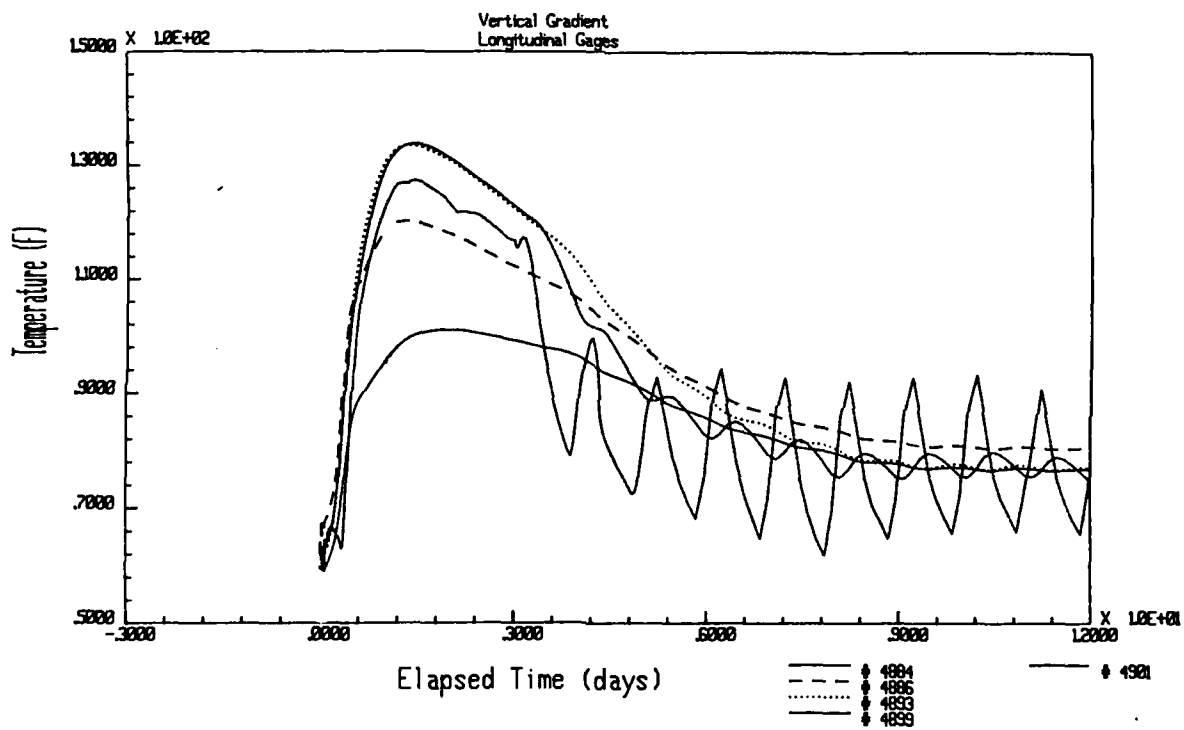


Figure 33c. Measured temperatures along vertical centerline of lift 6 in Test Wall

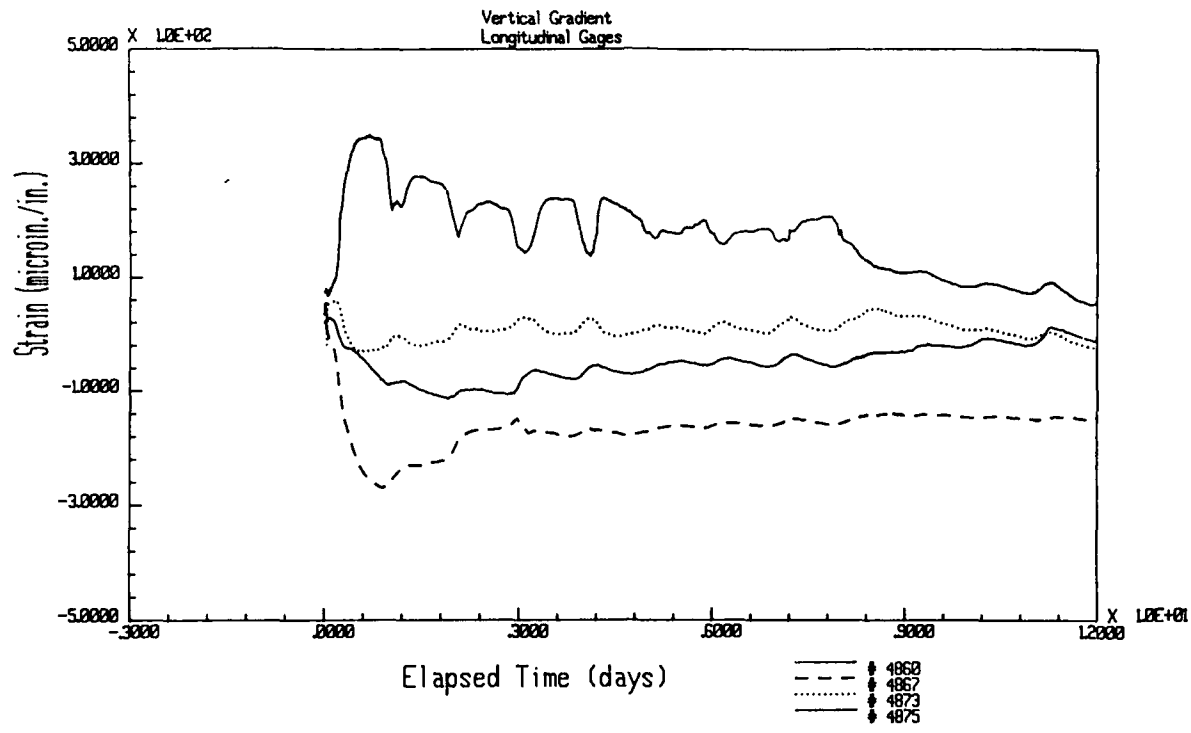


Figure 34a. Measured strains along vertical centerline of lift 5 in Test Wall due to thermal gradient in Figure 33a

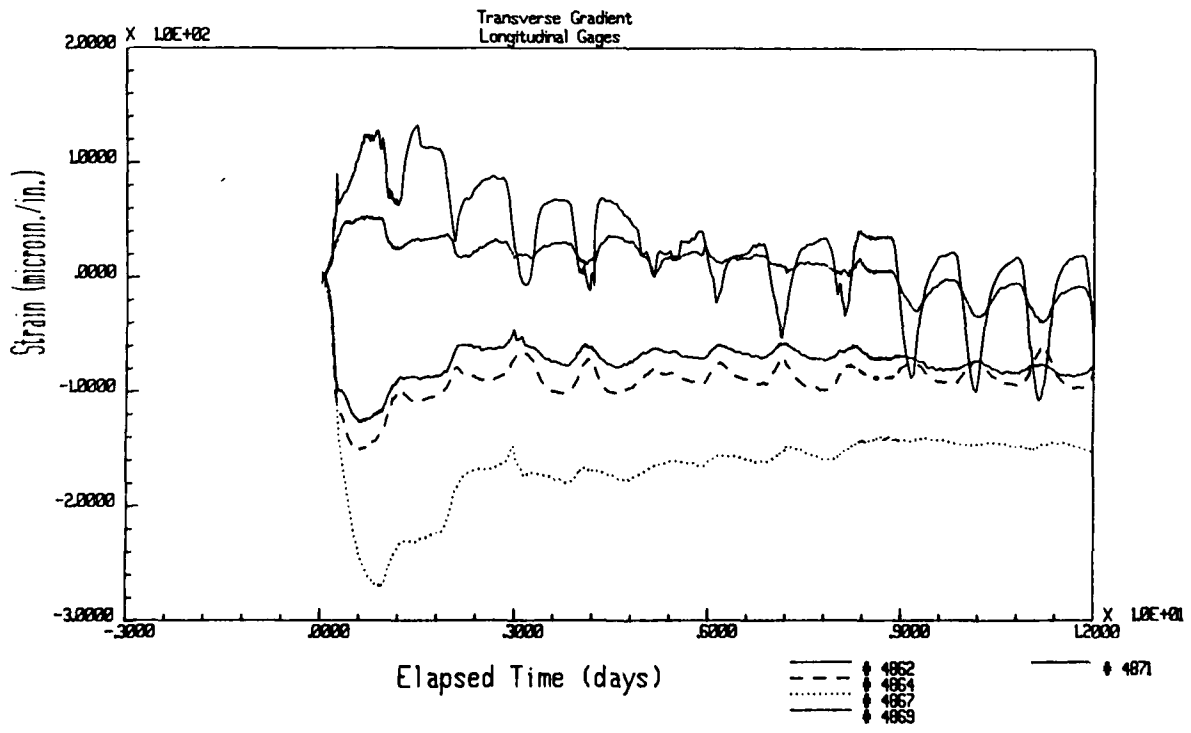


Figure 34b. Measured strains across width of lift 5 in Test Wall due to thermal gradient in Figure 33b

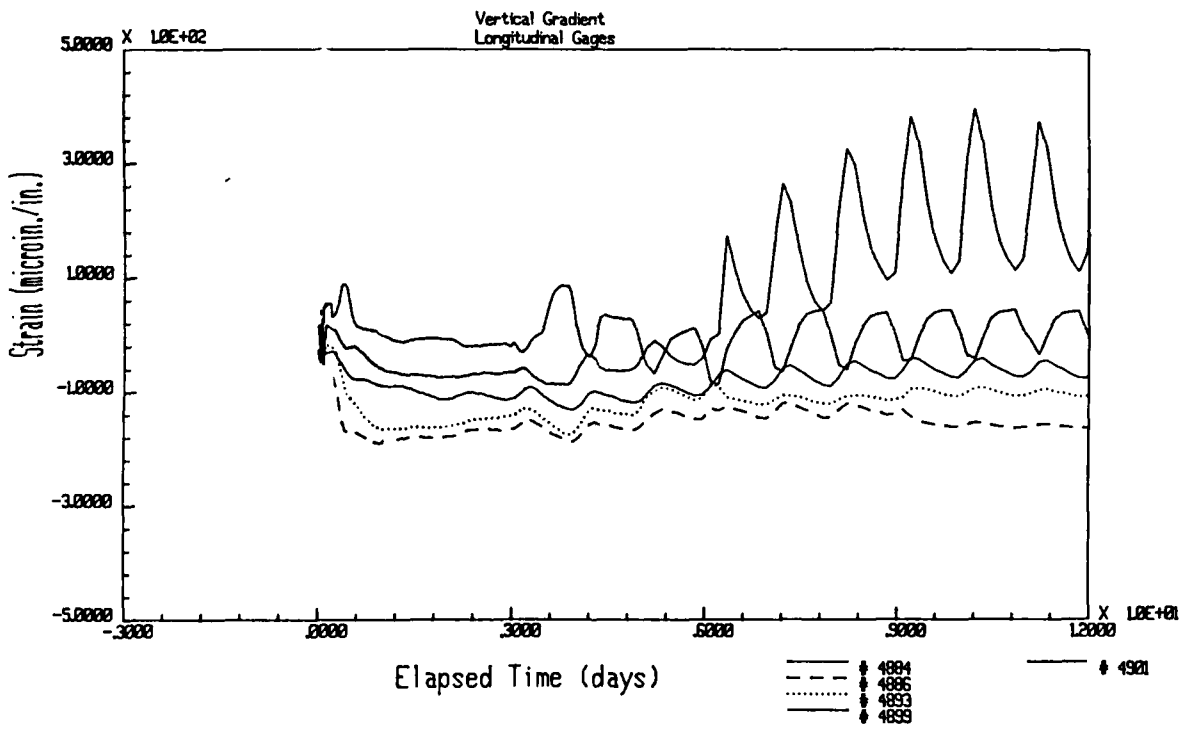


Figure 34c. Measured strains along vertical centerline of lift 6 in Test Wall due to thermal gradient in Figure 33c

described above. These analyses were conducted using finite-element models representing the transverse plane of the WES Test Wall so that comparisons against measured data could be made. The longitudinal versus transverse distance ratio of each monolith for lifts 3 - 6 was 2.50. Measurements made in this plane were considered to be nominally acceptable for comparison with 2-D thermal analysis. Error due to longitudinal heat flow (through the plane) was considered minimal and was consequently ignored.

Lift heights

62. The heights of lifts 3 - 6 were nominally specified to be 5 ft. Actual placement heights were 5 ft for lift 3, 4 ft 8 in. for lifts 4 and 5, and 5 ft 8 in. for lift 6. This variation in lift height was caused by limitations in the forming system employed by the contractor. The difference in height of lifts 5 and 6 caused a compromise to be made between vertical element size and number of elements per lift for the two lifts when designing the finite-element grids.

Finite-element models

63. Four finite-element models were used in the incremental formulation analyses. These models are shown in Figures 35 - 38. The eight-node planar heat transfer element DC2D8 was used in all models. The coarsest model designated as the "W-model" consists of one element vertically per lift and one element horizontally in the half-symmetry model (or two elements wide). The coarse model designated as the "C-model" includes two elements per lift vertically in lifts 3 - 6 and one element horizontally in the half-symmetry model. The medium-grid, "M-model" includes three elements per lift vertically in lifts 4 - 6 and two elements horizontally per half-symmetry model. Finally, the fine-grid, "F-model" includes three elements per lift vertically for lift 4 - 6 and four elements horizontally per half-symmetry model. Grid density vertically was the same for the M- and F-models. Table 6 summarizes the grid size variation.

64. All four models represent a transverse section through the west monolith wall with a symmetry boundary along the left side. When comparing results with measured data, these models represent a north-south orientation with north to the right. The north surface received no direct solar heating. It is assumed that diffuse solar heating was present, however all solar heating effects were ignored so that air temperatures provided the sole external thermal environment. The four models represent the entire height of

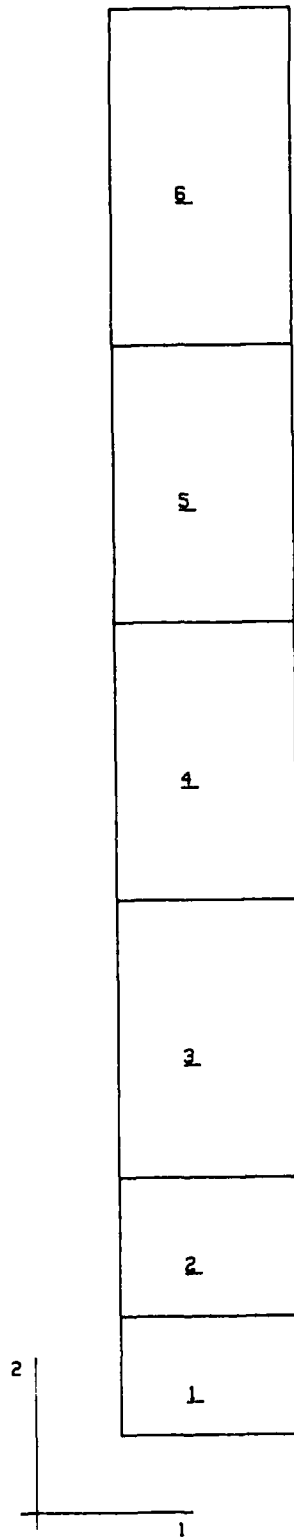


Figure 35. Finite element model for the very coarse grid "W-model"

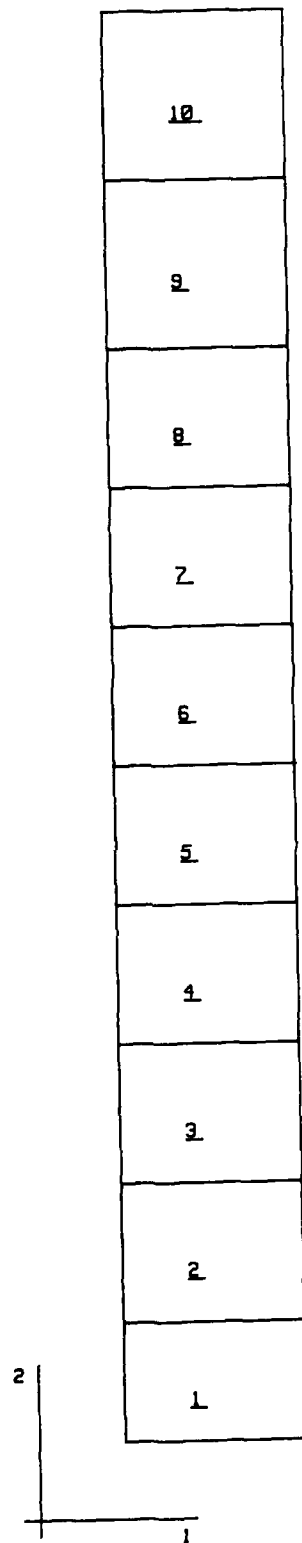


Figure 36. Finite element model for the coarse grid "C-model"

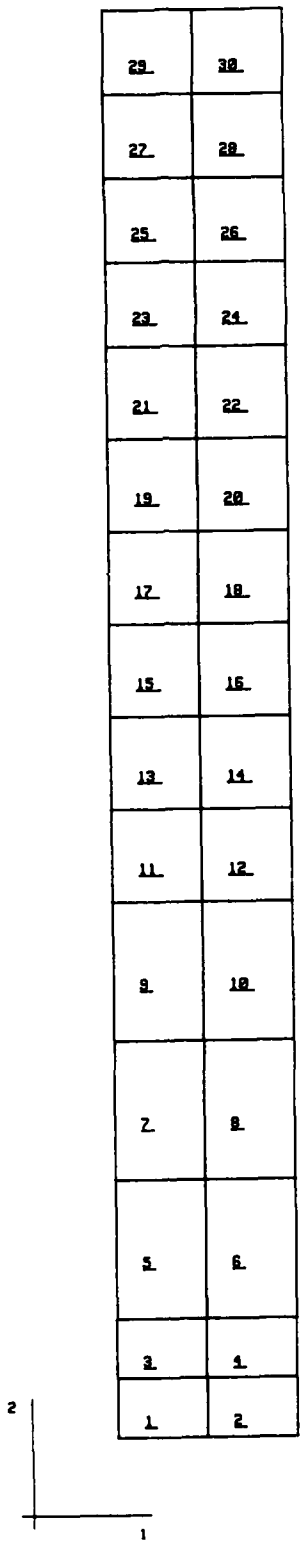


Figure 37. Finite element model for the medium grid "M-model"

| | | | |
|----|----|----|----|
| 57 | 58 | 59 | 60 |
| 53 | 54 | 55 | 56 |
| 49 | 50 | 51 | 52 |
| 45 | 46 | 47 | 48 |
| 41 | 42 | 43 | 44 |
| 37 | 38 | 39 | 40 |
| 33 | 34 | 35 | 36 |
| 29 | 30 | 31 | 32 |
| 25 | 26 | 27 | 28 |
| 21 | 22 | 23 | 24 |
| 17 | 18 | 19 | 20 |
| 13 | 14 | 15 | 16 |
| 9 | 10 | 11 | 12 |
| 5 | 6 | 7 | 8 |
| 1 | 2 | 3 | 4 |

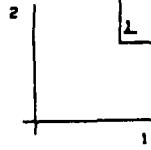


Figure 38. Finite element model for the fine grid "F-model"

Table 6
Finite-element Investigation - Grid Size Variation

| <u>Finite-element Model</u> | <u>Elements/lift Vertically</u> | <u>Elements/width* Horizontally</u> |
|-----------------------------|---------------------------------|-------------------------------------|
| W-model | 1 | 1 |
| C-model | 2 | 1 |
| M-model | 3** | 2 |
| F-model | 3** | 4 |

* Number of elements wide in symmetry model of one-half of structure.

** Four (4) elements used in lift 6 because of its extra height and the desire to keep element size nearly the same in lifts 5 and 6.

the Test Wall. Since, the primary emphasis was with lifts 5 and 6, the first two lifts were modeled with the same thickness as lifts 3 - 5. The grids for lifts 5 and 6 were designed with different criteria to address the difference in lift height. In the W- and C-models the same number of elements per lift, vertically, were used with different element heights in each lift. In the M-model and F-model vertical element size was nearly equal, but with a different number of elements per lift.

Concrete placement scheme

65. The concrete placement of the west monolith of the WES Test Wall was simulated as closely as possible during the finite-element thermal analyses. Primary interest was with lifts 5 and 6 where the bulk of measured data existed. It was felt that simulation of the entire wall was unnecessary if the temperature distribution in existing concrete and subsequent heat generation thereof could be approximated at the time of initiation. Therefore, all simulations were initiated to coincide with placement of lift 4. The concrete comprising lifts 1 - 3 was assumed to have completed heat generation and concrete temperatures at this time were approximated from several thermocouples located in these lifts.

Weather conditions

66. The WES Test Wall was constructed during the months of February and March. Weather conditions varied considerably as would be expected for this time of the year. Figure 39 shows the three ambient air temperature curves

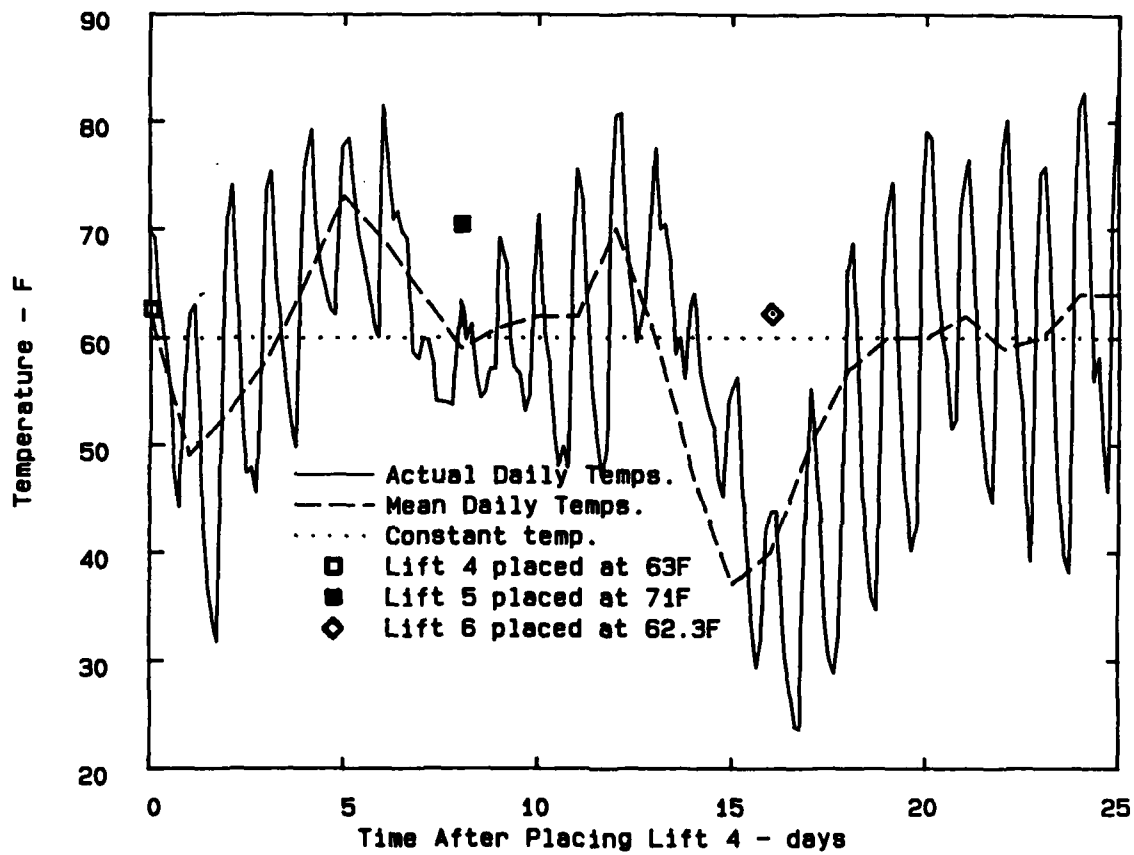


Figure 39. Ambient air temperature curves used in Test Wall analyses

used as external temperature environments in the thermal analyses. The first curve shows the actual daily temperature variation during the period beginning with placement of lift 4 through eight days following placement of lift 6. Since lifts 4 - 6 were each placed eight days apart, the total time shown is 24 days. The second curve represents mean daily temperatures while the third is the average air temperature during this time period. Also included are placement times and temperatures of lifts 4 - 6 to show air temperature exposure during placement and subsequent curing of the concrete.

67. During the time period shown, weather conditions were generally fair for the 8-day curing period following placement of lift 4, generally overcast during the curing period for lift 5, and fair during the curing period for lift 6. The effect of solar radiation was minimized during the curing period for lift 5 due to the overcast. Solar radiation was also minimized for lift 6 concrete during the period of insulation because the foil side of the insulation panels were on the outside. Most of the solar radiation was reflected by the foil surface. Because of these factors, solar radiation was not considered during this investigation.

68. Resultant wind velocity, which is the vector sum of wind speed and direction divided by number of observations, obtained from the Jackson, Mississippi NOAA Weather Station was 6.7 miles per hour during the 24-day construction period described above. Resultant wind direction was 330 degrees clockwise from north (from the north northwest) during this same time. These values for resultant wind velocity and direction indicated that the primary effects of the wind for this time were on the north face of the Test Wall used in the analyses. Figure 40 shows daily resultant wind velocities during construction of lifts 4 - 6 in the west monolith. It should be noted that wind velocities were moderate during the several days following placement of these three lifts. As a result, the cooling effect on internal temperatures from the wind during the initial temperature rise in each of these lifts was minimized. The effects of cooling by the wind were further minimized by the surface curing conditions following placement of lifts 5 and 6.

Concrete placement times

69. The actual time required for placement of lifts 4 - 6 ranged from 45 minutes to one hour and 15 minutes. Since lift 6 was one foot higher than lifts 4 and 5 concrete placement took longer because one additional ready-mix truckload of concrete was required. In all cases placement of the three lifts

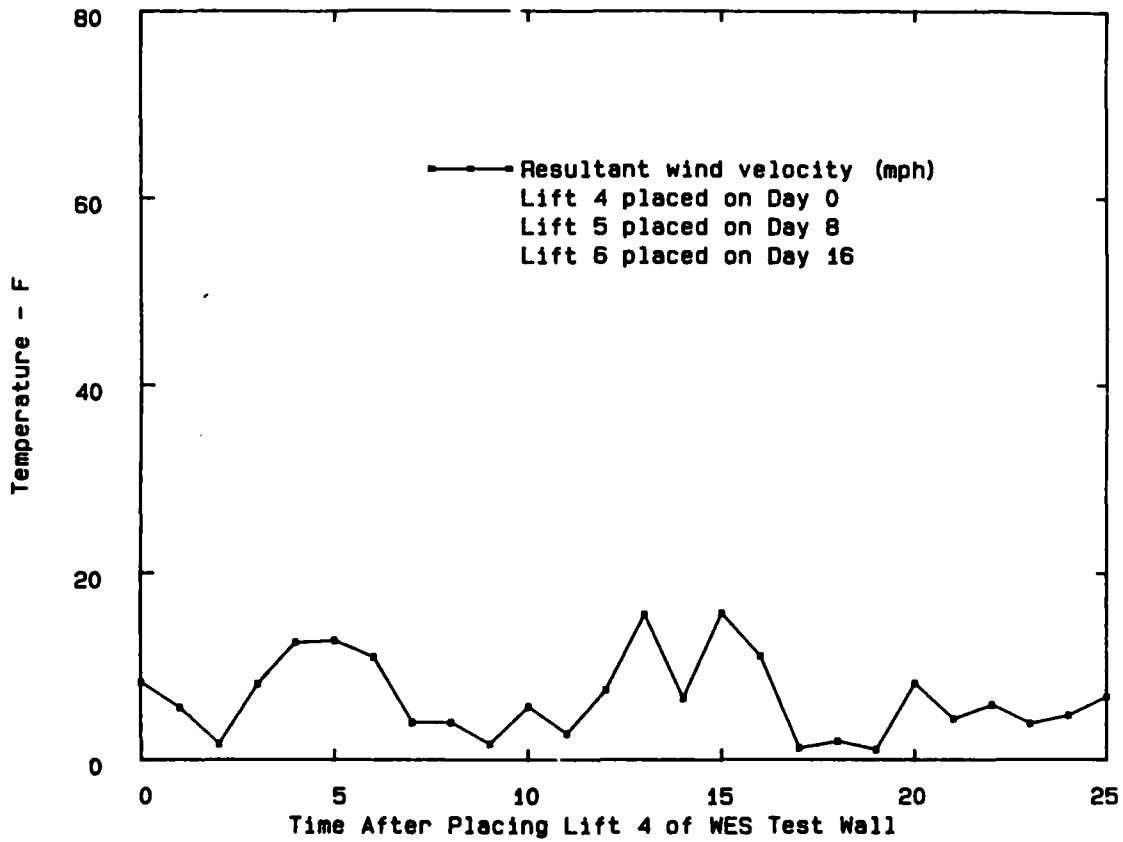


Figure 40. Actual resultant daily wind velocities during construction of Test Wall lifts 4-6

was made during the morning hours between 9:15 AM and 11:45 AM. For convenience, simulated placement of concrete in the thermal analyses was assumed to be instantaneous for each lift at 12:00 noon on the day of placement with a placement rate of eight days between lifts.

Placement temperatures

70. Placement temperatures of concrete varied by approximately 10°F between lifts primarily as a result of rather large variations in air temperature from day to day. Variation in delivered concrete temperatures per lift was 1°F to 2°F. Placement temperatures selected for lifts 4 - 6 of the thermal analyses were the average placement temperatures within the lift at the time placement was completed or 63°F, 71°F, and 62.3°F, respectively. Placement temperatures selected in this manner were generally 1°F higher than the average delivered temperatures prior to pumping and vibration. As indicated earlier, placement temperatures of lifts 4 - 6 are shown in Figure 39 along with comparative air temperature data.

Normal curing conditions

71. Curing of concrete in the Test Wall was done with a combination of water and membrane curing. This was accomplished by wetting the top surface of a freshly placed lift with a garden-type soaker-spray hose and also covering the concrete with a polyethylene membrane. The membrane was kept away from the upper surface to permit the water to be sprayed on to the entire horizontal surface. This caused a slow-running, thin film of water to flow down the sides of the wall. It was concluded, from visual observations and measured surface temperatures, that water flow on the north face actually was only enough to keep the surface wet and not to draw away heat. Measured surface temperatures suggested that the flow on the south face was high enough to contribute to some surface cooling. Since the exposed face in these thermal analyses was the north face, the effect of the water curing was not considered. The manner of placing the polyethylene membrane against the vertical concrete surfaces resulted in a layer of air separating the membrane from the surface. The thickness of the air layer varied considerably.

Curing convection film coefficient

72. The exchange of heat between a body and air is a function of a surface heat transfer film coefficient. The film coefficient is composed of a convection or surface conductance coefficient that defines heat exchange with surrounding air as a function of air velocity and a conduction heat transfer

coefficient that defines the heat flow through formwork and/or insulation applied to a surface. The film coefficient is needed by ABAQUS for computing concrete temperatures. The general equation used for the composite film coefficient is

$$h = \frac{1}{\frac{1}{h_{\text{air}}} + \frac{1}{C_{\text{formwork}}} + \frac{1}{C_{\text{insulation}}} + \frac{1}{C_{\text{other}}}} \quad (14)$$

in (BTU/day-in.²-°F), where

h_{air} = convection coefficient

C_{formwork} = conductance of formwork (when in use)

$C_{\text{insulation}}$ = conductance of insulation (when in use)

C_{other} = conductance of other factors such as an entrapped air layer.

A film coefficient was required for the time during the curing period when water and polyethylene membrane were in use. For purposes of computing the film coefficient the membrane was considered as an insulation layer, but one so thin as to cause its conductance to be ignored. The effect of using the membrane isolated the air trapped between it and the concrete reducing the effective air velocity to nearly zero. The combined effect of these assumptions was that of an exposed concrete surface exposed to air with a velocity of zero. Assuming air velocity $V = 0$ and using the approximate expression for computing surface conductance when air velocities are less than or equal to 16.5 ft/s and the surface has a rough texture (11)

$$h = h_{\text{air}} = 1.087 + 0.225V \quad (15)$$

where

V = air velocity in ft/s

produced a value of $h = 0.182$ BTU/day-in.²-°F, with units appropriate for ABAQUS. When used in analyses where actual daily air temperature environment was applied, near-surface temperatures resulting from use of this film coefficient were lower than measured. It is believed that assuming still air was the resultant environment when covering surfaces with a polyethylene membrane was not totally correct, but the best assumption under the conditions that existed. It is probable that the insulating effect of the air layer under the membrane was needed. However, the method of application of the membrane made determination of the thickness of the air layer very difficult. In addition the air layer must be less than 0.75-in. and still for the conduction effects of the air to be used. Otherwise convection effects are

introduced. Under these circumstances it is believed that the method used was a good approximation. If the insulating effect of the air layer had been used, it would have been included as the C_{other} term in equation 14 along with the convection coefficient due to the actual air velocity.

Insulation curing condition

73. Cold weather, characterized by night-time temperatures well below freezing, occurred during each of the first two nights following placement of lift 6. This lift had been tentatively selected to be insulated to generate measured data for this condition. Strangely, the cold weather occurred at precisely the right time to require insulation to prevent the concrete from freezing when night-time temperatures dropped to about 20°F for the two nights following placement. One-inch foil-backed polystyrene insulation panels were applied as snugly as possible to all surfaces of lift 6 about six hours after placement. A small air gap between concrete and insulation was typical. Measurements after placement indicated that the insulation had maintained surface temperatures at least 25°F higher than normal. In order to minimize cracking due to induced thermal shock following insulation removal, insulation was removed at 9:00 AM three days after placement. At insulation removal, the air temperature had risen above the morning low temperature and was continuing to rise which served to minimize the difference between air temperature and surface temperature. This effectively spread cooling of the surface over an additional one-half day, thereby reducing the thermal shock at insulation removal. Insulation of lift 6 was simulated in all thermal analyses.

Insulation curing film coefficients

74. Several values for the surface heat transfer film coefficients were used during the course of these analyses. Since the insulation was foil backed, the surface conductance was computed using the equation for a smooth surface texture (11)

$$h_{smooth} = 0.984 + 0.212 V \quad (16)$$

in BTU/hr-ft²-°F, where

V = air velocity in ft/s.

Equation 14, employing only the convection and insulation terms, was used for computing the composite surface film coefficient. Initially the film coefficient was calculated for an insulation thickness of 0.75 in. ($C = 0.375$ BTU/hr-ft²-°F) and the wind velocity arbitrarily set at 10 mph or 14.16667 ft/s. A film coefficient of 0.0571 BTU/day-in²-°F was computed for use in

ABAQUS. Most of these analyses used a constant air temperature environment over the duration of the simulation for simplicity. Since the initial runs were conducted to test the effects of grid size and time step variation, primarily in lift 5, the function of lift 6 in these analyses was to supply an appropriate thermal environment for lift 5. In analyses when the actual mean daily temperature environment began to be used, it was observed that near-surface temperatures in lift 6 were excessive. Although records showed that 0.75-in. insulating panel were used, examination of photographs taken during construction indicated that 1-in. insulation panels ($C = 0.25 \text{ BTU/hr-ft}^2\text{-}^\circ\text{F}$) were actually used which produced a film coefficient of $0.0393 \text{ BTU/day-in}^2\text{-}^\circ\text{F}$ for use in ABAQUS. Most of the subsequent thermal analysis runs used this new film coefficient. In addition some of the earlier runs were repeated to determine if the results changed appreciably. Correlation of measured versus calculated near-surface temperatures in lift 6 improved, but needed further refinement of the film coefficient when actual daily air temperature variation was used. Air velocity was changed to 4.5 mph or 6.6 ft/s to represent the mean velocity for the 5 days following lift 6. A conductance term was introduced for the air trapped (C_{other} in equation 14) between the insulation and the exposed aggregate concrete surface. This term was determined by the following procedure. It was estimated that uniformly distributing the volume of entrapped air over the surface area would produce an layer of air about 0.3-in. thick. If the conductivity of still air is $0.0156 \text{ BTU-ft/hr-ft}^2\text{-}^\circ\text{F}$ at 100°F , the conductance of a 0.3-in. air layer is then $0.61 \text{ BTU/hr-ft}^2\text{-}^\circ\text{F}$. The film coefficient resulting from the revised air velocity and inclusion of the air-layer conductance term was $0.0275 \text{ BTU/day-in}^2\text{-}^\circ\text{F}$. This value was used in Runs M-4AQ and F-4AQ and provided better correlation between measured and predicted results. Correlation can be further improved on pre- or post-construction thermal analyses if the film coefficient is changed continuously to reflect the predicted or actual air velocity variation. This requires the film coefficient to be changed for successive time increments. An ABAQUS user subroutine will be required to implement this capability.

Concrete Mixture and Properties

75. Specifications for the concrete mixture used in the Test Wall required a minimum compressive strength of 4,000 psi at 28-days. No specific

requirements were necessary for the structure with respect to type of cement, type of aggregate, and maximum aggregate size. Consideration was given to the need for larger aggregate and cements with heat of hydration limit. It was determined that concrete with 1-1/2-in. nominal maximum-size aggregate and Type I cement produced by a local ready-mix plant was acceptable. This concrete could be reproduced if necessary and was relatively easy to place around embedded instrumentation. It was acknowledged that the use of Type I cement would produce higher temperature rise. Minor thermal cracking was acceptable from the lock-wall repair standpoint. It was determined that the purposes for instrumentation of the structure were better served if the temperature rise, thermal gradients, and resulting thermal strains were higher. Table 7 lists the mixture proportions for the concrete used in the Test Wall.

DFLUX subroutine and the adiabatic temperature rise of concrete

76. Heat generation of concrete in ABAQUS is input by the user subroutine DFLUX. DFLUX passes heat generation rates to ABAQUS for each integration point per element. When used in an incremental construction

Table 7

WES Test Wall Concrete Mixture Proportions

| | |
|---|-------------|
| Cement, Type I | 564.0 lb |
| Coarse Aggregate (1-1/2-in. nominal maximum size) | 1,900.0 lb |
| Fine Aggregate | 1,200.0 lb |
| Water | 233.0 lb |
| Water-Cement ratio | 0.41 |
| Plastic unit weight | 144.5 pcf |
| Designed Compressive strength at 28 days | 4,000.0 psi |

application, DFLUX must be programmed to keep track of heat generation rates versus elapsed time relative to the placement time for each lift. Heat generation of concrete is normally determined by an adiabatic temperature rise test. At the outset of this project, the user was required to convert the adiabatic temperature rise versus age data to heat generation rate versus age data for elapsed times corresponding to calculation times. DFLUX was modified to calculate heat generation rates from user-entered adiabatic temperature

rise data, density, and specific heat for the concrete mixture, and to interpolate between data points when data was not supplied at exact elapsed times corresponding to the calculation time step.

77. Adiabatic temperature rise data for concrete used in the Test Wall was formulated from the initial portion of the measured temperature data at the centers of lifts 4 - 6 and from assumptions of heat generation at later times. It was concluded that the centers of lifts 4 and 5 remained near adiabatic for less than three-fourths of a day. Due to the insulation, the center of lift 6 remained in an adiabatic condition slightly longer. It was apparent that concrete placed at approximately 71°F in lift 5 produced higher temperatures at early times than concrete placed at an average temperature of 63°F in lifts 4 and 6. The phenomenon of accelerated hydration at elevated temperature was expected. Initially, a single adiabatic temperature rise curve from lift 5 was used in the thermal analyses. Later, dflux was modified to permit multiple adiabatic curves to be used and data was entered for the two adiabatic temperature rise functions. The two adiabatic functions used in the thermal analyses are shown in Figure 41. Concrete thermal properties input to dflux for use in the thermal analyses were obtained from tests on the WES Test Wall concrete are listed in Table 8.

Table 8

Thermal Properties of Concrete used in Finite-element Investigation

| | |
|----------------------|--|
| Thermal Conductivity | 2.35 Btu-in/day-in ² -°F |
| Specific Heat | 0.19 Btu/lb-°F |
| Density | 0.08391 lb/in ³ (145 lb/ft ³) |

Summary of Thermal Analyses

78. Over 30 complete finite-element thermal analyses based upon the WES Test Wall were performed during this investigation. Table 9 summarizes the thermal analyses as functions of grid size and time step length. Ambient temperature environments applied and adiabatic temperature rise functions used are also indicated. Table 10 provides a complete list of the analyses that were performed along with pertinent parameters.

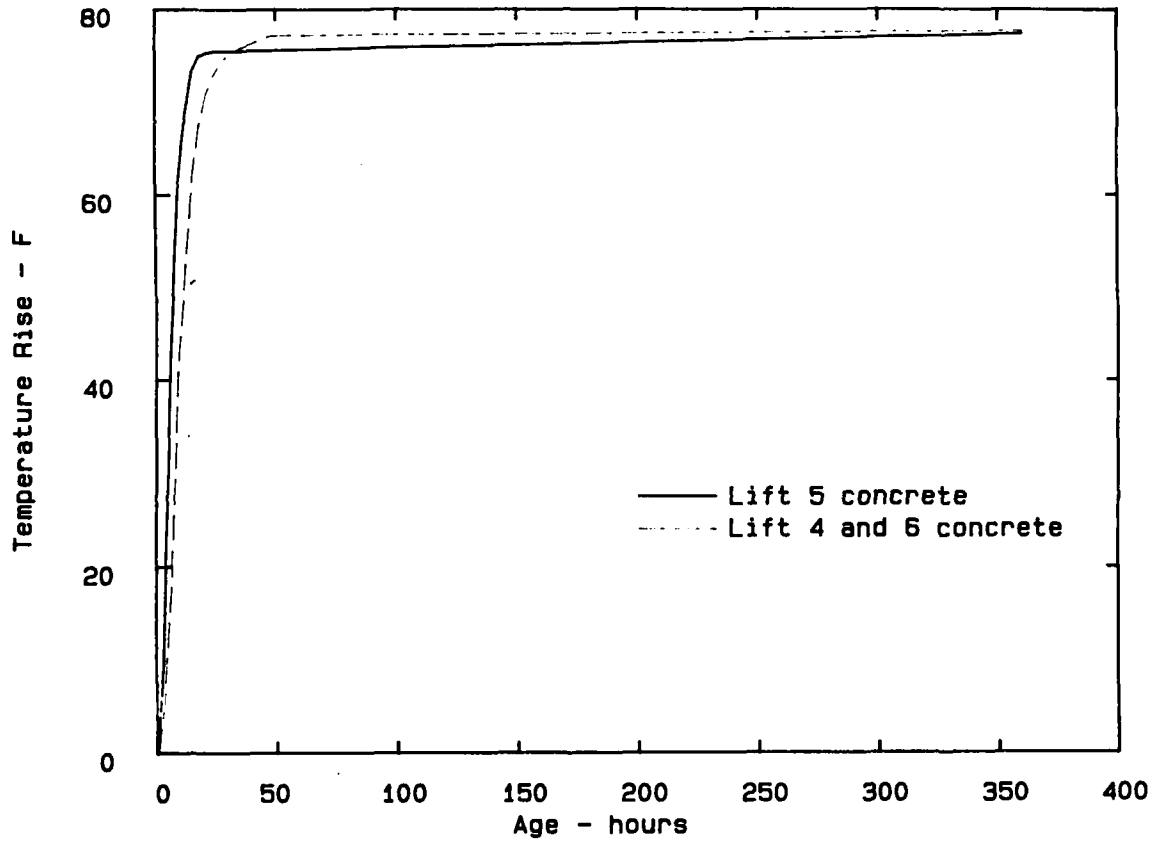


Figure 41. Adiabatic temperature rise curves of concrete for Test Wall

Table 9

Thermal Analysis Run Summary Showing Grid Size/Time Step/
Ambient and Adiabatic Temperature Relationship

| <u>Finite-element Model</u> | <u>Time Step Length in Days</u> | | |
|---------------------------------|----------------------------------|--|----------------|
| | <u>0.125</u> | <u>0.250</u> | <u>0.500</u> |
| W-model | A ¹ | A ^{1,2} | A ¹ |
| C-model | A ¹ ,C ² | A ^{1,2} | A ¹ |
| M-model | A ¹ ,C ^{1,2} | A ^{1,2} ,B ² ,C ² | A ¹ |
| F-model | A ¹ ,C ^{1,2} | A ¹ ,B ² ,C ¹ | A ¹ |

Notes:

Ambient Temperature Environments:

- A - Constant (average) air temperature.
- B - Actual mean daily air temperature variation.
- C - Actual daily air temperature variation.

Adiabatic temperature rise functions used:

- 1 - Adiabatic function from lift 5 used throughout.
- 2 - Adiabatic functions for lift 5 and lift 6 both used.

Table 10
Incremental Construction Formulation
Thermal Analyses Computer Runs

| Finite Element Model** | Run No. | Grid Size* | | Time Step Length (days) | Ambient Air Temperature | Adiabatic Temperature Rise Functions† | Insulated Surface h' for Lift 6†† |
|------------------------|-----------|--------------------|------|-------------------------|-------------------------|---------------------------------------|-----------------------------------|
| | | As In Lift 5 Horiz | Vert | | | | |
| W-model | W-1A | 1 | 1 | 0.250 | T=Const=60F | Single | 0.0571 |
| W-model | W-1B | 1 | 1 | 0.250 | T=Const=60F | Multiple | 0.0571 |
| W-model | W-2 | 1 | 1 | 0.500 | T=Const=60F | Single | 0.0571 |
| W-model | W-3, 3R | 1 | 1 | 0.125 | T=Const=60F | Sngl & Mult | 0.0571 |
| C-model | C-1A | 1 | 2 | 0.250 | T=Const=60F | Single | 0.0571 |
| C-model | C-1B | 1 | 2 | 0.250 | T=Const=60F | Multiple | 0.0571 |
| C-model | C-2 | 1 | 2 | 0.500 | T=Const=60F | Single | 0.0571 |
| C-model | C-3A, 3AR | 1 | 2 | 0.125 | T=Const=60F | Sngl & Mult | 0.0571 |
| C-model | C-4A, 4AR | 1 | 2 | 0.125 | T=Act. Daily | Multiple | 0.0571 |
| M-model | M-1 | 2 | 3 | 0.250 | T=Const=60F | Single | 0.0393 |
| M-model | M-1A | 2 | 3 | 0.250 | T=Const=60F | Single | 0.0571 |
| M-model | M-1B | 2 | 3 | 0.250 | T=Const=60F | Multiple | 0.0571 |
| M-model | M-2 | 2 | 3 | 0.500 | T=Const=60F | Single | 0.0393 |
| M-model | M-2A, 2AR | 2 | 3 | 0.125 | T=Const=60F | Sngl & Mult | 0.0571 |
| M-model | M-3 | 2 | 3 | 0.250 | T=Act. Daily | Single | 0.0393 |
| M-model | M-3A | 2 | 3 | 0.250 | T=Mean Daily | Multiple | 0.0571 |
| M-model | M-4 | 2 | 3 | 0.125 | T=Act. Daily | Single | 0.0393 |
| M-model | M-4A, 4AR | 2 | 3 | 0.125 | T=Act. Daily | Multiple | 0.0571 |
| M-model | M-4AQ | 2 | 3 | 0.125 | T=Act. Daily | Multiple | 0.0275 |
| F-model | F-1 | 4 | 3 | 0.250 | T=Const=60F | Single | 0.0571 |
| F-model | F-1A | 4 | 3 | 0.250 | T=Const=60F | Single | 0.0571 |
| F-model | F-2 | 4 | 3 | 0.500 | T=Const=60F | Single | 0.0393 |
| F-model | F-2A, 2AR | 4 | 3 | 0.125 | T=Const=60F | Sngl & Mult | 0.0571 |
| F-model | F-3 | 4 | 3 | 0.250 | T=Act. Daily | Single | 0.0393 |
| F-model | F-3A | 4 | 3 | 0.250 | T=Mean Daily | Multiple | 0.0571 |
| F-model | F-4 | 4 | 3 | 0.125 | T=Act. Daily | Single | 0.0393 |
| F-model | F-4A, 4AR | 4 | 3 | 0.125 | T=Act. Daily | Multiple | 0.0571 |
| F-model | F-4AQ | 4 | 3 | 0.125 | T=Act. Daily | Multiple | 0.0275 |

* Elements/lift horizontally in half-symmetry model (elements/half of wall).
 ** Model designations are based upon fineness of the grid.
 † Adiabatic temperature rise as a function of placement temperature.
 Adiabatic Function 1: for 60°F placement as in lifts 4 and 6. Adiabatic Function 2: for 70°F placement as in lift 5. SINGLE uses the 70°F adiabatic in lifts 4 - 6. MULTIPLE uses the 70°F adiabatic in lift 5 and the 60°F adiabatic in lifts 4 and 6, respectively.
 †† Surface film coefficient, h' (Btu/day-in²-°F) for lift 6 based upon one or more of: 0.75-in. or 1-in. foil-backed polystyrene insulation, air gap between rough concrete and insulation, and wind velocity. See Paragraph 74.

Discussion of Results

79. At the beginning of Part IV, questions were raised about the criteria needed in the selection of finite-element grid density and time step length for incremental construction analyses. Some of the potential limitations on these parameters are due to restrictions imposed by the finite-element program itself. ABAQUS documentation warns that use of the heat transfer routine must be implemented within the guidelines of element size, thermal properties, and time step length as specified in Equation 13 in Paragraph 50. Determination of optimum finite-element grid density or element size in incremental construction analyses must be considered in the context of the width and height of individual lifts as well as the entire structure. The rate at which heat is internally generated and rates that the thermal boundary environments change are additional considerations in determining optimum grid size/time step length relationships.

80. Obviously, selection of small elements and small time steps would guarantee accurate results. However, the computer hardware resources and computational time for even small problems can easily become unbearable. Optimization of grid density and time step length is necessary for practical problems involving prototype mass concrete structures using two-dimensional analysis. This optimization is critical when performing three-dimensional analysis because computer resources can easily be exceeded. Resources can be severely taxed even in a supercomputer environment especially when memory or disk storage limitations or both are imposed on individual applications.

81. The finite-element analyses in this investigation were based upon construction of the WES Test Wall. Obviously, simulation of the actual conditions of construction would not have easily provided fundamental relationships between grid density and time step requirements because of the complexity of the problem. Therefore, the initial phase of the analyses were performed with a simplified boundary environment and with a single adiabatic temperature-rise function for all concrete placements. The objective was directed toward comparative analyses across the matrix of grid densities and time step lengths. Later, improved adiabatic functions, surface heat transfer coefficients, and actual daily temperature variations were incorporated. This was done to assess grid density and time step lengths for problems where the effects of daily temperature or daily heat flux (such as solar radiation)

variation or both are desired. This final series of analyses were also used as validation of computed results when compared with measured values. It also provided a means to evaluate and fine-tune surface boundary conditions.

Element size and time step sensitivity analyses with constant air temperature

82. A large portion of the finite-element analysis runs in this investigation were conducted to evaluate basic element size and time step length sensitivity. In all cases these analyses used a constant air temperature of 60°F which was the mean temperature during the construction of lifts 4 - 6 in the Test Wall. Time steps of 0.125, 0.25, and 0.50 days were used in analyses of each of the four finite-element models. The selection of the finite-element models encompassed a range of finite-element grids that extended from very coarse to very fine. It was felt that the grid densities selected ranged from too coarse to too fine so that limits on grid density could be determined.

83. Some of the element size/time step combinations were intended to violate the restrictions in equation 13 discussed earlier. Table 11 shows the matrix of element sizes versus time steps lengths. The fundamental analyses designated by "A" were conducted for all 16 cases of element size and time steps. The solid line drawn through the table is a partition between those runs that met and those that did not meet the criteria.

84. Figures 42 - 44 show predicted temperatures versus element size for 0.125-, 0.25-, and 0.5-day time steps, respectively. The results from the medium-grid M-model and the fine-grid F-model were identical and are assumed to be accurate, limiting values. In all cases predicted temperatures from the W- and C-models at the center of lift 5 deviate from the desired results obtained with the M- and F-models. This is to be expected because the element dimension/time step requirements of equation 13 are violated for all analyses with the W- model and those with 0.125- and 0.25-day time steps with the C-model. From Table 9, the element dimension/time step criteria are not violated for a time step of 0.5 days. However, predicted temperatures with the C-model at a time step of 0.5 days show about the same difference as with the smaller time steps when compared with temperatures from the M- and F-models. This seems to indicate that the C-model is too coarse for precise temperature calculations. Comparison of these data indicated that the observations noted above apply primarily to predicted temperature during the

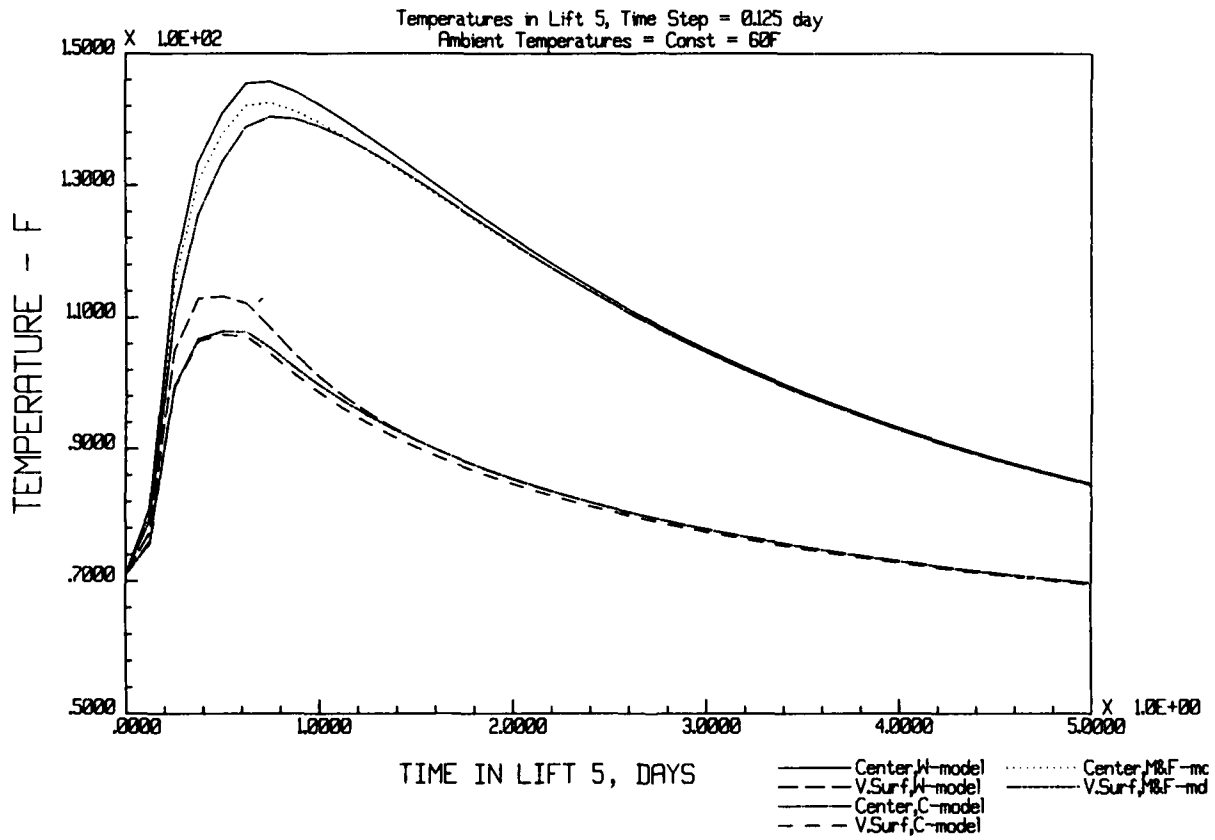


Figure 42. Predicted temperatures versus element size for time step of 0.125 days

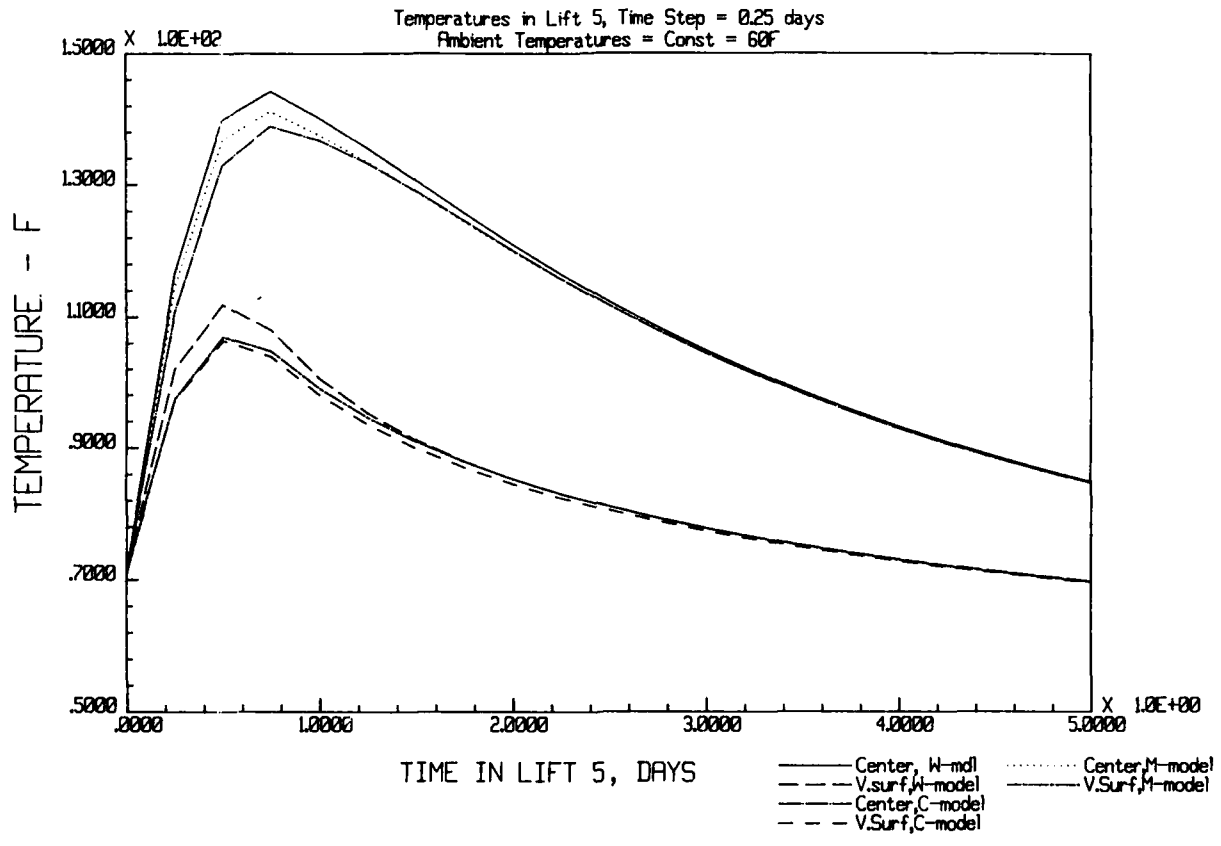


Figure 43. Predicted temperatures versus element size for time step of 0.25 days

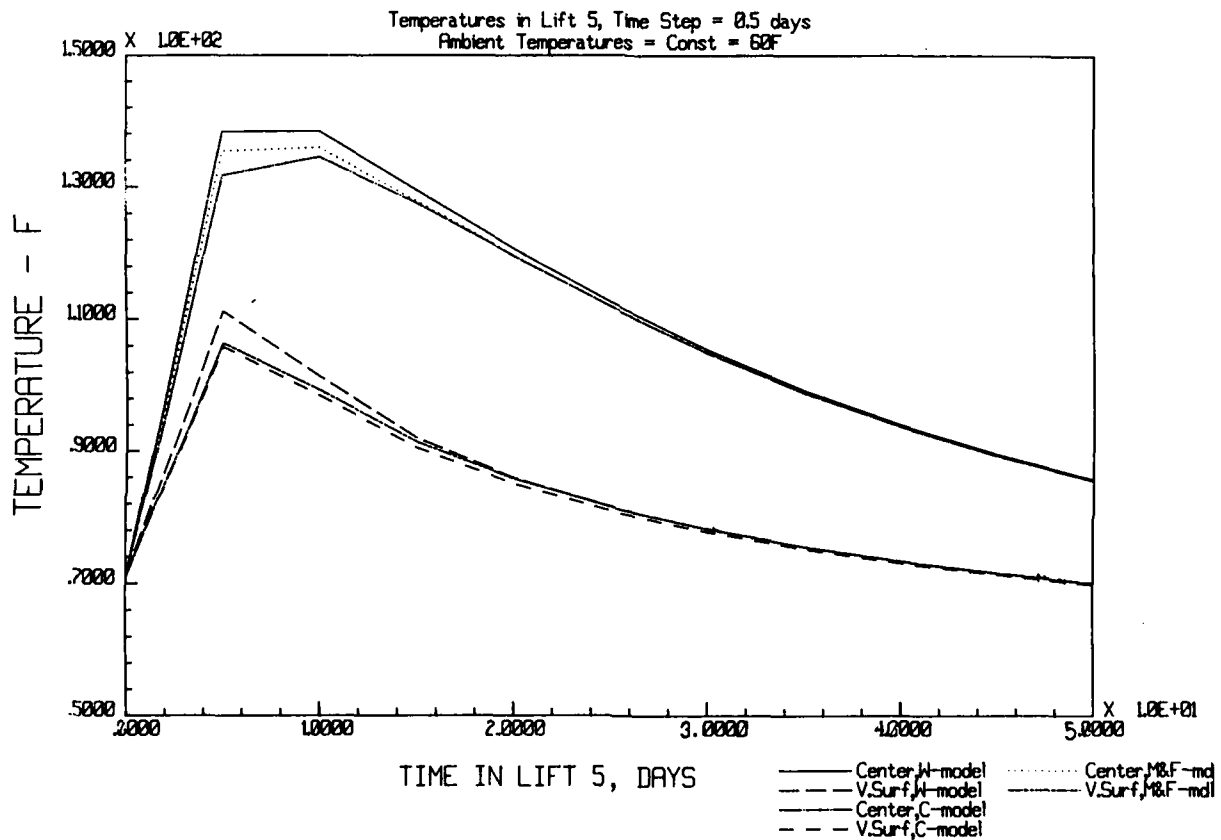


Figure 44. Predicted temperatures versus element size for time step of 0.50 days

Table 11

Minimum Time Step Lengths, t (days) Required by ABAQUS from Equation 13
for Incremental Construction Thermal Analyses of WES Test Wall.

Computed for Typical Element Dimension (l) Equal
to One-Half Length of a Side of an Element

| Finite-element Model | l (in.) | Direction of l | Time Step Lengths Used | | |
|-------------------------|------------|-------------------|------------------------|--------|--------|
| | | | 0.125 | 0.250 | 0.500 |
| W-model | 28 | Vertical | 0.886* | 0.886* | 0.886* |
| | 18 | Horizontal | 0.366* | 0.366* | 0.366* |
| C-model | 14 | Vertical | 0.222* | 0.222 | 0.222 |
| | 18 | Horizontal | 0.366* | 0.366* | 0.366 |
| M-model | 9.33 | Vertical | 0.098 | 0.098 | 0.098 |
| | 9 | Horizontal | 0.091 | 0.091 | 0.091 |
| F-model | 9.33 | Vertical | 0.098 | 0.098 | 0.098 |
| | 4.5 | Horizontal | 0.023 | 0.023 | 0.023 |

* Required minimum time step exceeds time step used. Time step length criteria violated for values above dividing line in table.

first 1 - 2 days after placement. It is important to note that after an elapsed time of 2 days, the differences in results from the four models become small.

85. Figures 45 - 47 show predicted temperature gradients horizontally across the width of lift 5 at 0.25, 0.50, and 1.0 days after concrete placement with a time step of 0.25 days. It is apparent that the results from the M- and F-models are virtually identical at all locations. Only two points are computed with the W-model, at the center and surface. In all cases the center and surface temperatures are higher than those produced from the finer grids. Predicted temperatures from the C-model compare favorably with those

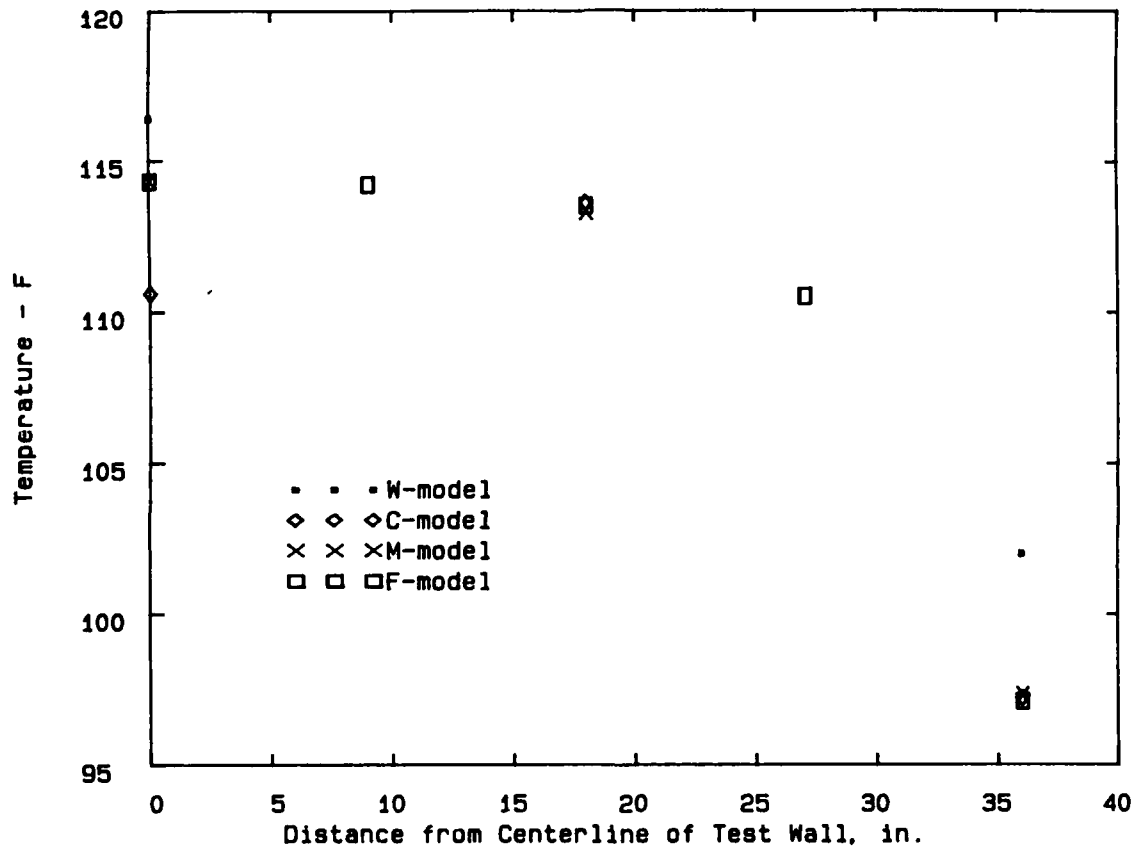


Figure 45. Horizontal temperature gradients versus element size at 0.25 days after placement of lift 5

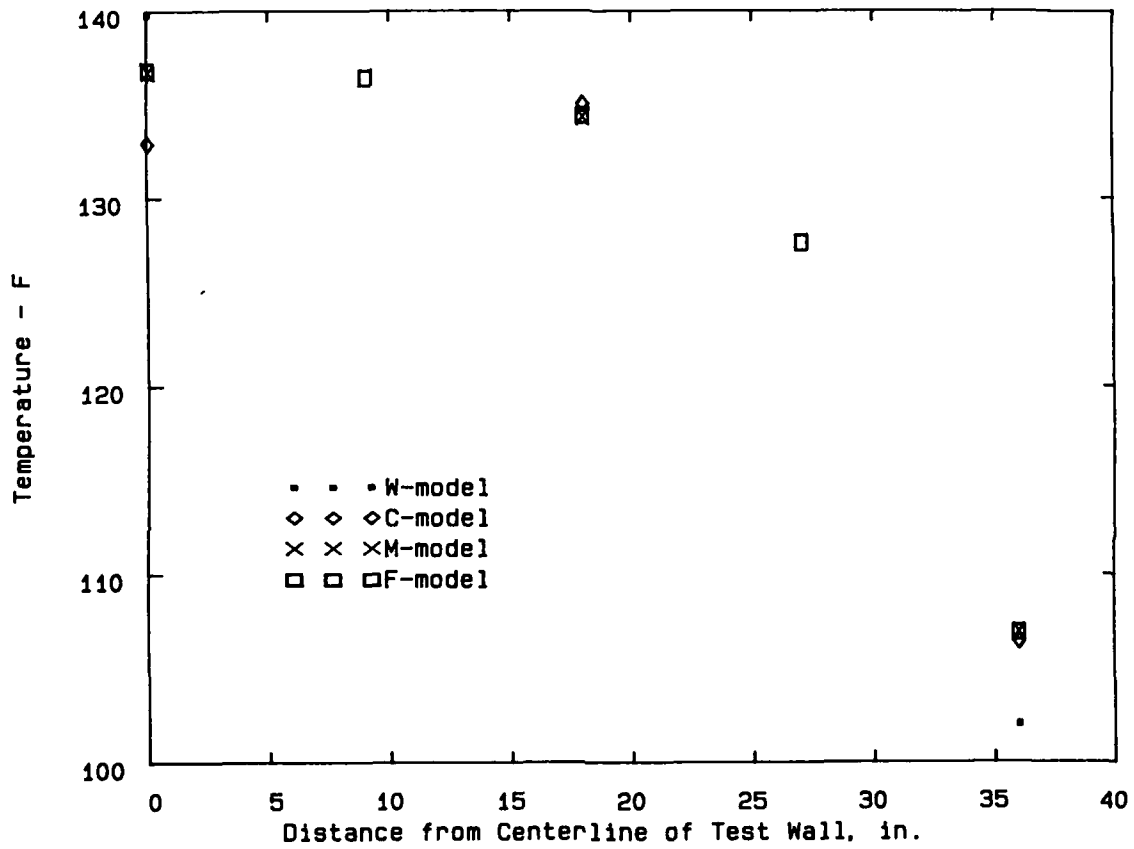


Figure 46. Horizontal temperature gradients versus element size at 0.50 days after placement of lift 5

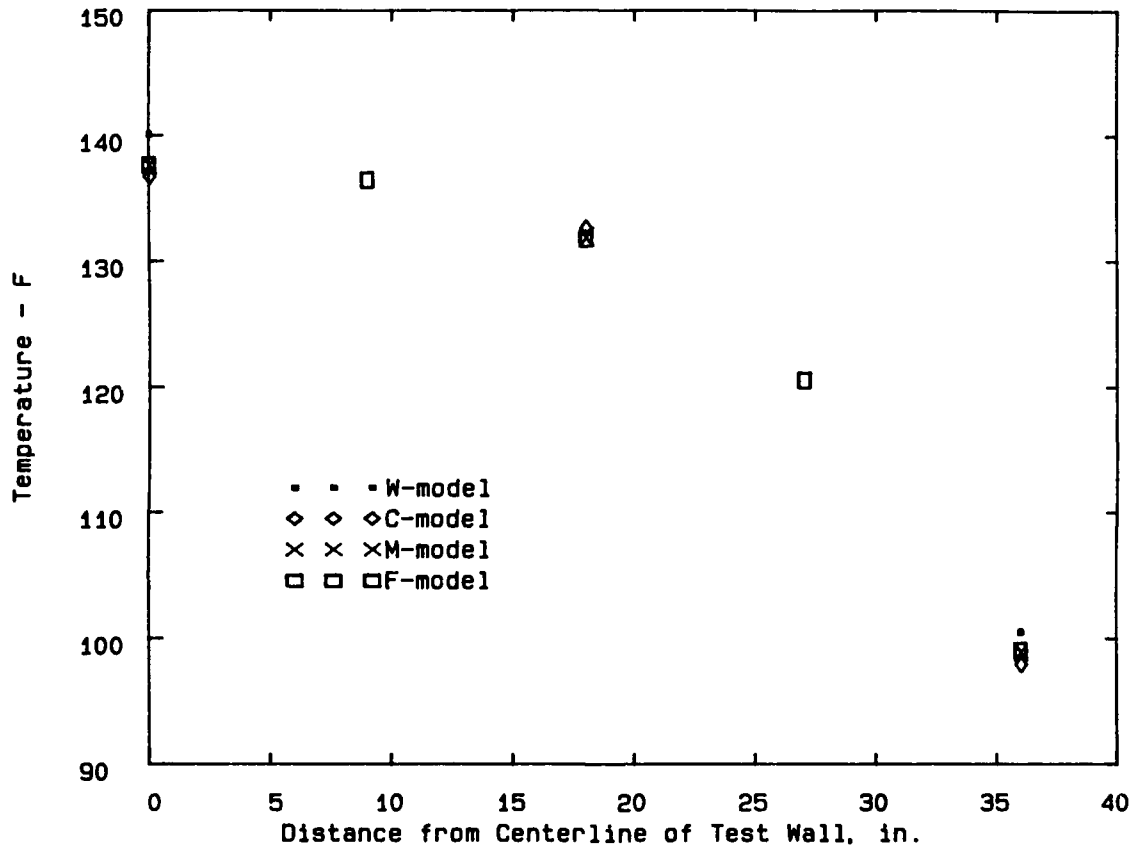


Figure 47. Horizontal temperature gradients versus element size at 1.0 days after placement of lift 5

from the M/F-models at the surface and a point half way to the center. Lower temperature actually occurred at the centerline. Predicted temperatures at the centerline were less than at the half-way point at elapsed times of 0.25 and 0.50 days. This is a clear indication of the spurious oscillations referred to in the ABAQUS manual. By an elapsed time of 1.0 days, predicted temperatures for all models had converged to within 1°F of each other.

86. Figures 48 - 50 show predicted temperatures at the center of lift 5 for time steps of 0.125, 0.25, and 0.50 days with the W-model, C-model, and M/F- models, respectively. Peak temperatures in lift 5 are reached at around 0.75 days. Predicted temperatures in Figures 48 - 50 are affected similarly by increased time step length. Peak temperatures are reduced by approximately 10 percent at a time step of 0.5 days due to the large time step. In all cases predicted temperatures at elapsed times greater than 2.0 days are within 2°F of each other for all models and time step lengths.

Element size and time step sensitivity
with variable ambient air temperatures

87. During most of the incremental construction thermal stress investigations conducted to date, ambient air temperature histories used have been the expected mean daily temperatures for the location of the structure being investigated. The effects of daily air temperature variation have essentially been ignored or were not considered to be significant. However, initial crack surveys of some structures seem to indicate that the surfaces of mass concrete structures that face to the south experience more cracking than those surfaces facing north*. The effect of daily air temperature variation supplemented by the effects of solar radiation and re-radiation on mass concrete surfaces during the period following placement invites analysis. In order to minimize computer costs it is important that the finite-element grids contain the minimum number of elements and that computation time steps be as large as possible while still accurately reproducing the effects of daily temperature variations.

88. Figure 51 shows predicted temperatures at the center and vertical surfaces of lift 5 for the C-model, M-model, and F-model at a time step of 0.125 days when exposed to the actual daily air temperatures that were measured during and following placement of lift 5 in the Test Wall. It should

* in the northern hemisphere.

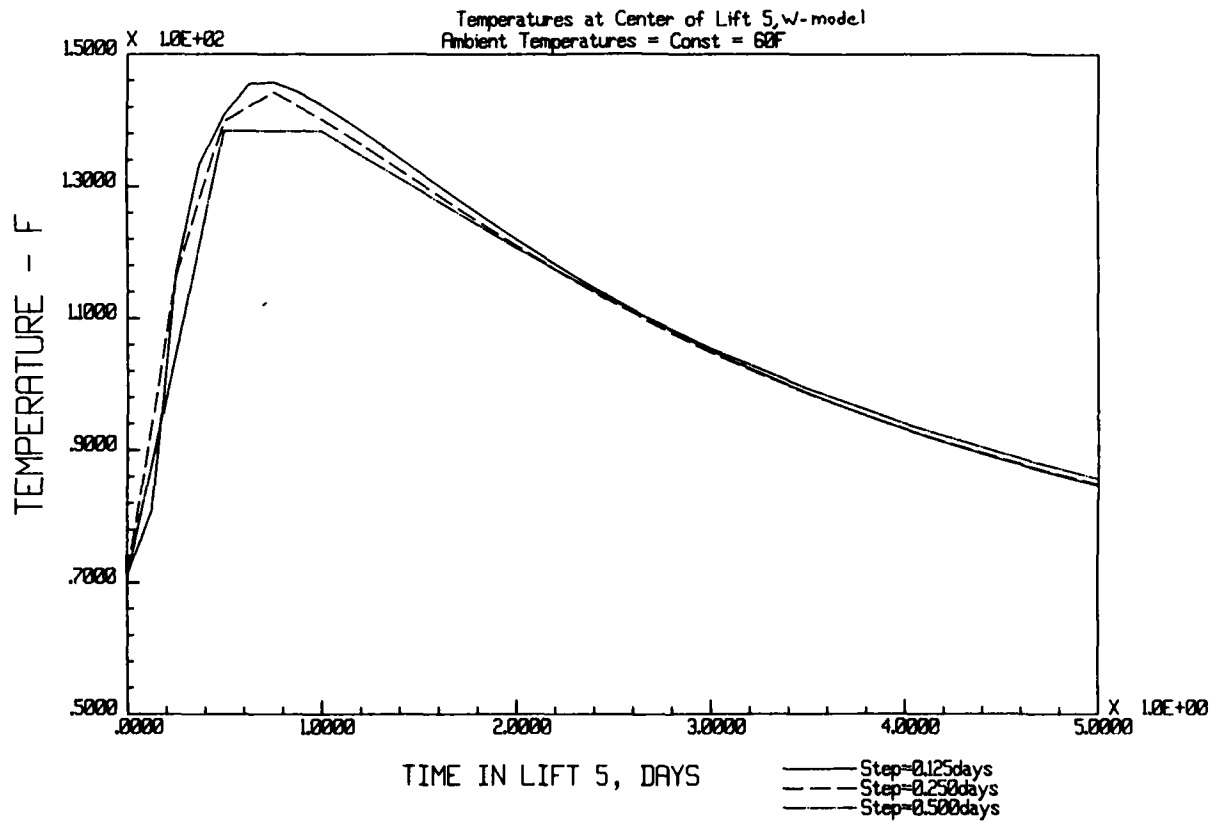


Figure 48. Predicted temperatures versus time step length in W-model

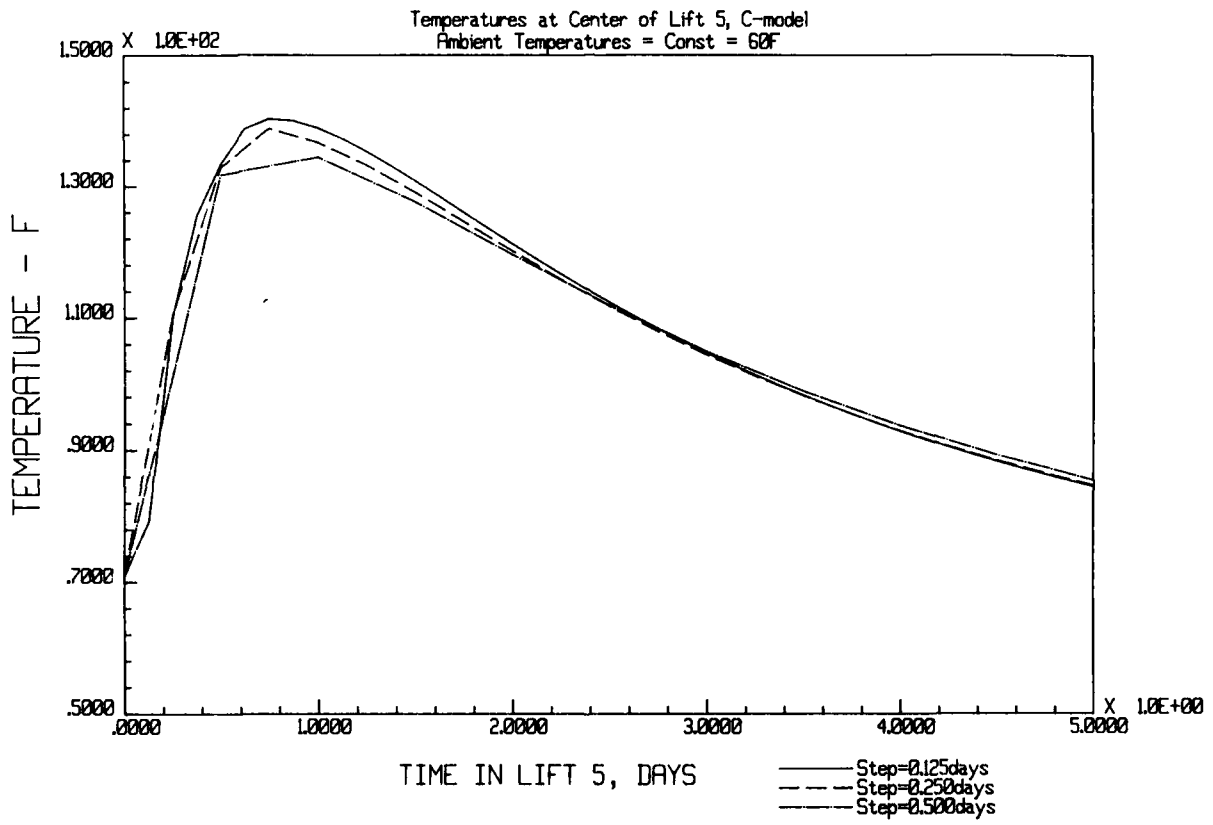


Figure 49. Predicted temperatures versus times step length in C-model

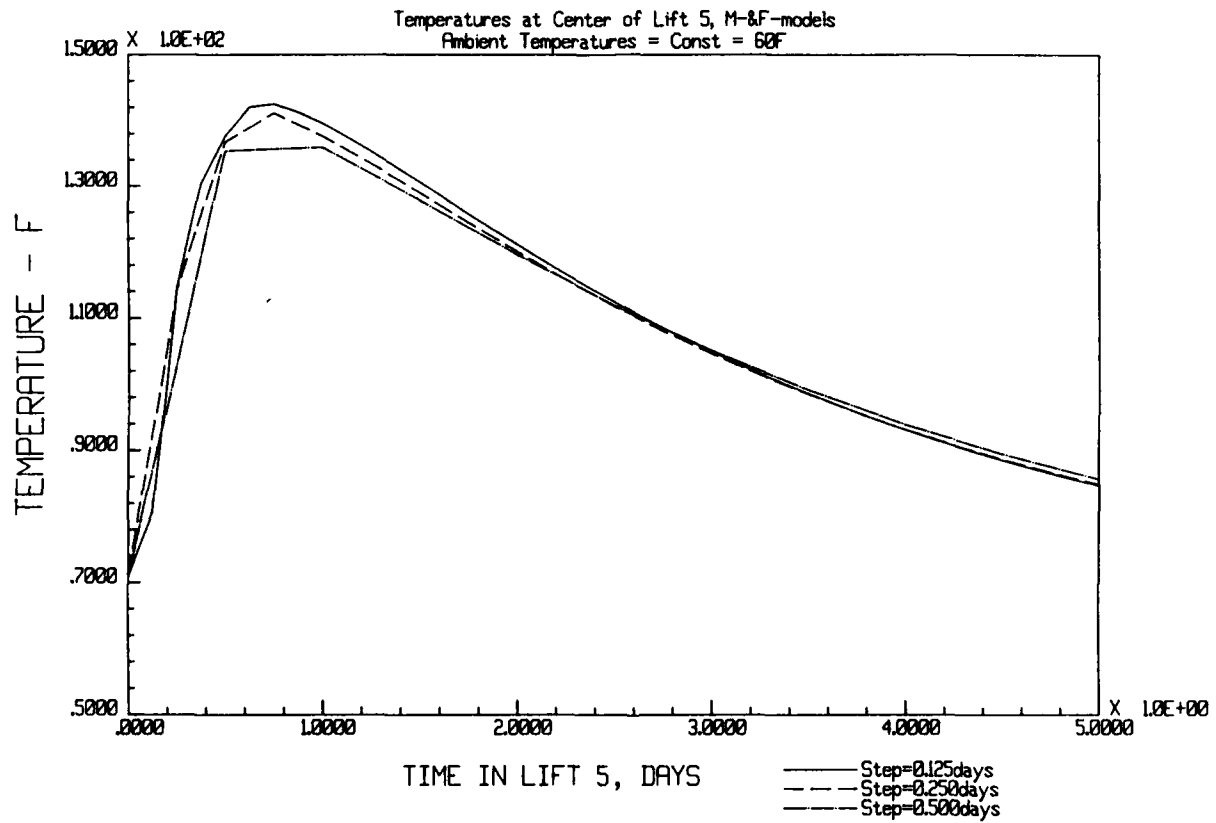


Figure 50. Predicted temperatures versus time step length in M- and F-models

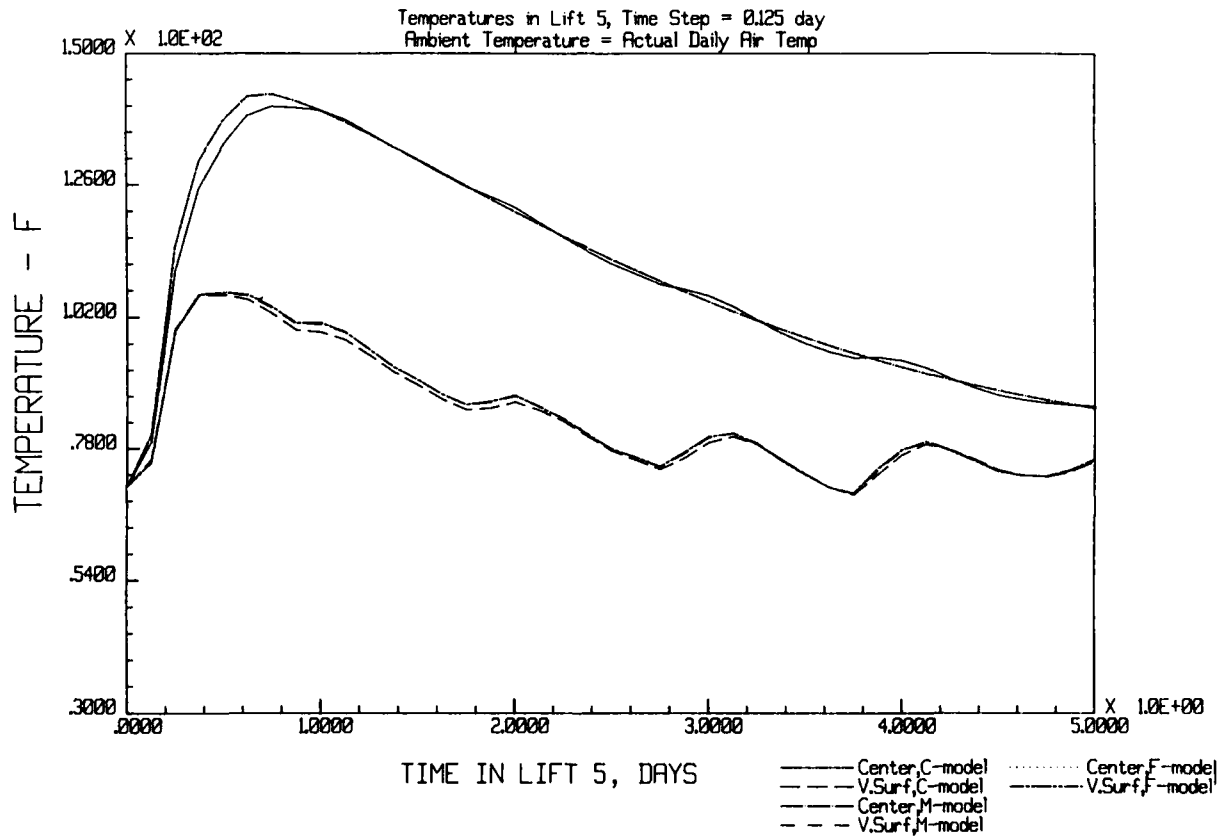


Figure 51. Predicted temperatures versus element size
with actual daily air temperatures

be noted that the C-model violates the restrictions of equation 13 when used with this time step. The predicted temperatures from the M- and F-models are identical. Surface temperatures computed with the C-model compare favorably within 1 - 2°F to those of the M- and F-models for the daily air temperature variation that followed placement of lift 5. It is not known if the differences in results between the C-model and the finer models are due to violation of equation 13 or because of the coarseness of the model horizontally. Therefore, it would be prudent to meet the criteria of equation 13 especially when reproduction of the near-surface gradient is critical for thermal stress computation with daily air temperature or other daily surface heat flux variation.

89. Figure 52 shows predicted temperatures in the F-model at time step lengths of 0.125 and 0.50 days when exposed to actual daily air temperature variation. Although not shown here, the results using the M-model were virtually identical. The results shown in Figure 52 indicate that a time step of 0.25 days will model temperatures adequately especially at times greater than 1.0 days after placement.

Comparison of measured and predicted results

90. Up to this point, all comparisons have been made against predicted results. It is important to establish that predicted temperatures compare well with measured temperatures. Figure 53 shows predicted and measured temperatures in lift 5 with daily air temperature variation and predicted temperatures with average daily air temperature variation. These were achieved with the M-model using a time step of 0.25 days. Virtually identical results were obtained with the F-model at the same time step. During the first 5 days after placement the concrete surfaces were covered with polyethylene membrane and cured with water as described in Paragraph 71. A composite heat transfer coefficient equivalent to still air was used as described in Paragraph 73. The results shown in Figure 53 show reasonable comparison between measured and computed results considering the problem of modeling the complex curing condition used. This is especially true for analyses where mean daily air temperature environment was used. The predicted surface temperatures representing average surface temperatures compare well with measured values. Computed temperatures at the center also correlated very well with measured temperatures.

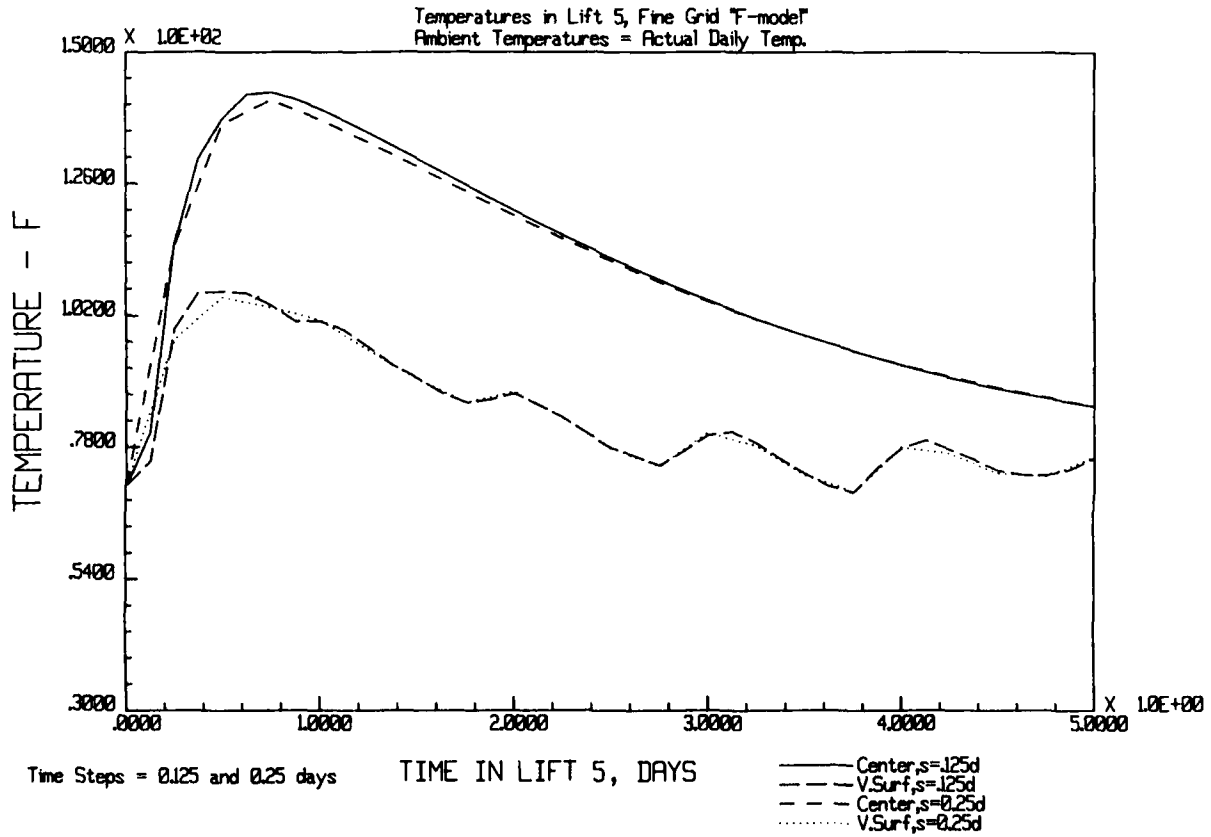


Figure 52. Predicted temperatures versus time step length in F-Model with actual daily air temperatures

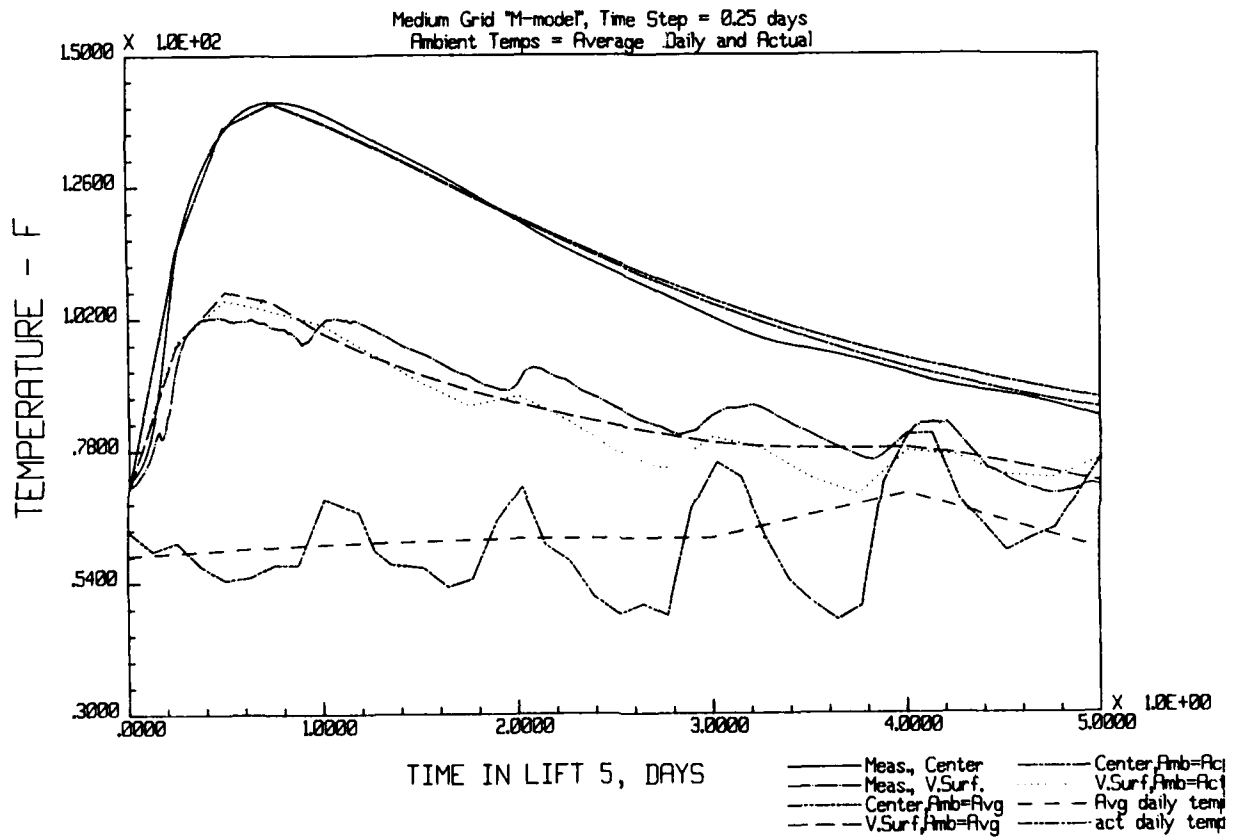


Figure 53. Measured and predicted temperatures at the center and vertical surface of lift 5 with mean daily and actual daily air temperatures

91. Computed surface temperatures when actual daily air temperatures were used do not correlate quite as well with measured surface temperatures. It is believed that the heat transfer coefficient for polyethylene membrane curing discussed in paragraph 72 should have included an insulation component for the conductance of entrapped air instead of assuming that the polyethylene membrane merely reduced the air velocity. Adding the insulating effect for the entrapped air would have lowered the film coefficient, thereby, increasing surface temperatures resulting in better agreement with measured values. However, the thickness of the entrapped air layer would have been arbitrary because the film was not maintained at constant thickness. Although it was concluded that the effect of water curing on the north face of lift 5 was negligible due to the very low flow rate, water curing added to the complexity of the problem.

92. Figure 54 shows predicted and measured temperatures in lift 6 which was insulated for most of the first 3 days after placement. These results were obtained with the M-model at time steps of 0.125 days. Because the air temperatures were much colder during and immediately following placement of lift 6, the boundary conditions were treated differently than for lift 5. A composite surface heat transfer film coefficient sequence was developed to represent the changes in boundary conditions during the time following placement of lift 6. This information is listed in Table 12.

93. The results shown in Figure 54 compare favorably with measured results. The air velocity of 4.5 mph used was an average for the 5 days following placement. If the actual variation in wind velocity was used by varying the heat transfer coefficient several more times, the correlation during the time step would have been even better. A question did arise regarding the measured temperature on the north surface of lift 6 during the insulation period. The manner of applying the insulation did permit some heat losses especially from the vertical surfaces.

94. Figure 55 presents comparison of measured temperatures from the south, north, and top surfaces of lift 6 with calculated vertical surface temperatures. When compared to these data the predicted temperature history lies within the band of measured temperatures at least during the 3 days before the insulation is removed. After 3 days the predicted temperatures are cooler. The heat transfer coefficient based upon 4.5 mph is probably excessive during this time.

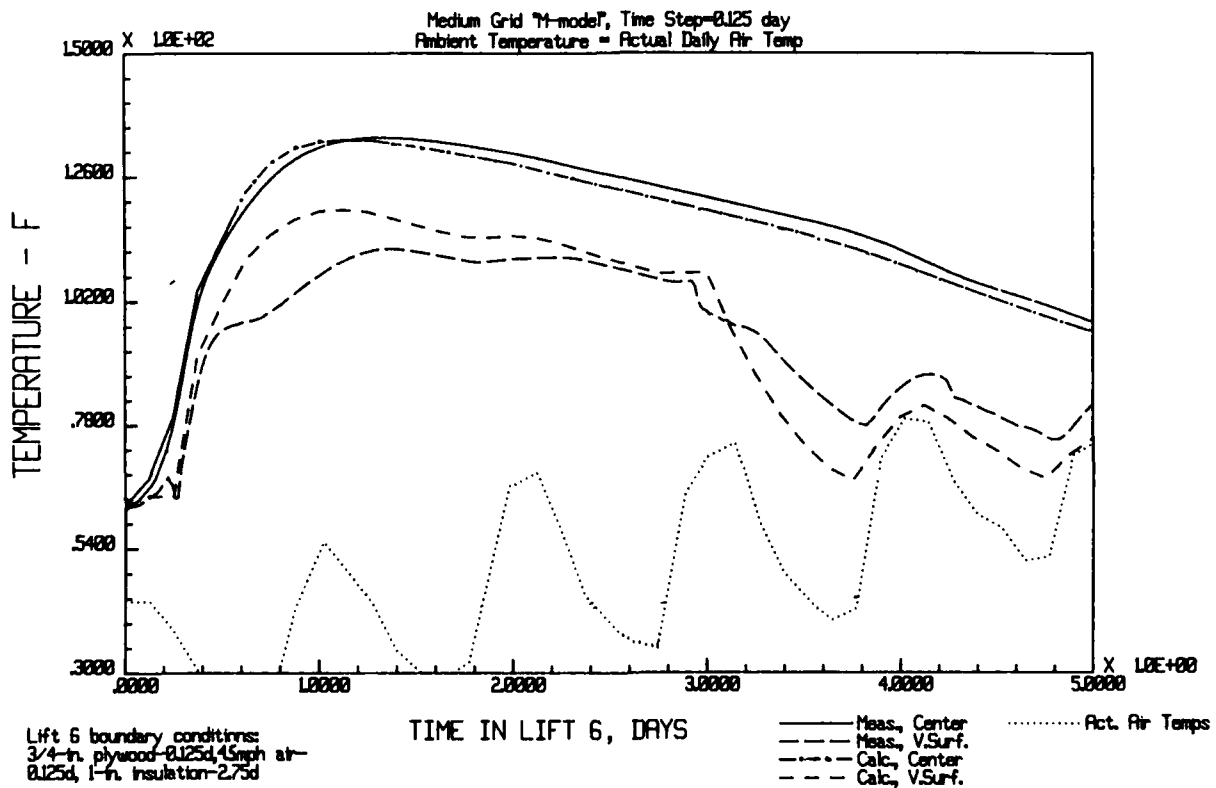


Figure 54. Measured and predicted temperatures in insulated lift 6 with actual daily air temperatures

Table 12

Final Sequence of Heat Transfer Film Coefficients Used for Lift 6

| <u>Elapsed Time After Placing Lift 6 (days)</u> | <u>Description of the Boundary Condition</u> | <u>Surface Heat Transfer Coeff. (h') (Btu/day-in²-°F)</u> |
|---|---|--|
| 0.000 - 0.125 | <u>Vertical Surface:</u> 3/4-in. plywood + 4.5-mph air velocity | 0.1000 |
| | <u>Top Surface:</u> 4.5-mph air velocity | 0.3200 |
| 0.125 - 0.250 | <u>All Surfaces:</u> Exposed Concrete + 4.5-mph air velocity | 0.3200 |
| 0.250 - 3.000 | <u>All Surfaces:</u> 1-in. styrene w/foil + 4.5-mph air velocity | 0.0275 |
| 3.000 - 8.000 | <u>All Surfaces:</u> Exposed Concrete + 4.5-mph air velocity | 0.3200 |

Lift interface equilibration

95. New concrete is often pre-cooled as a means of controlling subsequent thermal stress due to heat of hydration-induced temperature changes and the interaction with ambient temperatures. This usually causes the temperature of the freshly placed concrete to be substantially cooler than the temperature of the surface upon which it is placed. During placement, the interface temperature will immediately equilibrate to an intermediate temperature. This process rapidly cools the existing concrete surface possibly inducing damaging tensile strains.

96. When this condition is expected in a structure being investigated using incremental finite-element thermal stress analysis, it may be necessary to explicitly model the thermal equilibration of lift interfaces. Otherwise, incorrect thermal loading and incorrect computed thermal stains may result. Interface equilibrium is accomplished in ABAQUS by using a thermal interface element between the old and new concretes that effectively has infinite conductivity and is able to average the surface temperatures of the existing concrete and the new concrete at the common nodal points. Use of this modeling technique was to be performed in this investigation and results evaluated with measurements in the Test Wall. However, it was discovered that

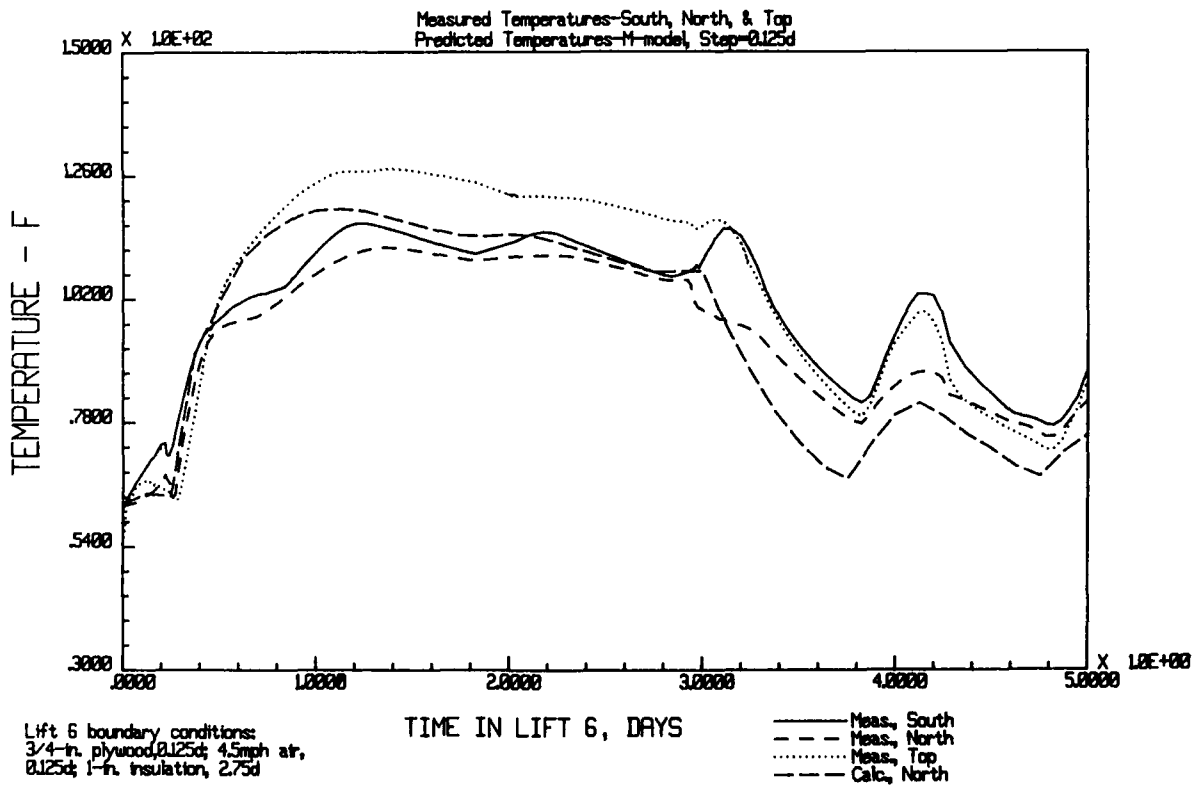


Figure 55. Comparison of predicted surface temperatures with variation in measured surface temperatures in insulated lift 6

the concrete placement temperatures and exposed top surfaces of existing concrete were nearly equal for every placement. Apparently ambient temperatures affected placement temperatures of fresh concrete, which were not controlled, and the old concrete surfaces similarly. By late morning when placement of concrete was made, surface temperatures warmed to near placement temperature. Thus, when temperature differences between new and old concrete did exist, the old concrete was always slightly cooler. Since, no appreciable difference in temperature existed between placement temperatures of the new concrete and the top surface temperature of the existing concrete, the procedure to model interface temperature equilibrium was not implemented.

97. Figure 56 shows measured temperatures in the vicinity of the lift 5/lift 6 interface prior to and following placement of lift 6. It is apparent that the existing temperatures at the top of lift 5 are nearly the same as the initial concrete placed in lift 6. No abrupt change in the lift 5 concrete is seen at time = 0 days which occurs at the time of placing lift 6. In reviewing the measured strain data, similar behavior was observed. That is, no abrupt change in strain was observed at placement time.

Conclusions

98. The conclusions that follow are presented as criteria to be applied in selection of certain parameters used in incremental construction analyses and to identify the state-of-the-art. All conclusions relative to grid density or element size and time step sensitivity are based upon results obtained with the two-dimensional, 8-node heat-transfer element (DC2D8). For purposes of evaluating compliance with ABAQUS requirements with Equation 13, basic element side dimensions are one-half the length of the side of the element or the distance from mid-side to corner nodes.

Element size and time step sensitivity with constant air temperatures

99. Presented below are concluding remarks based upon the thermal analyses conducted with constant air temperatures or slowly changing air temperatures such as those characteristic of seasonal rather than daily temperature variations. The guidance supplied should be followed to avoid calculating errors in temperature distribution or thermal stress during thermal studies that can result from improper grid selection or calculational

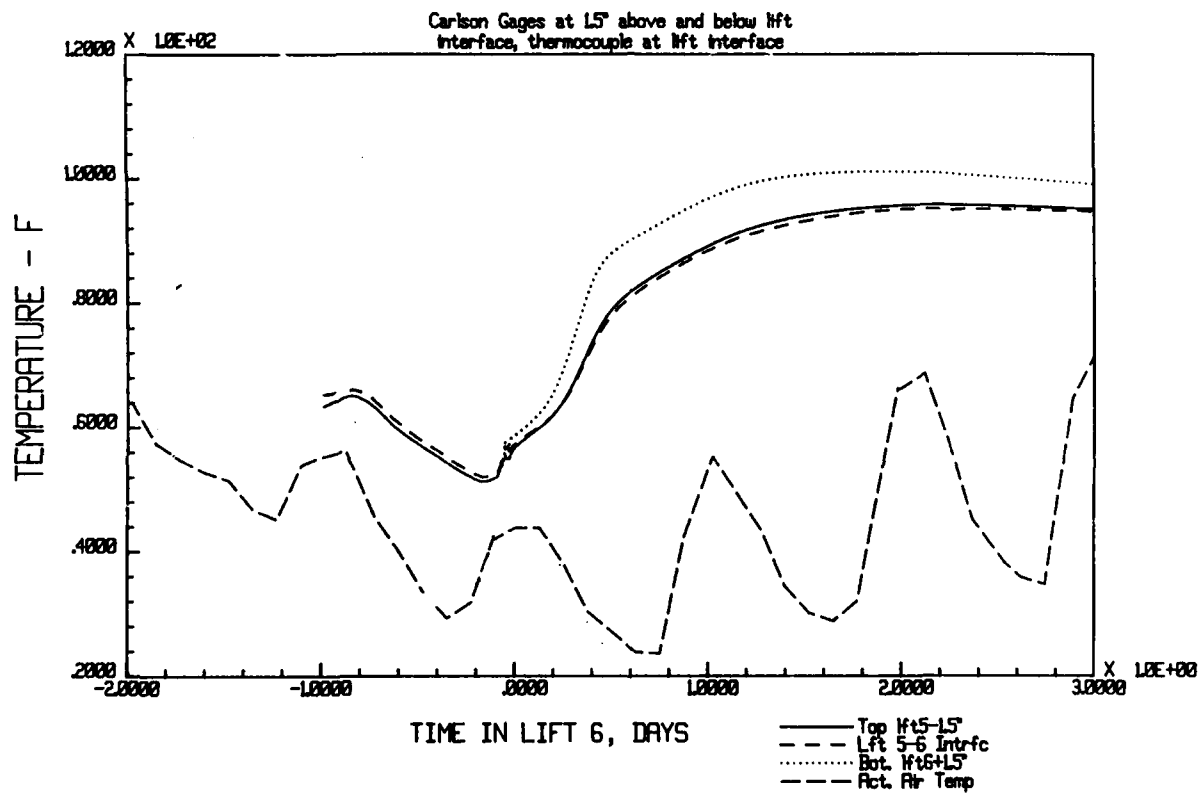


Figure 56. Measured temperatures at lift 5/lift 6 interface before and after placing lift 6

time steps. The guidance supplied is intended to apply to small and large structures or structural elements. It is recommended that the requirements of equation 13 for grid size and calculational time step be carefully considered. Otherwise, spurious oscillations can occur within the computed temperature distributions to cause error in resulting thermal stresses.

- a. Use of one element per lift vertically in massive monoliths with many lifts or one element per lift horizontally in a narrow segment of a structure should be avoided. If used, analyses should be limited to those cases in which only rough estimates of temperature distribution are needed and no subsequent thermal stress analyses should be made.
- b. Use of two elements per lift in the vertical direction and two elements (one element in a half-symmetry model) horizontally in a narrow segment of a structure should also be avoided. This is especially the case when the heat of hydration rate is very high during the first day or so after placement. The exception is when the height and width dimensions of the lift are much less than 5 ft. Otherwise the criteria of Equation 13 will be violated and temperature errors up to at least 10 percent can then be expected during the first day. If this level of error can be accepted during the first day or so after placement, this grid density will produce adequate results thereafter.
- c. Use of at least three elements per lift in the vertical direction and at least four elements (two elements in a half-symmetry model) in the horizontal directions are recommended for all lifts when these dimensions are 5 - 6 ft or when a higher degree of accuracy is required. This should avoid violating the time step criterion of Equation 13.
- d. A different criterion should be used for lifts higher than or structure segments wider than 6 ft. From the practical standpoint, elements in the center of lifts that are 7 to 10 ft high may be larger for a given time step required by Equation 13 as long as the width of the section is at least equal to the height and temperature changes across the element within the time step are small. Similarly, continuous, horizontal structural segments much wider than 10 ft and with reasonable lift height may be composed of elements whose horizontal dimensions substantially exceed the requirements of Equation 13 provided that very small or insignificant temperature changes are expected, horizontally. Sporadic oscillation can be expected to be very small or non-existent. Elements must still have acceptable aspect ratios consistent with subsequent stress analyses and have acceptable numbers of elements in the primary direction of heat flow. Tests to verify grid density may be necessary if doubt exists for a particular finite-element modeling problem.

- e. A time step of 0.125 day is necessary to guarantee accurate results during rapid temperature changes that can occur during the first several days after placement or at any other time when rapid temperature change occurs. However, a time step of 0.25 day usually produces reasonable and probably acceptable results in most applications. Time steps equal to 0.5 days can usually be applied safely at times greater than 2 to 3 days after placement. Use of shorter time steps should always be employed when doubt exists and tests for the appropriate time step to be used in a specific situation have not been made.

Element size and time step sensitivity
with variable ambient air temperature

100. Presented below are concluding remarks based upon the thermal analyses conducted with actual daily air temperatures. They are offered to provide additional guidance beyond the criteria presented above in paragraph 99 when thermal analyses include daily temperature variation or rapid changes in temperature such as during passage of cold weather fronts.

- a. Use of at least three elements per lift in the vertical direction and four elements (two elements in a half-symmetry model) in the horizontal directions are recommended for all lifts whose dimensions are nominally 5 ft or when a higher degree of accuracy is required.
- b. A time step of 0.125 day is necessary to produce accurate results. A time step of 0.25 day, however, does produce reasonable results as long as the daily temperature change is moderate and solar radiation effects are not considered. Time steps greater 0.25 days should not be used. These criteria should be applied during the times when any heat flux or rapid cooling phenomena are applied.
- c. The element size criteria permitting large elements in thick lifts or wide structural sections presented in Paragraph 99 may be applied safely for interior elements as long as temperature changes within a time step for these elements are small.

Concrete properties

101. Certain concrete properties are strongly affected by placement temperature and certain concrete constituent materials. This is the case for adiabatic temperature rise during the first day or so after placement as well as some of the early-age mechanical properties of concrete such as modulus of elasticity and creep. Knowledge of the potential variability of concrete properties as functions of placement temperature, age, and concrete materials for a specific project is important if incremental finite-element thermal stress analyses of mass concrete structures are to reflect the field conditions during construction. In certain projects where placement

temperature will be constant year around, the concrete properties should be determined for the given placement temperature. However, if the placement temperature specifications are such that a range of placement temperatures are possible, seasonally, concrete properties used in incremental construction thermal studies should reflect the potential variation.

Curing, boundary conditions, and modeling of surface heat transfer film coefficients

102. Simulation of the thermal boundary conditions and curing procedures used during construction of the WES Test Wall presented certain problems during this investigation that have implications for future finite-element analyses of structures incrementally constructed. The problems are two-fold. First, when a complex curing condition is employed, such as the combination of water and application of a polyethylene membrane on a rough surface, a scheme to model the heat exchange provided by this condition must be developed resulting in a single, composite surface heat-transfer coefficient. Secondly, the heat-transfer coefficient(s) must reflect the effects caused by variability in the application or implementation of the curing condition.

103. The first problem is primarily one of idealizing how the prescribed curing treatment should be modeled. The second problem is induced by variability in the application of the curing treatment. For example, modeling the effect of water curing during which the surface was also covered by a plastic film required several trial finite-element analyses each with different surface heat-transfer film coefficients before an acceptable value was found. The task involved integrating effects of the flow of a thin film of water at an unknown rate, application of plastic film on a rough surface, and the wind velocity into a single coefficient value. The value finally used (equivalent to still air) in evaluating the north face of lift 5 was actually reasonable for the combined conditions where a low rate of water flow caused little cooling, a layer of air existed between the plastic film and concrete, and the sky was generally overcast. This value had not evident initially, however, and was found to require additional refinement when daily air temperature variation was simulated.

104. The second problem in simulating the surface film coefficient was variability in application of the curing condition. This problem is characterized by the following examples. In one example differences in the rate at which water flowed down the south and north surface was apparent

because the two surfaces cooled differently on overcast days following placement when direct solar radiation was not a factor. Another example was variability in the air space between the plastic film and concrete surface. A final example was variability in application of the insulation on lift 6 following placement. Apparently, small gaps between adjoining insulating panels or poor contact with the concrete surface caused differences between measured surface temperatures in lift 6 at several locations.

105. With these factors in mind it is important during future finite-element incremental construction investigations of mass concrete structures to realistically identify the curing conditions and the variability expected in their implementation. Otherwise, considerable error between predicted and actual conditions is possible.

Recommended future efforts

106. Additional efforts are desirable beyond the scope of this investigation to further define the incremental construction formulation for use in future mass concrete projects. First, a thermal stress analysis investigation based upon thermal analyses from this investigation which should include verification of results against measured strains in the WES Test Wall is necessary to develop similar guidance in element size and time step sensitivity. In addition, existing Test-Wall and weather-bureau data can be used to further refine boundary condition guidance. Modeling solar radiation and re-radiation to develop simplified criteria for use in incremental construction investigations can be based upon Test Wall data taken after the initial complicating effects of heat of hydration, curing condition, early shrinkage, and other age dependent properties have stabilized. A considerable amount of measured data exists from which future investigations can be based.

107. It is evident that additional, but identifiable efforts are necessary to complete the thermal and mechanical aspects of the finite-element incremental construction formulation begun here. Completion of these efforts will more rapidly transform incremental construction investigations of proposed mass concrete structures from the research level to a application-level engineering tool.

REFERENCES

1. A. A. Bombich, C. D. Norman and H. W. Jones. 1987. Thermal Stress Analyses of Mississippi River Lock and Dam 26(R)," Technical Report SL-89-6, USAE Waterways Experiment Station, Vicksburg, MS.
2. ABAQUS Users Manual, Version 4. 1988. Hibbit, Karlsson & Sorensen, Inc., Providence, RI.
3. Y. R. Rashid and R. S. Dunham. 1986. "Development of a General Three-Dimensional UMAT Model for Concrete Considering Aging, Viscoplasticity, and Cracking," Technical Report ANA-85-0041, ANATECH International Corporation, La Jolla, CA.
4. ACI Committee 209. 1989. "Prediction of Creep, Shrinkage, and Temperature Effects in Concrete Structures," Report 209R-82, Manual of Concrete Practice, American Concrete Institute, Detroit, Michigan.
5. C. C. Norman, R. L. Campbell and S. B. Garner. 1988. "Analysis of Concrete Cracking on Lock Wall Resurfacing," Technical Report REMR-CS-15. USAE Waterways Experiment Station, Vicksburg, MS.
6. Z. P. Bazant and F. H. Wittmann. 1982. Creep and Shrinkage in Concrete Structures. John Wiley and Sons, New York, NY.
7. D. Pirtz. 1968. "Creep Characteristics of Mass Concrete for Dworshak Dam," Report No. 65-2, University of California, Berkeley, CA.
8. A. A. Bombich, R. R. Sullivan and J. E. McDonald. 1977. "Concrete Temperature Control Studies, Tennessee-Tombigbee Waterway Projects," Miscellaneous Paper C-77-8. USAE Waterways Experiment Station, Vicksburg, MS.
9. A. M. Neville. et. al. 1983. Creep of Plain and Structural Concrete. Construction Press, Longman, Inc., New York, New York.
10. W. Jürges. 1924. "Der Wärmeübergang an einer ebenen Wand" (Heat Transfer to a Plane Wall), *Beih. z. Ges. Ing.* 1, No. 19.